Westfälische Wilhelms-Universität Münster

Mathematical Models for Pedestrian Motion

Diplomarbeit

Institut für Numerische und Angewandte Mathematik

eingereicht von
Bärbel Angelika Schlake

Betreuer
Prof. Dr. Martin Burger

Münster, April 2008

Abstract

Subject of this work is the mathematical modelling of pedestrians, whose motion can be described in terms of ordinary and partial differential equations.

We introduce the most interesting models and their output. Models that are continuous in space (social force models) are as well considered as spatially discrete models (cellular automaton models).

We analyze in particular a one-dimensional, continuous in space model, for which we introduce some extensions. We investigate existence and uniqueness for local solutions of this extended model. In addition we present our numerical results. We investigate also the case that the number of pedestrians tends to infinity.

Furthermore we analyze for the continuous in space models under which conditions motion around homogeneous flow is stable.

In addition we present a numerical simulation for a two dimensional social force model and give an outlook about the work which is still open.

Zusammenfassung

Die vorliegende Arbeit befasst sich mit der mathematischen Modellierung von Fußgängern, deren Bewegung durch gewöhnliche und partielle Differentialgleichungen beschrieben werden kann.

Wir stellen die interessantesten Modelle sowie deren Output vor. Sowohl räumlich kontinuierliche Modelle (social force models) als auch räumlich diskrete Modelle (zelluläte Automaten) werden betrachtet.

Wir beschäftigen uns im Besonderen mit einem eindimensionalen, räumlich kontinuierlichem Modell, welches wir erweitern. Für dieses erweiterte Modell untersuchen wir Existenz sowie Eindeutigkeit lokaler Lösungen. Darüberhinaus präsentieren wir unsere numerischen Simulationen. Wir untersuchen auch den Fall, dass die Anzahl der Fußgänger gegen unendlich geht.

Außerdem untersuchen wir für die raumlich kontinuierlichen Modelle, unter welchen Bedingungen die Bewegung um den homogenen Fluß stabil ist.

Wir präsentieren auch eine numerische Simulation für ein zweidimensionales, räumlich kontinuierliches Modell und geben einen Ausblick über die Arbeit, die noch getan werden kann.

Acknowledgments

First of all, I want to thank my advisor Prof. Dr. Martin Burger for giving me the chance to work on this interesting topic and for taking his time to answer all my questions. His guidance has been a great help for me.

Furthermore, I would like to express my gratitude to Marzena Franek for the useful conversations during the last months.

I would also like to thank Jan for his techical support.

Last but not least I want to thank my family, especially my parents, for their support through all the years.

Contents

1 Introduction **1**

2 Literature Review **3**

2.1 Generalized Force Model of Pedestrian Dynamics 3
2.1.1 Observations 3
2.1.2 The Model 5
2.1.3 Simulation and Self-Organization Phenomena 6
2.1.4 Collective Phenomena in Panic Situations 7
2.1.5 Optimization 10
2.1.6 Conclusions 11
2.2 1D Social Force Model 11
2.2.1 Hard Bodies without Remote Action 12
2.2.2 Hard Bodies with Remote Action 13
2.2.3 Algorithms 13
2.2.4 Model Results 13
2.2.5 Conclusions 14
2.3 Social Force Model with Finite Reaction Times 14
2.3.1 Basic Model 14
2.3.2 Instantaneous Model including Anisotropy 14
2.3.3 Model including Finite Reaction Time 15
2.3.4 Comparison of the Models 15
2.3.5 Results 16
2.3.6 Conclusions 17
2.4 Optimal Velocity Model 18
2.4.1 The Model 18
2.5 Cellular Automaton Models 18
2.5.1 Results 19
2.5.2 A Model of Pedestrian Motion 19
2.5.3 Testing the Model 20
2.5.4 Conclusions 21
2.6 Discrete Microscopic Model 21
2.6.1 The Model 21
2.6.2 Results 22
2.6.3 Emergency Cases 23
2.6.4 Conclusions 23
2.7 The ASEP with shuffled Update 24
2.7.1 The Model 24
2.7.2 Steady State Distribution and Fundamental Diagram 24
2.7.3 Generalizations 25

2.7.4 Conclusions . . . 26
2.8 A Model based on a Lagrangian Approach . . . 26
2.8.1 The Model . . . 26
2.8.2 Another Formulation of the Model . . . 28
2.8.3 Theoretical Results . . . 28
2.8.4 Numerical Method . . . 29
2.8.5 Approximative Calculation of the effective Velocity . . . 30
2.8.6 Conclusions . . . 31
2.9 Model based on Continuum Dynamics . . . 31
2.9.1 The Model . . . 32
2.9.2 Conclusions . . . 34
2.10 Model for Crowds . . . 34
2.10.1 The Model . . . 34
2.10.2 Optimal Path Computation . . . 36
2.10.3 Speed . . . 36
2.10.4 Minimum Distance Enforcement . . . 37
2.10.5 Implementation . . . 37
2.10.6 Conclusions . . . 37

3 1D Movement 39
3.1 Experimental Setup . . . 39
3.1.1 Measurement Setup . . . 39
3.1.2 Empirical Results . . . 40
3.2 Results . . . 41
3.3 Investigations of the Model . . . 41
3.4 Implementation . . . 44
3.5 Conclusions . . . 45

4 Limiting Behaviour based on the BBGKY Approach 47
4.1 Special Case: Deterministic Locations . . . 47
4.1.1 Equation for V . . . 49
4.1.2 Conclusion . . . 50
4.2 General Case . . . 50
4.2.1 Link between Special and General Approach . . . 52
4.2.2 Conclusions . . . 54

5 Linear Stability 55
5.1 1D Social Force Model . . . 55
5.2 2D Social Force Model of Helbing . . . 57
5.2.1 Conclusions . . . 60
5.3 NOMAD Model . . . 60
5.3.1 Conclusions . . . 61
5.4 Optimal Velocity Model . . . 62
5.4.1 Linear Analysis . . . 62
5.4.2 Conclusions . . . 64

6 Numerical Results for a 2D Social Force Model 65

7 Outlook 71

A Experimental Data 73

B Details for Linear Stability of Helbings Model **75**
B.1 Exact Forms of A, B, C and D 75
B.2 Modes along the x-axis 76
B.2.1 Longitudinal Modes 76
B.2.2 Transverse Modes 76
B.3 Modes along the y-axis 77
B.3.1 Longitudinal Modes 77
B.3.2 Transverse Modes 77
B.4 Modes in General Direction 78
B.4.1 Longitudinal Modes 78
B.4.2 Transverse Modes 79

C Details for Linear Stability of the NOMAD Model **81**
C.1 Exact Forms of A, B, C and D 81
C.2 Modes along the x-axis 82
C.2.1 Longitudinal Modes 82
C.2.2 Transverse Modes 82
C.3 Modes along the y-axis 82
C.3.1 Longitudinal Modes 82
C.3.2 Transverse Modes 83
C.4 Modes in General Directon 83
C.4.1 Longitudinal Modes 83
C.4.2 Transverse Modes 84

Chapter 1

Introduction

The modelling for pedestrian motion, especially the modelling of evacuation scenarios, has become very important in the last recent years. This is due to the fact that events for crowds are getting larger at all times. Thousands of people have to be guided safe and fast out of buildings. It is a sad matter of fact that crowds are favoured by terrorists due to the number of victims and the attention they get. Furthermore, density of population is increasing which is problematic in case of natural disasters. Even districts or major cities sometimes have to be evacuated. Therefore it is essential to optimize escape routes.

It is necessary to simulate evacuation scenarios because running several simulations makes it easy to identify weak points in escape routes of public buildings like airports, stations or hotels. These weak points can be eliminated by means of technical, operational and architectural media.

We want to point out that a scientifical definition of the word 'panic' is still missing. Three states have to be distinguished: Non-compeditive evacuation (pedestrians leaving a room), compeditive evacuation (pedestrians leaving a room and every person wants to be outside first) and panic. The state of panic is rare, e.g. panic would include two pedestrians starting a fight in front of an exit because each person wants to be the first to get out. This leads to neither of them, nor of the following pedestrians, getting out. Fortunately the state of panic occurs seldomly, only in about two percent of all states commonly called 'panic' (in newspaper, television, etc.). In moste cases when the term 'panic' is used one deals with compeditive evacuation, as in this thesis.

It is essential to understand the behaviour of pedestrians under normal condition before modelling pedestrians in case of panic. Pedestrian's motion has been investigated since over forty years until now. The investigations are based on observations, photos and videos. Helbing evaluated many video records and summarized the results of further pedestrian studies ([8], [9], [11]). He presented a social force model which reproduces the observed phenomena quite realistically. The model is based on superposition of forces of walls and surrounding persons. The social force model is a microscopic model. Every person is taken into account individually. There are various models based on the social force model.

Another type of model used for modelling pedestrian motion are cellular automaton models. These models are discretized in space. A regular lattice is used as basis. The motion to other cells is determined by the transition probability which is stored in each pedestrian's preference matrix. Advantages of this type of model are their speed and their efficiency. There are a lot of models based on other approaches. We present the most interesting ones within this theses.

It is desirable to have a model that describes both, pedestrian's behaviour under normal

condition and in case of panic. In Helbing's social force model only one parameter, the nervousness, changes at the alterning of cases. Nevertheless all observed phenomena appearing in case of panic can be simulated well.

This thesis is organised as follows: In Chapter 2 we present several models. We begin with Helbing's model, his observations and results. We describe microscopic models as well as macroscopic ones, and discuss their output.

We investigate a 1D model based on the social force model in Chapter 3. We make some extensions and show existence and uniqueness for local solutions of the extended model. Furthermore, we present our numerical results, especially the velocity-density diagram obtained from our simulation.

In Chapter 4 we investigate the limiting behaviour (number of pedestrians tends to infinity) of the generalized 1D model on large time scales. Our approach is an analogon of what is called the BBGKY hierarchy used in classical kinetic literature.

In Chapter 5 we investigate linear stability around homogeneous flow. We want to know under which condition perturbations in homogeneous flow do not increase in time. We consider only continuous in space models here.

We simulated Helbing's social force model for pedestrians who are not in the state of panic. We present our results in Chapter 6.

In Chapter 7, we give an outlook about the work still have to be done.

Chapter 2

Literature Review

There are several modelling approaches for pedestrian dynamics. Accordingly, we want to give a review over the exsisting literature first. All the models considered here are generated on the basis of observed data. These data are rare in the case of panic situations.

The first aim of modelling is to reproduce the observed data. After calibrating the models that they fit the data, one hopes that they predict the changes in dynamics in the case of panic. We start with the model approaches of D. Helbing [8], [9], [11], because the other models considered here partly go back on his model.

2.1 Generalized Force Model of Pedestrian Dynamics

Helbing models the collective phenomena of escape panic with respect to self-driven many-particle systems, every pedestrian corresponding to one particle. First of all, we reflect his observations of pedestrians under normal and troubeling situations [8], [9].

2.1.1 Observations

Under normal Condition

- Pedestrians normally take the *fastest* route to their destination, and not the *shortest* one. They take into account detours as well as the comfort of walking. They try to minimize the effort to reach their destination. Their paths can be approximated by polygons.
- Pedestrians like to walk with an individual speed which corresponds to the most comfortable (equally least energy-consuming) one, as long as it is not necessary to walk faster. The individual speed is dependent of age, sex, purpose of the trip, time of day, etc. The desired speeds are Gaussian distributed with a mean value of approximately 1.34m/s and a standard deviation of about 0.26m/s. There are slightly different values in other articles,e.g. 1.24m/s ($\pm$0.15m/s) [25], which result from different conditions (in this case people were told not to hurry).
- Pedestrians keep a certain distance from other pedestrians and boundaries (walls, streets, etc.). The distance gets smaller the more hurried the person is. Furthermore, it decreases with increasing pedestrian density.
- Resting pedestrians (waiting for a train, etc.) are uniformly distributed among the available space, unless they belong to a group (family, friends).

- Groups behave similarly to individuals. Group sizes are Poisson distributed.
- Pedestrian's density increases around points of interest. It decreases with growing velocity invariance.

At medium Densities

- Footprints of pedestrian crowds look similar to streamline of fluids.
- At borders between opposite walking direction one can observe 'viscous fingering': The borderline between the pedestrians is unstable against small perturbations and gives rise to finger-like structures.
- The emergence of pedestrian streams through standing crowds appears analogous to the formation of river beds.
- If the pedestrian's density is high enough, pedestrians spontaneously organize into lanes of uniform walking direction.
- At bottlenecks the passing direction oscillates.
- Propagation of shock waves emerges in dense crowds pushing forward.

In Case of Panic (high Densities)

- Pedestrians are getting nervous and tend to move rather irrationally.
- Pedestrians try to move faster than usual.
- Individuals start pushing, and hence interactions between individuals become physical in nature.
- Moving and in particular passing of a bottleneck becomes uncoordinated.
- Jams build up. Arching and clogging are observed at exits.
- Physical interactions in the jammed crowd add up and can cause dangerous pressures up to 4500 N/m.
- Escape is slowed down by injured or fallen persons, who become obstacles for other pedestrians.
- People tend to show herding behaviour (they do what other people do), hence alternative exits are often overlooked or not efficiently used in escape situations.

In general, pedestrian motion is similar to the dynamics of gases or fluids or granular media, depending on wheather the density is low, medium, or high.

2.1.2 The Model

For modelling, Helbing uses the fact that the motion of each pedestrian can be described as a superposition of several forces. These forces are approximately vectorially additive, as concluded from a couple of experiments. Helbing assumes that these forces are a mixture of socio-psychological and physical forces [9]: each pedestrian i (weighing mass m_i) of N pedestrians likes to move with a certain desired speed v_i^0 in a certain direction $\mathbf{e}_i^0(t)$ and therefore tends to adapt his actual velocity $\mathbf{v}_i(t)$ within a certain characteristic time τ_i. Furthermore he tries to keep a velocity-dependent distance from other pedestrians j and walls W. This can be modelled by 'interaction forces' $\mathbf{f}_{ij}(t)$ and $\mathbf{f}_{iW}(t)$. The change of velocity in time t is then given by the equation of motion

$$m_i \frac{d\mathbf{v}_i}{dt} = m_i \frac{v_i^0 \mathbf{e}_i^0 - \mathbf{v}_i}{\tau_i} + \sum_{j(\neq i)} \mathbf{f}_{ij} + \sum_W \mathbf{f}_{iW}. \tag{2.1}$$

The change of position $\mathbf{r}_i(t)$ is as usual given by the velocity $\mathbf{v}_i(t) = d\mathbf{r}_i/dt$. The psychological tendency of two pedestrians i and j to stay away from each other is described by a repulsive interaction force

$$\mathbf{f}_{ij}^{interact} = A_i \cdot \exp[(R_{ij} - d_{ij})/B_i] \cdot \mathbf{n}_{ij}, \tag{2.2}$$

where A_i and B_i are fix the strength and range of the force. $d_{ij}(t) = \|\mathbf{r}_i - \mathbf{r}_j\|$ denotes the distance between the pedestrian's centres of mass, and $\mathbf{n}_{ij}(t) = (n_{ij}^1, n_{ij}^2) = (\mathbf{r}_i - \mathbf{r}_j)/d_{ij}$ is the normalized vector pointing from pedestrian j to i. Accordingly, pedestrians touch each other if their distance d_{ij} is smaller than the sum $R_{ij} = (R_i + R_j)$ of their radii R_i and R_j. This case is very important for understanding the behaviour of panicking crowds, as in crowds people tend to push each other. If pedestrian i comes to close to j, Helbing assumes two additional forces: a 'body force'

$$\mathbf{f}_{ij}^{body} = k(R_{ij} - d_{ij}) \cdot \mathbf{n}_{ij} \tag{2.3}$$

counteracting body compression and a 'sliding friction force'

$$\mathbf{f}_{ij}^{slid} = \kappa(R_{ij} - d_{ij}) \Delta v_{ji}^t \mathbf{t}_{ij} \tag{2.4}$$

impeding relative tangential motion. Here, $\mathbf{t}_{ij}(t) = (-n_{ij}^2, n_{ij}^1)$ means the tangential direction and $\Delta v_{ji}^t(t) = (\mathbf{v}_j - \mathbf{v}_i) \cdot \mathbf{t}_{ij}$ means the tangential velocity difference, while k and κ are large constants. In summary, we have

$$\begin{aligned} \mathbf{f}_{ij} = &\{A_i \cdot \exp[(R_{ij} - d_{ij})/B_i] + kg(R_{ij} - d_{ij})\} \mathbf{n}_{ij} \\ &+ \kappa g(R_{ij} - d_{ij}) \Delta v_{ji}^t \mathbf{t}_{ij}, \end{aligned} \tag{2.5}$$

here $g(x)$ is zero if the pedestrians do not touch each other ($d_{ij} > R_{ij}$), otherwise it is equal to the argument x. The interaction with walls is treated analogously:

$$\begin{aligned} \mathbf{f}_{iW} = &\{A_i \cdot \exp[(R_i - d_{iW})/B_i] + kg(R_i - d_{iW})\} \mathbf{n}_{iW} \\ &- \kappa g(R_i - d_{iW})(\mathbf{v}_i \cdot \mathbf{t}_{iW}) \mathbf{t}_{iW}, \end{aligned} \tag{2.6}$$

here $d_{iW}(t)$ denotes the distance to wall W, $\mathbf{n}_{iW}(t)$ denotes the direction perpendicular to it, and $\mathbf{t}_{iW}(t)$ means the direction tangential to it.

One can take into account that the situation in front of a pedestrian has a larger impact on his behaviour than things happening behind him [8]. Then the socio-psychological force has to be improved by a factor which reflects the anisotropic character of pedestrian's interaction:

$$\mathbf{f}_{ij} = A_i \cdot \exp[(R_{ij} - d_{ij})/B_i]\mathbf{n}_{ij} \cdot \left(\lambda_i + (1-\lambda_i)\frac{1+\cos\varphi_{ij}}{2}\right) \tag{2.7}$$

With the choice $\lambda_i < 1$ happenings in front of the pedestrian are weighted more than events behind him. φ_{ij} denotes the angle between the direction $\mathbf{e}_i = \mathbf{v}_i / \|\mathbf{v}_i\|$ of motion and the direction $-\mathbf{n}_{ij}$ of the object exerting the repulsive force. It is not necessary to take into account other details such as velocity dependence of the forces and noncircular-shaped pedestrian bodies, because this has no qualitative effect on the dynamics of the simulations.

Moreover, one can consider time-dependent attractive interactions towards sights or special attractions α by forces of the type (2.7) [8]. In comparison with repulsive interaction, the corresponding interaction range $B_{i\alpha}$ is here usually larger, whereas the strength parameter $A_{i\alpha}$ is smaller, negative and time-dependent.

The joining behaviour of friends, families or groups can be reflected by forces of the type $\mathbf{f}_{ij}^{att} = -C_{ij}\mathbf{n}_{ij}$. This guarantees that acquainted individuals rejoin, after being seperated by other pedestrians.

Finally, Helbing adds a fluctuation term ξ_i, taking into account unsystematic variations of individual behaviour.

In the following, we drop attraction effects and assume $\lambda_i = 0$ for simplicity (interaction forces become isotropic), according to Helbing [8]. In addition, the physical interactions are only relevant if pedestrians touch each other, i.e. in panic situations, so normally we have only repulsive social and boundary interactions to consider.

2.1.3 Simulation and Self-Organization Phenomena

The generalized force model of pedestrian's motion has been simulated for different situations and a large number of pedestrians. It describes the observed phenomena quite realistically, in spite of its simplifications. Futhermore, it explains various self-organized spatio-temporal patterns which are not externally influenced (traffic signs, etc.).

The above model is completly symmetric. Anyway, there are symmetry-braking phenomena resulting from the non-linear interactions of pedestrians. They are discussed below.

Segregation

Helbing's model reproduces the phenomenon of lane formation: pedestrians with the same desired walking direction prefer to walk in lanes. For open boundary conditions, these lanes are varying dynamically. The lane number depends on the width of the street, pedestrian's density and the level of fluctuation. One observes a noise-induced ordering: Medium noise amplitudes result in a more pronounced segregation (smaller number of lanes) than lower ones, high noise amplitudes lead to 'freezing by heating'.

Helbing's model explains lane formation without assuming that pedestrians prefer a special walking side (they do, in Europe (exept Britain) they like moving on the right, in Japan and Britain they walk on the left). Pedestrians walking against the stream have a high relative velocity, leading to many and strong interactions. As a consequence, at every interaction they change their walking direction sideways to avoid collisions. This moving sideways finally leads to separation. The resulting collective pattern of motion minimizes avoidance maneuvers if fluctuations are weak. The most stable configuration corresponds to a state with minimal interaction strength (assuming identical desired velocities $v_i^0 = v^0$):

$$-\frac{1}{N}\sum_{i\neq j}\tau\mathbf{f}_{ij}\cdot\mathbf{e}_i^0 \approx \frac{1}{N}\sum_i\left(v^0-\mathbf{v}_i\cdot\mathbf{e}_i^0\right)=v^0(1-E). \tag{2.8}$$

This is related to a maximum efficiency of motion

$$E=\frac{1}{N}\sum_i\frac{\mathbf{v}_i\cdot\mathbf{e}_i^0}{v^0}. \tag{2.9}$$

The efficiency E ($0\leq E\leq 1$) describes the average fraction of the desired speed v_0, with which pedestrians actually approach their destination ($N=\sum_i 1$ is the number of pedestrians i). As a consequence, formation of lanes globally maximizes the average velocity in the desired direction of motion. This is interesting, because in this model pedestrians do not even try to optimize their behaviour locally.

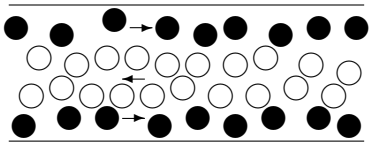

Figure 2.1: Lane Formation

Oscillations

In simulations at bottlenecks (doors) one observes an oscillation of the passing direction. Once a pedestrian is able to pass the bottleneck, other pedestrians can easily follow. Pedestrians on the other side have to wait. People may start pushing, so a 'pressure' builds up. Once this pressure is larger than on the other side, the chance of taking over the passage grows. This leads to a deadlock situation and finally the direction of passing changes.

Getting through a bottleneck is easier if it is broad and short, so that the direction of passing changes more frequently. It is more efficient to have two small doors instead of a large one. Each door is then used by one passing direction for a long time because of self-organiztion (a pedestrian passing through one door clears it for his successors).

Intersections

At intersections, the collective pattern of motion is alternating, short-lived and unstable. There may be phases at which the intersection is crossed in either vertical or horizontal direction, but also phases at which roundabouts arise. Roundabout traffic is connected with small detours, but the movement becomes more efficient on average because of minimal deceleration and stopping maneuvers. The chance of getting a roundabout can be improved by putting an obstacle (tree, column) in the centre of the intersection.

2.1.4 Collective Phenomena in Panic Situations

In panic situations pedestrian's motion changes in the following way:

- Pedestrians get nervous, resulting in a higher level of fluctuations.
- They try to escape from the cause of panic and therefore have a higher desired velocity.

- They are insecure and do not know what to do, thus they orientate at other peoples behaviour (herding behaviour).

In the following, we discuss the consequences of fluctuations, higher increased velocities and herding behaviour. We do not take into consideration that people might behave associally, although they sometimes do so [8], [9].

'Freezing by Heating'

First of all, we give a measurement for the fluctuations:

$$\eta_i = (1 - n_i)\eta_0 + n_i\eta_{max}. \tag{2.10}$$

Here, n_i denotes the nervousness of pedestrian i ($0 \leq n_i \leq 1$), η_0 denotes the normal und η_{max} the maximum fluctuation strength. If density of pedestrians is high enough, the formation of lanes occurs. But by increasing the fluctuation strength ('heating'), these lanes are destroyed. The 'fluid' state does not transform into the 'gaseous' disordered state, as expected, but into a solid state ('freezing'). It is characterized by a blocked situation with a regular structure. The blocked state shows a higher degree of order, although the internal energy is higher and the resulting state is metastable with respect to structural perturbations. 'Freezing by heating' is the opposite of what one would expect for equilibrium systems.

Preconditions for 'freezing by heating' are the additional driving term $v_i^0\mathbf{e}_i^0/\tau_i$ and dissipative friction $-\mathbf{v}_i/\tau_i$. Inhomogenities inside the corridor or other perturbations bring the transition forward. Transition is also observed if a certain density is exceeded.

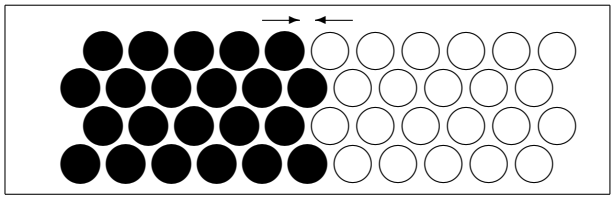

Figure 2.2: 'Freezing by heating'

'Faster is Slower Effect'

In this section, we discuss what happens if people try to leave a room fast. Simulated leaving of a room is well coordinated if the desired velocities are normal, but for desired velocities above 1.5m/s, one observes irregular succesion of archlike blockings of the exit and avalanchelike accumulation of leaving people if the arches break. This is compatible with empirical observations and similar to clogging found in granular flows.

Clogging is always connected with delays, so trying to leave a room fast may end up in a less average leaving speed, which is particularly tragic in the presence of fire. The driving term does not slow people down if the walls are sufficiently remote, so clogging presupposes a combination of several effects: First of all, slowing down beacause of a bottleneck, secondly, strong interpersonal friction, appearing only if pedestrians come to close to each other. ('Faster is slower' also accurs if the sliding friction force is assumed to be smooth).

The danger of clogging can be minimized by avoiding bottlenecks in the construction of public buildings. We mention that jamming may also appear at widenings of corridors, due

to pedestrians trying to overtake each other. So at the end of the widening people have to squeeze into the stream again and cause jamming.

Outflows can be improved by placing columns asymmetrically in front of the exits. This reduces the pressure and the injuries, because people can escape more easily.

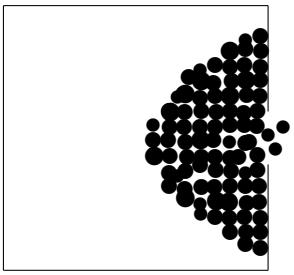

Figure 2.3: Archlike Blockings at the Exit

'Phantom-Panics'

In the past, panics have occured without any comprehensible reason. They were caused by small counterflows of pedestrians. Counterflows lead to delays in the leaving crowd. Pedestrians who cannot see the reason become impatient and start pushing. The increased desired speed is formulated as follows:

$$v_i^0(t) = [1 - n_i(t)]v_i^0(0) + n_i(t)v_i^{max}, \tag{2.11}$$

where, v_i^{max} is the maximum desired speed and $v_i^0(0)$ the initial one, correspondig to the expected velocity of leaving. The function

$$n_i(t) = 1 - \frac{\bar{v}_i(t)}{v_i^0(0)} \tag{2.12}$$

reflects the nervousness, $\bar{v}_i(t)$ beeing the average velocity in the desired direction of walking. As a consequence, long waiting times increase the desired velocities, and this leads to an inefficient outflow. This again leads to longer waiting times and so on. This tragic feedback leads to such high pressures that people are squashed or trampled after falling. This shows the importance of wide exits and prevention of counterflows if large crowds want to leave.

Herding Behavior

We investigate a situation where people try to leave a smoky room [8], [9], [11]. The exits are not visible. Each pedestrian i chooses either an individual direction $\mathbf{e}_i$ or follows the average direction $\left\langle \mathbf{e}_j^0(t) \right\rangle_i$ of his neighbours j in a certain Radius ρ_i or tries a mixture of both. In Helbings model, both strategies are weighted with the nervousness n_i:

$$\mathbf{e}_i^0(t) = N\left[(1 - n_i)\mathbf{e}_i + n_i \left\langle \mathbf{e}_j^0(t) \right\rangle_i\right]. \tag{2.13}$$

Here, $N(\mathbf{z}) = \mathbf{z}/\left\|\mathbf{z}\right\|$ denotes the normalization of a vector $\mathbf{z}$ to unit length. If n_i is low, pedestrian i shows pure individualistic behavior, otherwise he shows herding behavior. The above model suggests that neither pure individualistic nor pure herding behavior performs well. Pure individualistic behaviour means that only a few pedestrians find the exits. On the

other hand, pure herding behaviour means that the whole crowd moves into the same (maybe wrong) direction, so other exits are overlooked (as a sad matter of fact in agreement with observations). Optimal chances of survival are expected for a mixture of both: individualistic behavior allows some people to find the exits and herding guarantees that small groups follow.

2.1.5 Optimization

Streams of pedestrians are largely dependent on the geometry of the boundaries. They should be simulated during planning of buildings for optimizing the structure of the building in varying borders, exits, etc. Besides the efficiency E, the measure of comfort $C = 1 - D$ can be defined with respect to the discomford D [7]:

$$D = \frac{1}{N} \sum_i \frac{\overline{(\mathbf{v}_i - \overline{\mathbf{v}}_i)^2}}{(\mathbf{v}_i)^2} = \frac{1}{N} \sum_i \left(1 - \frac{\overline{\mathbf{v}}_i^2}{\overline{(\mathbf{v}_i)^2}} \right), \tag{2.14}$$

$0 \leq D \leq 1$. D reflects the frequency and dimension of sudden velocity changes. Thus the optimal walking state for pedestrians is the one with most efficiency and comfort. For the optimization, the following elements can be varied:

1. Arrangement and shape of the planned building.
2. Arrangements of pavements, entrances, exits, staircases, elevators, escalators and corridors.
3. Shape of rooms, corridors, entrances and exits.
4. Function and time schedule of the room-use.

It is also possible to use the optimization for existing bottlenecks and exits. We show some examples how the geometry of boundaries can be improved [9], [7]:

1. Lanes of opposite walking direction disturb each other at high pedestrian densities, due to impatient pedestrians using every gap for overtaking and impeding pedestrians on the other lane. A series of coloums in the middle of the corridor stabilizes the lanes. They still allow overtaking, but they appear like a wall for walking pedestrians. Moreover, it takes a detour to change the lane through the columns and consequently it is less attraktive.
2. Streams of pedestrians at bottlenecks can be improved by a funnelshaped geometry, which is also space-saving. The optimal shape is a convex one.
3. Two doors are more efficient than one doors which is twice as broard, by reason of every door beeing used by one direction of motion via self-organization. At a single broad door, the direction of walking just changes more frequently.
4. At intersections streams of opposite walking directions cross each other. Oscillating changes of the walking direction occur and jams build up in the meantime. Guidance arrangements like balustrades, which lead to a roundabout, reduce the resulting drop of efficiency. A roundabout can even be stabilized by an obstacle in the center.
5. It is better to have slim queues, because pedestrians advance faster then. Thus they do not start pushing. If waiting people are guided in zigzag shaped queues, dangerous pressures cannot build up.

6. Staircases are dangerous in panicking crowds, because pedestrians fall down due to being pushed, and are trampled. They turn to obstacles for other pedestrians, who fall down, too. So staircases should be subdivided in adequate small segments with zigzag walking directions. This breaks the pushing direction. One avoids dangerous pressures. Upside staircases are less dangerous than downstairs ones, because they straighten the crowd out in vertical direction and reduce the pressure in the crowd.

7. Escape routes have often a constant width. In many buildings, this is often barly hold. But it is not wise that escape routes have a constant width. The top level of a hotel, e.g., has to cope with the smallest number of persons. With every level the number of persons who have to be evacuated grows. The waiting times grow in inverse proportion to the distance to the exit. It is reasonable to built escape routes the more width, the smaller the distance to the exit is. It is not necessary that the medial width has to be larger than before.

8. A column placed asymmetrically in front of the exit can absorb the pressure like a wave-braker. It is placed asymmetrically for avoiding balance of forces.

The complex cooperation of several streams of pedestrians can lead to unexpected results, due to non-linear dynamics. The conventional methods can not prevent jams or blockades. But by optimizing pedestrian flows, one is able to increase the efficiency and even to save space.

2.1.6 Conclusions

Helbing's continuous pedestrian model is based on plausible interactions and is, by reason of its simplicity, robust with respect to parameter variations. It is therefore suitable for drawing conclusions about the possible mechanics underlying the effects of escape panic (increased desired velocity, strong friction effects during physical interactions and herding behaviour). After having calibrated the model parameters to avaliable data on pedestrian flows, it has reproduced many observed phenomena, such as 'freezing by heating', building up of fatal pressures, clogging at bottlenecks, jamming at widenings, faster is slower effect, phantom panics and herding behavior.

The model could be used to test buildings for their suitability in emergency situations. Moreover, it accounts for the different dynamics in normal and panic situations by changing a single paramet, the nervousness n_i.

Based on Helbings model, one could take into account direction- and velocity-dependent interpersonal interactions, specify the individual variation of parameters, study the effect of fluctuations, consider falling people, integrate acoustic information exchange, implement more complex strategies and interactions, or allow for switching of strategies. A superior theory would have to repoduce the empirical findings equally well with less parameters, reach a better quantitative agreement with data with the same number of parameters or reproduce additional observations.

2.2 1D Social Force Model

We consider the social force model of Helbing again, but only in the one-dimensional case. We modify it according to [25], in order to investigate hard bodies with and without remote action. The equations of motion for pedestrian i read

$$\frac{dr_i}{dt} = v_i, \quad m_i \frac{dv_i}{dt} = f_i = \sum_{j \neq i} f_{ij}(r_j, r_i, v_i). \tag{2.15}$$

They describe the movement of pedstrian i at position $r_i(t)$ with velocity $v_i(t)$ and mass m_i. The summation over j accounts for the interaction with other pedestrians. We neglect friction at the boundaries and random fluctuations, thus we only have a driving and a repulsive term: $f_i = f_i^{driv} + f_i^{rep}$. Seyfried *et al.* chose

$$f_i^{driv} = m_i \frac{v_i^0 - v_i}{\tau_i}, \tag{2.16}$$

$$f_i^{rep} = \sum_{j \neq i} -\nabla A_i (\|r_j - r_i\| - d_i)^{-B_i}. \tag{2.17}$$

Again, v_i^0 is the desired velocity and τ_i controlls the acceleration. The hard core d_i reflects the size of the pedestrian i acting with a remote force to other pedestrians. In one-dimensional systems, a repulsive force which is symmetric in space can lead to undesired effects: First of all, it may yield velocities which are in opposite direction to the intended speed. Secondly, the velocity of a pedestrian can exceed the desired speed through the impact of the forces of other pedestrians. These effects do not necessarily occur in two-dimensional systems. They can be avoided through the introduction of additional forces like lateral friction and an appropriate choice of the interaction parameters.

For our model we modify the reduced one-dimensional social force model in order to get the following properties: First of all, the force is always pointing in the direction of the desired velocity v_i^0. Secondly, the movement of a pedestrian is only influenced by effects which are directly positioned in front. Furthermore, the required length d of a pedestrian to move with velocity v is composed of a velocity independent term a and a velocity dependent term bv: $d = a + bv$. [25]. To investigate the influence of the remote action, we introduce a force which treats pedestrians as simple hard bodies as well as a force according to (2.16) und (2.17), where a remote action is present [25]. We set $v_i^0 \geq 0$, $r_{i+1} > r_i$ and $m_i = 1$ for simplicity.

2.2.1 Hard Bodies without Remote Action

Seyfried *et al.* modelled the force for hard bodies without remote action in the following way:

$$f_i(t) = \begin{cases} \frac{v_i^0 - v_i(t)}{\tau_i} & \text{, if } r_{i+1}(t) - r_i(t) > d_i(t) \\ -\delta(t) v_i(t) & \text{, if } r_{i+1}(t) - r_i(t) \leq d_i(t), \end{cases} \tag{2.18}$$

where $d_i(t) = a_i + b_i v_i(t)$. It depends only on the position of pedestrian i, his velocity, and the position of pedestrian $i+1$ in front. If the distance between pedestrians i and $i+1$ is larger than the required length d_i, only the driving term influences the movement of pedestrian i. If the required length is smaller than the distance, pedestrian i stops. This ensures that the velocity is restricted to the interval $v_i = [0, v_i^0]$ and that the movement is only influenced by the pedestrian $i+1$ in front. The required length d_i increases with growing velocity v_i.

2.2.2 Hard Bodies with Remote Action

Seyfried *et al.* modelled the force for hard bodies with remote action according to

$$f_i(t) = \begin{cases} G_i(t) & \text{, if } v_i(t) > 0 \\ \max(0, G_i(t)) & \text{, if } v_i(t) \leq 0, \end{cases} \tag{2.19}$$

with

$$G_i(t) = \frac{v_i^0 - v_i(t)}{\tau_i} - e_i \left(\frac{1}{r_{i+1}(t) - r_i(t) - d_i(t)} \right)^{g_i}. \tag{2.20}$$

Again, $d_i(t) = a_i + b_i v_i(t)$. The force depends only on pedestrian $i+1$. Due to d_i depending on v_i, the range of the interaction is a function of the velocity. The parametrs e_i and g_i fix the range and the strength of the force. We have to change the condition for setting the velocity to zero: The pedestrian stops if the force would lead to a negative velocity. With the proper choice of e_i and g_i and sufficiently small time steps this condition gets active mainly during the relaxation phase. This becomes important in case without remote action: If the influence of the driving term is large enough to get positive velocities, the person can advance.

2.2.3 Algorithms

Seyfried *et al.* used different update algorithms for the forces [25]. For the hard body model with remote action, an explicit Euler method with a timestep of Δt=0.001s works well. The case for the hard body model without remote action is more complicated because of the distribution on the right-hand side of (2.18), since its position is not known. The procedure is as follows: In a simple time-step each person is advanced one step (Δt=0.001s) according to the local forces. If after this step the distance to the person in front is smaller than the required length, the velocity is set to zero and the position is set to the old position. Additionally, the step of the next following person is controlled. If it is still possible, the update is completed. Otherwise, the velocity is set to zero again and the position is set to the old position, and so on. This is an approximation of the parallel update, though is not completely correct. It was tested for different arrangements of persons. The differences were minute and not more than expected from rearranging of arithmatic operations.

2.2.4 Model Results

Seyfried *et al.* tested the model as follows [25]: They chose a length L=17.3m. Values for v_i^0 were distributed according to a normal-distribution with mean μ=1.24m/s and σ=0.05m/s. τ, a, b, e and g were identical for all pedestrians. They presented their results in the dependency between mean velocity and density. To demonstrate the influence of the required length dependent on velocity, they chose different values for b. For hard bodies without remote actions, b=0.56s resulted in good agreement with the empirical data.

The influence of the interaction for hard bodies with remote action is small. For the same b, one observes a similar velocity-density relation, but one notices a gap at $\rho \approx 1.2\text{m}^{-1}$. It is generated through the development of distinct density waves [8]. The width of the gap can be changed by variation of the parameter g, which controls the range of the remote force. Near the gap the occurence of density waves depends on the distribution of the individual velocities.

2.2.5 Conclusions

The above modified one-dimensional social force model takes into account that the required length for moving with a certain velocity is a function of the current velocity. The model parameter can be adjusted to yield good agreements with empirical values [25]. This is valid for hard bodies with and without remote action. In case of remote action, one observes distinct density waves, which lead to a velocity gap in the fundamental diagramm. The model could be improved by taking into account that the movement of a pedestrian is not only influenced by the pedestrian directly in front, but also by the situation further ahead. As the model describes the one-dimensional case, it can be applied to for evacuation routes guiding through corridors, etc.

2.3 Social Force Model with Finite Reaction Times

We consider now a simplified version of the NOMAD model, which is similar to Helbing's social-force model [11]. We present the basic model and some extensions. Hoogendoorn *et al.* compared the models [14]. We present the results.

2.3.1 Basic Model

The basic model predicts the two-dimensional acceleration vector $\mathbf{a}_i(t)$ as a function of the desired velocity $\mathbf{v}_i^0$, the current speed $\mathbf{v}_i(t)$, and the distance $d_{ij}(t)$ between pedestrians i and j as follows:

$$\frac{d\mathbf{v}_i(t)}{dt} = \mathbf{f}_i(\mathbf{v}_i(t), \mathbf{r}_i(t) - \mathbf{r}_j(t), ...) = \frac{\mathbf{v}_i^0 - \mathbf{v}_i(t)}{\tau_i} - A_i \sum_{j \in Q_i} \mathbf{u}_{ij}(t) e^{-\frac{d_{ij}(t)}{B_i}}. \tag{2.21}$$

Here,

$$d_{ij}(t) = \|\mathbf{r}_i(t) - \mathbf{r}_j(t)\|, \quad \mathbf{u}_{ij}(t) = (\mathbf{r}_j(t) - \mathbf{r}_i(t))/d_{ij}(t).$$

We remark that $\mathbf{u}_{ij}$ is the same as $-\mathbf{n}_{ij}$ in Helbing's model. Q_i denotes the set of pedestrians that influence pedestrian i:

$$Q_i = \{j, \quad d_{ij} \leq c_i\}.$$

Pedestrians j having a smaller distance than c_i influence the movement of pedestrian i.

The four pedestrian specific parameters are the desired speed $V_i^0 = \left\|\mathbf{v}_i^0\right\|$, the acceleration time τ_i, the interaction constant A_i and the interaction distance B_i. They have to be estimated from the data. The desired walking direction $\mathbf{e}_i^0 = \mathbf{v}_i^0/V_i^0$ is assumed known.

2.3.2 Instantaneous Model including Anisotropy

Anisotropy means that pedestrians will only - or at least mainly - react to pedestrians in front of them. NOMAD can be extended to include anisotropy as follows [14]:

$$\frac{d\mathbf{v}_i(t)}{dt} = \frac{\mathbf{v}_i^0 - \mathbf{v}_i(t)}{\tau_i} - A_i \sum_{j \in Q_i} \mathbf{u}_{ij}(t) e^{-\frac{d_{ij}^*(t)}{B_i}} 1_{\mathbf{u}_{ij}(t) \cdot \mathbf{v}_i(t) > 0} \tag{2.22}$$

with

$$d_{ij}^*(t) = \frac{\mathbf{u}_{ij}(t)\cdot\mathbf{v}_i(t)}{\|\mathbf{v}_i(t)\|} + \eta_i\frac{\mathbf{w}_{ij}(t)\cdot\mathbf{v}_i(t)}{\|\mathbf{v}_i(t)\|}.$$

Here, $\eta_i > 0$ is a pedestrian specific factor that describes differences in pedestrian's reaction to stimuli directly in front and stimuli from the sides of the pedestrians. It has to be estimated from the avaliable microscopic data. The indicator function $1_{\mathbf{u}_{ij}\cdot\mathbf{v}_i>0}$ equals one if pedestrian j is in front ($\mathbf{u}_{ij}\cdot\mathbf{v}_i > 0$) of i and zero otherwise. This implies full anisotropy: A pedestrian does not take notice of any pedestrians behind him.

2.3.3 Model including Finite Reaction Time

Models for pedestrian motion do generally not include a finite reaction time. To determine if the reaction time can be neglected or not, we consider the following retarded model [14]:

$$\frac{d\mathbf{v}_i(t+T_i)}{dt} = \frac{\mathbf{v}_i^0 - \mathbf{v}_i(t)}{\tau_i} - A_i\sum_{j\in Q_i}\mathbf{u}_{ij}(t)e^{-\frac{d_{ij}^*(t)}{B_i}}1_{\mathbf{u}_{ij}(t)\cdot\mathbf{v}_i(t)>0}, \tag{2.23}$$

where $T_i > 0$ is the pedestrian specific reaction time (the perception-response time). T_i has to be estimated from the microscopic data. In this model, pedestrians have a delayed response to the observations they make at time instant t. The reaction times are between 0.1s and 0.8s.

This method can be applied to the former models as well: Finite reaction time is taken into account by replacing in the respective formulas $a_i(t)$ by $a_i(t+T_i)$.

2.3.4 Comparison of the Models

Hoogendorn *et al.* [14] compared the models introduced above. They estimated the parameters from experimental data. The group of pedestrians participating in the experiment consisted of people of different ages and genders. The experiment was characterized by a high pedestrian demand trying to pass through a narrow bottleneck of 1m width. The demand was larger than the bottleneck capacity, therefore the bottleneck became oversaturated resulting in congestion.

For the comparison, Hoogendorn *et al.* used the maximum likelihood estimation. Most continuous time microscopic walker models, including the models above, can be expressed in the following form:

$$\frac{d\mathbf{v}_i(t+T_i)}{dt} = \mathbf{a}_i(t+T_i) = \mathbf{F}_i(\mathbf{v}_i(t), \mathbf{r}_i(t) - \mathbf{r}_j(t), ...|\theta_i) + \epsilon_i. \tag{2.24}$$

Here, ϵ_i reflects errors in the modeling, θ_i desnotes the model parameters. Since we can determine all relevant variables directly from available experimental data, we can use (2.24) to determine a prediction for the retarded acceleration directly from the data. The prediction $\mathbf{a}_i(t_k + T_i|\theta_i)$, ($t_k$ being the time instant, $k = 1, ..., n$) is clearly dependent on the model parameters θ_i to be estimated and can be compared with the observed acceleration $\mathbf{a}_i^{obs}(t_k + T_i)$.

The maximum log-likelihood for an entire sample of subsequent acceleration observations $\mathbf{a}_i(t+T_i|\theta_i) = \mathbf{F}_i(\mathbf{v}_i^{obs}(t), \mathbf{r}_i^{obs}(t) - \mathbf{r}_j^{obs}(t), ...|\theta_i)$ neglecting correlation between subsequent samples reads (n denotes the number of time instants t_k)

$$\tilde{L}(\theta_i, \hat{\sigma}_i) = -\frac{n}{2}\ln\left(\frac{2\pi}{n}\sum_{k=1}^{n}(\mathbf{a}_i^{obs}(t_k+T) - \mathbf{a}_i(t_k+T_i|\theta_i))^2\right) - \frac{n}{2}. \tag{2.25}$$

In the following, the likelihood-ratio test is used to test whether one model performs better than the other. The zero-acceleration model is used as a reference model: $\mathbf{a}_i(t) = \epsilon_i$ with log-likelihood

$$\tilde{L}_0 = -\frac{n}{2}\ln\left(\frac{2\pi}{n}\sum_{k=1}^{n}\mathbf{a}_i^{obs}(t_k)^2\right) - \frac{n}{2}.$$

The likelihood-ratio (LR) test involves testing the statistic

$$S_i = 2\left(\tilde{L}(\hat{\theta}_i, \hat{\sigma}_i) - \tilde{L}_0\right), \tag{2.26}$$

which follows the χ^2 distribution with m degrees of freedom. m denotes the number of parameters of the model. The likelihood-ratio test is passed with 95% confidence if

$$2\left(\tilde{L}(\hat{\theta}_i, \hat{\sigma}_i) - \tilde{L}_0\right) > \chi^2(0.95, m). \tag{2.27}$$

2.3.5 Results

We present the results of cross-comparing the model predictions with the naive zero-acceleration reference model, according to [14]. The parameters of the models have been estimated from the experimental data discussed above. The performance of the models is cross-compared based on the overall relative increase in the log-likelihood ratio test.

Modeltype	**% Improvement log-likelihood**	**% of models passing likelihood ratio test**
Basic model	6.4%	71%
Anisotropic model	7.7%	76%
Retarded anisotropic model	19.7%	83%

Table 2.1: Overview of estimation results

Table 2.1 shows an overview of the estimation results. It shows that there are considerable differences between the model performances. Especially the difference between the instantaneous models and the retarded models is relatively large (6.6% or 7.7% improvement of the log-likelihood for the instantaneous models, compared to 19.7% in case of the retarded anisotropic model).

Hoogendorn *et al.* also investigated the statistics of the parameter estimates as well as inter-pedestrian differences [14]. We present the results here only briefly.

Basic Model

The basic model passed the LR test in 71% of all cases. For the remaining 29%, the basic model showed a higher log-likelihood than the null-model, but the improvement was not large enough to pass the LR test.

The inter-pedestrian differences are at most reflected by the differences in the acceleration times τ_i and the interaction distance B_i (mean 1.09s resp. 0.16m, standard deviation 0.35s resp. 0.08m). The inter-pedestrian correlations between the parameter estimates are generally small, except for a positive correlation between free speed and interaction distance (0.49)

Anisotropic Model

The anisotropic model with instantaneous reaction outperformed the basic model, but the improvement was rather small. The model improved significantly with respect to the naive zero-acceleration model in case of 76% of all parameters considered.

As to the parameter estimates, the acceleration time τ_i has a relative large standard deviation (0.24s compared to a mean of 0.96s). This implies that the inter-pedestrian differences in acceleration times are large. This holds equally for the interaction distance B_i (mean 0.33m, standard deviation 0.09m).

A considerable correlation is found between free speed and interaction distance (0.62). This implies that on average, pedestrians having a large free speed V_i^0 have large acceleration distances B_i. Other high correlations are found between the acceleration time τ_i and interaction factor A_i (-0.54), and between the interaction factor A_i and the interaction distance B_i (0.46).

Comparing the estimates of the basic model with the estimates of the anisotropic model, one notices that the estimates are similar, except for the interaction distance B_i. In the anisotropic model, the interaction distance is on average twice as large as in the non-anisotropic model. Regarding the inter-pedestrian parameter differences, it turns out that the variability in the acceleration time τ_i reduces considerably (from 0.35s to 0.24s (St-d.)).

Retarded Anisotropic Model

The importance of this model can clearly be seen in the Table 2.1: First of all, 83% of the considered cases pass the LR test. Secondly, the log-likelihood improvement over the naive zero-acceleration model of 19.7% was much higher than for the non-retarded models.

The standard deviations -and thus the inter-pedestrian differences- of the acceleration times and of the interaction distances are relatively large (0.23s (0.74s mean) or 0.11m (0.35m mean)). Mean of T_i is 0.28s, standard deviation is 0.07s. Free speed V_i^0 and interaction distance B_i are positively correlated (0.57), reaction time T_i and interaction factor A_i are negatively correlated, implying that the reaction time and the interaction factor are to a certain extent mutually exclusive.

For the distributions of the parameter estimates it has to be mentioned that their shape is rather skewed than symmetric. Especially the interaction factor A_i has few estimates with very large values. The median reaction time equals 0.3s, only few pedestrians have a reaction time larger than the median of 0.3s.

The parameter estimates determined by applying the approach to data from other experiments are consistent.

2.3.6 Conclusions

In this section, a generic approach for calibration of microscopic models was reviewed. The approach provides on the one hand insight into the statistical properties of the estimates. On the other hand one gains insight into the performance of the models to which the calibration is applied. Besides anisotropy, finite reaction times play an important role in correctly describing microscopic walking behaviour. Researches about the macroscopic properties of the microscopically calibrated pedestrian models have not been done until now. It is still an open problem how finite reaction times and inter-pedestrian differences are related to the dynamic flow properties.

2.4 Optimal Velocity Model

The optimal velocity model was literally used to describe one-dimensional traffic flow. In this section, we present a two-dimensional extension of the one-dimensional OV according to [22].

The concept for the one-dimensional OV model is simple: A driver maintains his optimal velocity depending on the distance to other vehicles. The two-dimensional OV model for pedestrians is constructed along the same concept. Pedestrians are treated as identical particles moving in a plane (2D). Each pedestrian chooses his optimal velocity depending on the distance to other pedestrians.

2.4.1 The Model

The two-dimensional OV model for pedestrian flow is a natural extension of the one-dimensional one [22]. The equation of motion for pedestrian i reads

$$\frac{d}{dt}\mathbf{v}_i(t) = a\left[\left(\mathbf{v}^0 + \sum_j \mathbf{f}(\mathbf{r}_j(t) - \mathbf{r}_i(t))\right) - \mathbf{v}_i(t)\right]. \tag{2.28}$$

Here, $\mathbf{r}_i = (x_i, y_i)$ and $\mathbf{r}_j = (x_j, y_j)$ are the positions of the i-th and j-th pedestrians. $\mathbf{v}^0$ denotes the desired velocity. A pedestrian moves with the desired velocity if he is alone. $\mathbf{f}$ expresses the interaction between particles. Nakayama *et al.* chose the following form [22]:

$$\mathbf{f}(\mathbf{r}_j - \mathbf{r}_i) = g(d_{ji})(1 + \cos\varphi)\mathbf{n}_{ji} \tag{2.29}$$

with

$$g(d_{ji}) = \alpha[\tanh\beta(d_{ji} - b) + c]. \tag{2.30}$$

Again, $d_{ji} = \|\mathbf{r}_j - \mathbf{r}_i\|$, $\mathbf{n}_{ji} = (\mathbf{r}_j - \mathbf{r}_i)/d_{ji}$ and $\cos\varphi = (x_j - x_i)/d_{ji}$. The interaction is determined by the distance d_{ji} between i-th and j-th pedestrians and the angle φ between $\mathbf{r}_j - \mathbf{r}_i$ and $\mathbf{v}^0$. The factor $(1+\cos\varphi)$ reflects the anisotropic character of pedestrian's motion.

Nakayama *et al.* investigated the instability of pedestrian flow. We present their results and conclusions in Section 5.4.

2.5 Cellular Automaton Models

We now change from models that are continuous in space to cellular automaton models. These models have in common that they are based on discretization of space into indentical cells of size Δx. The states of the cells are either empty or occupied. The update of the cells is performed at times $t = i\Delta t$ with an elementary time step Δt according to globally applied update rules. Due to this properties, cellular automaton models are in particular interesting for their speed and efficiency.

In a spatially and temporally discrete model the speed of a person is the number of cells which he advances during one time step. The time discretization fixes the real-world interpretation of the dimensionless speed. In the following, we consider in particular von-Neumann and Moore neighbourhoods, and a mixture of both. If a person takes a von-Neumann step, he is allowed to walk in horizontal and vertical direction. If he takes a Moore step, he is as well allowed to walk in diagonal direction. If a person moves into the diagonal direction, he is either $\sqrt{2}$ times as fast or as slow as if he moves horizontally or

vertically. The situation can be improved by taking a mixture of von-Neumann and Moore neighbourhoods. This results in a larger total neighbourhood of cells which can be reached during one round.

In the following, we deal with the question whether there is an optimal total neighbourhood for a given speed, and whether it can be composed of von-Neumann and Moore neighbourhoods, according to [17]. In vertical and horizontal direction, the neighbourhood contains for $v = v_m$ the cell of the agent and v_m cells in each vertical and horizontal direction. For any other directions it is not obvious which cell is part of the neighbourhood.

Definition: *Complete neighbourhoods are fourfold symmetrical neighbourhoods where all cells which belong to the neighbourhood are closer to the center cell than those which do not [17].*

Thus one can limit the search for an optimal neighbourhood to complete neighbourhoods. One is interested in which complete neighbourhood represents the number of cells in horizontal and vertical direction best. The criteria chosen in Kretz *et al.* are such that discretization effects concerning the axis of discretization of the original plan are minimized.

First of all, for each complete neighbourhood the speed $v(\phi)$ has to be written down, where ϕ denotes the angle for every direction. After this, the direction-averaged speed

$$\langle v \rangle = v_{av} = \frac{1}{2\pi} \int_{\phi} v(\phi) d\phi \tag{2.31}$$

and the squared deviation of speeds into each direction from this average

$$\Delta v = \sqrt{\frac{1}{2\pi} \int_{\phi} (v(\phi) - v_{av})^2 d\phi} \tag{2.32}$$

are calculated. The criteria for an optimal neighbourhood are then, according to [17]:

- The direction averaged speed should be close to an integer
- The deviation from this average into different directions should be small

Since all complete neighbourhoods have a fourfold axial-symmetry, it is sufficient to calculate $v(\phi)$ for $0 \leq \phi < \pi/4$. $v(\phi)$ is continuously composed from different functions resulting from different ranges of ϕ. The structure of those ranges depends on the shape of the edge of the neighbourhood.

2.5.1 Results

Kretz *et al.* obtained the choices of neighbourhood showed in Table 2.2. This choices resulted in the quarter of speed neighbourhoods illustrated in Figure 2.4 (a pedestrian with maximum speed v_m can reach all cells with a number $\leq v_m$).

2.5.2 A Model of Pedestrian Motion

We present the model that uses the above ideas only in brief [17]:

Space is discretized into quadratic cells. Length of a site is 0.4m, so each cell is occupied by at most one pedestrian. Individual parameters (such as maximum speed) are spread over all pedestrians. Then the pedestrians are assigned to their starting position. Round by round pedestrians repeat the following steps until all pedestrians have left the scenario

speed	neighborhood (d^2_{max})
1	2
2	5
3	10
4	18
5	29
6	40
7	53
8	72
9	89
10	109

Table 2.2: Speed and related neighbourhoods

via an exit: All pedestrians choose in parallel one of the cells (destination) within the neighbourhood according to their maximum speed. After this, they sequentially try to reach their destination.

The rules for the selection of a destination cell are quite complex and probabilistic while the rules of movement are rather simple and deterministic. Important for the decision of the destination is the higher probability to select a cell as destination if it is closer to the exit (probability $p \propto \exp(k_s(S_{max} - S))$, with coupling strength k_s and distance S to the exit). Herding behaviour, inertia, the distance towards other agents and walls may also play a role. The sequence in which the pedestrians carry out their steps is chosen randomly. Each pedestrian moves within a Moore neighbourhood to that cell lying closest to his destination cell. If no cell closer to the destination cell is available, he remains at his current position. A once used cell remains blocked for the rest of the round.

10	10	10	10							
9	9	9	10	10	10					
8	8	8	9	9	9	10				
7	7	7	8	8	9	9	10			
6	6	6	7	7	8	8	9	10		
5	5	5	6	7	7	8	9	9	10	
4	4	5	5	6	7	7	8	9	10	
3	3	4	4	5	6	7	8	9	10	10
2	2	3	4	5	5	6	7	8	9	10
1	1	2	3	4	5	6	7	8	9	10
0	1	2	3	4	5	6	7	8	9	10

Figure 2.4: Speed neighborhoods

2.5.3 Testing the Model

Kretz *et al.* carried several simulations out to test the model. In each of them every pedestrian moved a distance of 325 cells into eight different directions with two different

speeds [17]. Each simulation was carried out 100 times. k_s has been set to 10.0.

The overall evacuation time for v=1 was 302.6 rounds ± 7.00 rounds (2.30%). For v=5, it was 65.9 rounds ± 0.30 rounds (0.46%). This implies that the standard deviation of the overall average is roughly by the same factor (5) smaller as the speed is larger. If one wants to interpret the pedestrians moving in the two examples with 2m/s, for v=1 one round has to be interpreted as 0.2 seconds. For v=5 one round would be one second. On the other hand, for v=1, the time to move as far as 130 m would vary with the orientation of the discretization axis by more than 10 seconds. For v=5 it would only be 2.5 seconds.

Kretz *et al.* compared the simulated walking times of two alternative routes in another test. Route B is $\sqrt{2}$ times as long as route A. The average (ten simulations) walking times for pedestrians with a certain speed are shown in Table 2.3.

	T_A	T_B	T_B/T_A	$T_B/(\sqrt{2}T_A)$
v=1	291.1	328.4	1.13	0.80
v=2	147.0	202.4	1.38	0.98
v=3	98.6	155.2	1.57	1.11
v=4	74.2	102.9	1.39	0.98
v=1	59.4	86.7	1.46	1.03

Table 2.3: Average walking times

2.5.4 Conclusions

Kretz *et al.* presented two criteria to identify the best neighbourhoods for speeds larger than one. Furthermore they presented the results of simulations which compared motion in Moore neighbourhood steps with motion in steps within the best neighbourhood for v=5. The results showed the reduction of discretization artifacts by a factor of four or even five for the latter neighbourhood. This becomes interesting in case of finer discretizations, where a subsequent execution of steps within Moore or von-Neumann neighbourhoods would lead to the same dependance of evacuation times.

2.6 Discrete Microscopic Model

We examine a discrete microscopic model which is based on the common approach for cellular automaton models and social-force-based repulsion forces, according to [24]. Schultz *et al.* used this model is to investigate emergency situations in airport terminals.

2.6.1 The Model

As a cellular automaton model, this model is both spatially and time discrete. Space is devided into square cells with a side length of 0.4m. This equals the space requirement of a single person [30]. Again, the states of one cell are either empty or occupied. A person can reach all surrounding cells. The motion to other cells depends upon the transition probability which is stored in the preference Matrix $M_{q,p}$ (see Figure 2.5).

We assume independence of the longitudinal (p) and transverse (q) components of the passengers velocity. Thus the movement from $M_{0,0}$ to $M_{0,1}$ (M^{hor}) is determined by the common transition probability h calculated by the variance σ^2 and the expected value μ [1]:

$$h_{-1} = \frac{1}{2}(\sigma^2 + \mu^2 - \mu)$$
$$h_0 = 1 - (\sigma^2 + \mu^2)$$
$$h_1 = \frac{1}{2}(\sigma^2 + \mu^2 + \mu)$$

$$\mu_q = 0 \qquad 0 \leq \mu_p \leq 1 \qquad 0 \leq \sigma_q^2 \leq 1 \qquad \frac{1}{4} - \left(|\mu_p| - \frac{1}{2}\right)^2 \leq \sigma_p^2 \leq 1 - |\mu_p|^2$$

Direction dependent movement can be archieved by the superposition of M^{hor} and M^{diag}. M^{diag} is a copy of M^{hor}, turned by 45°. It allows considering the case of diagonal movement (further details in [1]).

$$M_{q,p} = [1 - \lambda]M_{q,p}^{hor} + \lambda M_{q,p}^{diag} \qquad \lambda = \tan\alpha \qquad 0° \leq \alpha \leq 45° \tag{2.33}$$

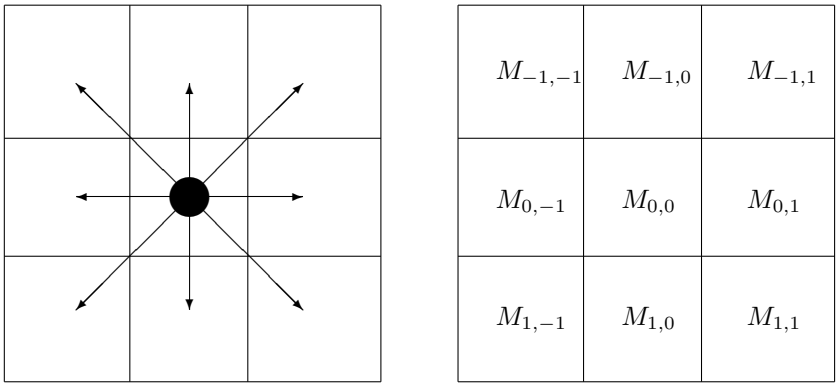

Figure 2.5: Cell Neighborhood and Preference Matrix

2.6.2 Results

Distance

As previously seen, periodic lattice structure composed of square cells has the negative side effect that there is not the same distance from one cell to every surrounding cell. If a person moves in diagonal direction, distance is seized by a factor of approx. 1.41. To compensate this effect, Schulz *et al.* propose a stop-and-go algorithm [24]. If a person stops after a couple of diagonal steps, the distance error will be scaling down. 3 horizontal steps approximate 2 diagonal steps (error -6%), as an example. The appropriate algotihm notation is 3/2. There are other algorithms, such as 4/3, 7/5, 17/12. In the following, the 17/12 algorithm will be used, because here variations of the distance error in positive and negative directions are the smallest (±1.5%) [24].

System immanent Variance

The transition probability for every neigbouring cell can be determined by the specification of a set of movement parameters $(\mu_p, \sigma_p^2, \sigma_q^2, \alpha)$. The above model generates a system immanent varicance σ^2, even without assuming a transverse variance. This happens due to the regular lattice: If the motion angle is not a multiple of 45°, a selection of two cells is generated. The influence of σ^2 is made smaller by variations of the horizontal/ vertical motion direction than by variations of the diagonal motion direction. To compensate the effect of the system immanent variance σ^2, the model will be calibrated by a weighing function $\sigma^2(\alpha, \sigma_q^2) \approx 3.95$. This leads to a loaded variance [24].

Repulsion Forces

Due to the interaction between the simulated persons (social forces), the cellular automaton model will be extended by a potential field $\Phi(x, y)$ approach, where x represents the longitudinal component and y represents the transverse component of the person's velocity.

$$\Phi = a \cdot \exp\left\{\frac{w_{x_1}}{w_{x_2}}\left(1 - \exp\left(-\frac{x}{w_{x_1}}\right)\right) - \frac{x}{w_{x_2}} - \frac{y^2}{w_y}\right\} \tag{2.34}$$

$$x < 0\,(w_{x_1} = \hat{w}_{x_1}; w_{x_2} = \hat{w}_{x_2})$$

Here, a is the amplitude and w represents the set of shape parameters for the potential field. There are two different sets of parameters: w is used for $x > 0$, $\hat{w}$ for $x < 0$.

Route Choice

To determine a person's path through complex building structures, the distance to the nearest exit is stored in every cell. Obstacles are taken into account. This algorithm leads to artifacts in the movement of the pedestrians [16]. Accordingly, this approach has to be extended. First of all, the shortest distance for each cell is specified. After this, the created distance matrix can determine how far any person can move directly to the destination in the horizontal/ vertical and diagonal direction. This results in the actually visible final cell. This cell is not hidden by any obstacles.

2.6.3 Emergency Cases

In this simulation environment, emergency cases are determined in three different ways: lack of orientation information, modification of motion parameters, and changing of the area surrounding a person (e.g. blocked exits). For simulating emergency cases it is necessary to determine the terminal areas which are influenced by the incident and the emerging consequences. The so called consequence area and its expansion depends on the mode and dimension of the emergency as well as on the surrounding environment.

2.6.4 Conclusions

Airport evacuation is important by reason of the masses of people which linger at an airport every day. The above discrete microscopic model allows a fast identification of weak points at the evacuation by simulating several airport scenarios. These weak points can be eliminated beforehand by means of technical, operational and architectural media.

2.7 The ASEP with shuffled Update

We consider a one-dimensional cellular automaton model that describes pedestrian's motion in a long and narrow corridor, according to [31]. This model is equivalent to the asymmetric simple exclusion process (ASEP) with periodic boundary conditions and shuffeled dynamics. The ASEP describes a particle system on a linear chain with hard core exclusion. Particles are allowed to jump one cell to their right if it is empty.

2.7.1 The Model

Before describing the model, we briefly explain the underlying automaton: We consider a corridor of of finite width W in y-direction, which is divided into square cells. As above, each cell can be occupied or empty. We assume periodic boundary conditions in x-direction, and impermeable walls in y-direction. This implies that the number of pedestrians is constant. A person moves to his neighbouring cells with different transition probabilities. The preferred direction of motion is along the positive x-axis. A parallel update could lead to conflicts, therefore a shuffeled update is chosen: At the beginning of a time step a random permutation of the particle numbers gives the order in which the particles move. We investigate the simplest case first, the one-dimensional case with $W = 1$. The corridor is so small that it is impossible for pedestrians to move 'side-by-side'. Since this results in a completely asymmetric movement to the right, the model is equivalent to the ASEP with shuffeled update.

In our model, we consider a one-dimensional lattice with L sites and periodic boundary conditions. Each site is either empty or occupied by one of the N pedestrians, labelled $n = 1, 2, ..., N$. In each discrete timestep a random permutation $\pi(1, ..., N)$ of pedestrian's numbers determines the update sequence. If the right neighbouring cell is empty, the relevant person moves one cell to the right with probability p. If it is occupied, the person stays in his cell.

2.7.2 Steady State Distribution and Fundamental Diagram

We assume that the probability to find a certain agglomeration of pedestrians in the steady state factorizes into probabilities for interparticle distances. This is usually not exact and motivates the car-oriented mean-field (COMF) theory. The mean field theory leads to the kinetic equations, e.g., the Liouville equation. If P_n denotes the probability to find a pedestrian with n holes in front, the resulting master equations are (for details, see [31]):

$$P_0(t+1) = P_0(t) - (p-g)(1-P_0(t)) + p\bar{g}P_1(t), \tag{2.35}$$

$$P_1(t+1) = (p-g)(1-P_0(t)) + (pg + (1-p)\bar{g})P_1(t) + p\bar{g}P_2(t), \tag{2.36}$$

$$P_n(t+1) = (1-p)gP_{n-1}(t) + (pg + (1-p)\bar{g})P_n(t) + p\bar{g}P_{n+1}(t), \qquad n > 1. \tag{2.37}$$

Here, $g = 1 - \bar{g}$. In the limit $t \to \infty$ we obtain:

$$P_0 = P_0 - (p-g)(1-P_0) + p\bar{g}P_1, \tag{2.38}$$

$$P_1 = (p-g)(1-P_0) + (pg + (1-p)\bar{g})P_1 + p\bar{g}P_2, \tag{2.39}$$

$$P_n = (1-p)gP_{n-1} + (pg + (1-p)\bar{g})P_n + p\bar{g}P_{n+1}, \qquad n > 1. \tag{2.40}$$

The probability for a person to have exactly $k-1$ pedestrians directly in front is approximated in COMF by $(1-P_0)P_0^{k-1}$ (due to factorization). One can calculate the probability with which the person has moved at the end of the time step:

$$g = \sum_{k=1}^{\infty} \frac{p^k}{k!}(1-P_0)P_0^{k-1} = \begin{cases} p & P_0 = 0 \\ \frac{1-P_0}{P_0}\left[\exp(pP_0)-1\right] & P_0 > 0. \end{cases} \tag{2.41}$$

Since g is the probability that an arbitrary person moves, it equals the average velocity. We obtain the fundamental diagram

$$J(\rho) = g\rho. \tag{2.42}$$

Here, ρ denotes the pedestrian's density. An implicit expression for P_0 reads:

$$P_0 = \frac{p(\rho-\bar{\rho}) - (p\rho-\bar{\rho})g}{p\rho\bar{g}}, \tag{2.43}$$

where $\bar{\rho} = 1-\rho$. If $p = 1$, P_0 becomes explicit, and the flow-density relation reads

$$J(\rho, p=1) = \begin{cases} \rho & \rho \le 1/2 \\ \frac{\rho(1-\rho)}{2\rho-1}\left[\exp\left(\frac{2\rho-1}{\rho}\right)-1\right] & \rho > 1/2. \end{cases} \tag{2.44}$$

In Wölki *et al.*, the fundamental diagrams $J(\rho)$ for $p = 1$ and $p = 0.5$ from the above calculations and from Monte-Carlo simulations are compared. It has to be mentioned that the COMF-theory applied here does not give the exact results for a general choice of p and ρ. However, the results are very good approximations.

2.7.3 Generalizations

In the following we consider two generalizations of the above model, according to [31]. Pedestrians move in a corridor of arbitrary width W. They are not allowed to change lanes. Therefore the pedestrian's density in a particular lane is fixed for all time steps. The probability of finding i pedestrians in a particular lane is given by the hypergeometric distribution

$$Hyp_{N,L,L(W-1)}(i) = \frac{\binom{L}{i}\binom{L(W-1)}{N-i}}{\binom{LW}{N}}. \tag{2.45}$$

Mean is $\rho = N/(LW)$. The fundamental diagram of the model with decoupled lanes reads [1]

$$\tilde{J}(\rho) = \sum_{i=0}^{L} Hyp_{\rho LW,L,L(W-1)}(i) \cdot J(i/L). \tag{2.46}$$

Here, $J(\rho)$ denotes the single-lane fundamental diagram. Comparing the decoupled-lane fundamental diagram with the single-lane fundamental diagram, one has to mention that the maximum in the decoupled-lane fundamental diagramm is smoother and a little bit lowered. Lane-changing, which is important for high densities, would lead to a reduction of the flow.

Wölki *et al.* introduce a larger maximum velocity v_{max} (a larger number of cells that can be passed during one time step) to reproduce the shift of the maximum flow to lower densities, which is observed in pedestrian dynamics. The simplest way is to allow a person to move the minimum of v_{max} cells and the number of empty cells in front with probability p at each time step. In the following, we consider only the case $W = 1$ and $p = 1$.

For densities less or equal to $1/(v_{max}+1)$, each of the pedestrians has at least v_{max} empty sites in front. The probability to find a person in front is P_0. The flow is deterministically given as $v_{max}\rho$. For higher densities it may happen that a pedestrian occupies a cell at time $t+1$ that has been occupied by a different pedestrian belonging to the cluster in front at time t. For relatively small v_{max} this can be neglected (concluding from computer simulations). Hence Wölki *et al.* describe the dynamics with parallel update. The probability to have at least one hole in front is in the above case $p = (1-\rho)/v_{max}$. The fraction of pedestrians which do not have a person in front is $(\rho - (1-\rho)/v_{max})/\rho$. This determines P_0, and we obtain for the fundamental diagram

$$J(\rho, v_{max}, p=1) = \begin{cases} v_{max}\rho & \text{if } \rho \leq 1/(v_{max}+1) \\ \frac{v_{max}\rho(1-\rho)}{(1+v_{max})\rho-1}\left[\exp\left(\frac{(v_{max}+1)\rho-1}{v_{max}\rho}\right)-1\right] & \text{else.} \end{cases} \tag{2.47}$$

For the fundamental diagram in case of $v_{max} = 3$ and $p = 1$ it has to be mentioned that the maximum of the fundamental diagram and the critical point $(1/(v_{max}+1), \rho v_{max})$ do not coincide, in contrast to the case of $v_{max} = 1$ and $p = 0.5$. This is qualitatively reproduced by the analytical result. To recover the exact result one would have to take into account longer ranged correlations.

2.7.4 Conclusions

The steady state distribution functions derived from the above model are in very good agreement with Monte-Carlo data. The fundamental diagram for $p = 1$ has a strong asymmetry with respect to $p = 1/2$. This is by reason of the fact that for small densities all pedestrians can move independently and deterministically. On the other hand, for higher densities jams are formed and the probability for a person in a jam to move decreases with the number of pedestrians directly in front, due to the shuffled dynamics. Thus the flow is increased in high density regions. Furthermore, Wölki *et al.* presented generalizations of the results to a two dimensional setting with decoupled lanes and higher velocities. The simulation are in good agreement with analytical results.

2.8 A Model based on a Lagrangian Approach

We present a model for pedestrian motion based on a Lagrangian approach, according to [19]. Each person is taken into account individually. Maury *et al.* show the well-posedness of this problem under reasonable assumptions and propose a numerical method.

2.8.1 The Model

In this model, Maury *et al.* consider N pedestrians. They are described as hard discs, which move through a two-dimensional plane containing obstacles. The coordinates of the disc's centres are given through

$$\mathbf{q} = (\mathbf{q}_1, \mathbf{q}_2, ..., \mathbf{q}_N) \in \mathbb{R}^{2N}, \tag{2.48}$$

their radii are $r_1, r_2, ..., r_n$. In this approach we consider two velocities: The desired and the actual velocity. A person would move with the desired velocity if he was alone. It is calculated individually: Each person tries to move as fast as possible to the exit. On the other hand one has to take into account that the pedestrians are not allowed to superpose

each other or to go through obstacles. Hence the actual velocity is the Euclidian projection from the desired velocity on the admitted velocities. To simplify the notations, we present here only the first type of constraint, because the constraints near obstacles can be treated similarly. The space of the admitted distributions is given as

$$Q_0 = \left\{ \mathbf{q} \in \mathbb{R}^{2N}, \quad \forall i, j \quad i \neq j \quad D_{ij}(\mathbf{q}) = |\mathbf{q}_i - \mathbf{q}_j| - r_i - r_j \geq 0 \right\}. \tag{2.49}$$

Desired Velocity

First of all, Maury *et al.* describe the desired velocity of an arbitrary person. The velocity depends basically upon the persons position. Hence they define for all points M of the space considered the desired velocity $\mathbf{U}_0(M)$, with which a person at this point would move to the exit if he was alone. The desired velocity is also a function of the geometry of space. A person moving with this velocity tries to minimize the distance to the exit. The choice of the velocity is not unique. One can get a reasonable set of data for the desired velocities if one considers the maximal velocity of a person and computes for all points in the space the shortest route from this point to a point outside. We assume the same behaviour for all pedestrians. Therefore the vector with the desired velocities for N pedestrians reads

$$\mathbf{U}(\mathbf{q}) = (\mathbf{U}_0(\mathbf{q}_1), ..., \mathbf{U}_0(\mathbf{q}_N)). \tag{2.50}$$

We do not consider the case that the desired velocity of a person depends on the surrounding pedestrians.

Remark 1: *The above model allows easy integration of improved dynamics: One can improve the desired velocities with regard to each person behaving differently, or having different maximum speeds. In this case the vector of the desired velocities reads* $\mathbf{U}(\mathbf{q}) = (\mathbf{U}_1(\mathbf{q}_1), ..., \mathbf{U}_N(\mathbf{q}_N))$. $\mathbf{U}_i$ *can differ in value and direction.*

This problem is well posed under the condition that $\mathbf{U}$ is Lipschitz-continuous in ratio to $\mathbf{q}$. It has to be mentioned that for real life scenarios, space is not simply connected any more. Thus the Lipschitz-character of $\mathbf{U}$ can not be preserved.

Actual Velocity

To avoid superposition of the discs, the actual velocity $\mathbf{u}$ is supposed to belong to the cone of the admitted velocities $C_{\mathbf{q}}$:

$$C_{\mathbf{q}} = \left\{ \mathbf{v} \in \mathbb{R}^{2N}, \quad D_{ij}(\mathbf{q}) = 0 \quad \Rightarrow \quad \mathbf{G}_{ij}(\mathbf{q}) \cdot \mathbf{v} \geq 0 \quad \forall i < j \right\}, \tag{2.51}$$

where

$$\mathbf{G}_{ij}(\mathbf{q}) = \nabla D_{ij}(\mathbf{q}) = (0, ..., 0, -\mathbf{e}_{ij}(\mathbf{q}), 0, ..., 0, \mathbf{e}_{ij}, 0, ..., 0),$$

and

$$\mathbf{e}_{ij}(\mathbf{q}) = \frac{\mathbf{q}_j - \mathbf{q}_i}{|\mathbf{q}_j - \mathbf{q}_i|}$$

is the normalized vector pointing from pedestrian i to j. If two pedestrians touch each other, the effective velocity increases the distance between them. In this model, the actual velocity $\mathbf{u}$ is defined as the Euclidian projection from the desired velocity $\mathbf{U}$ on all admitted velocities $C_{\mathbf{q}}$. The model finally reads

$$\begin{cases} \mathbf{q} = \mathbf{q}_0 + \int \mathbf{u} \\ \mathbf{u} = P_{C_\mathbf{q}} \mathbf{U}. \end{cases} \tag{2.52}$$

Here, $\mathbf{U}$ is the set of data for the desired velocities, and $C_\mathbf{q}$ is defined in (2.51). The study of this model is based on another formulation of (2.52), which is investigated in the next section.

2.8.2 Another Formulation of the Model

The polar cone of $C_\mathbf{q}$ is:

$$N_\mathbf{q} = C_\mathbf{q}^0 = \left\{ \mathbf{w} \in \mathbb{R}^{2N}, \quad \forall \mathbf{v} \in C_\mathbf{q} \quad \mathbf{v} \cdot \mathbf{w} \leq 0 \right\}. \tag{2.53}$$

Applying Farkas' Lemma to the vectors in $N_\mathbf{q}$, one obtains [19]:

Proposition 1:

$$N_\mathbf{q} = \left\{ -\sum \mu_{ij} \mathbf{G}_{ij}(\mathbf{q}), \quad \mu_{ij} \geq 0, \quad \mu_{ij} = 0 \quad \text{if} \quad D_{ij}(\mathbf{q}) > 0 \right\}.$$

Proposition 2:

$$P_{C_\mathbf{q}} + P_{N_\mathbf{q}} = \mathrm{Id}.$$

This basic feature, based on the decomposition of a Hilbert space into the sum of two polar cones, is investigated in [19]. We apply it to our model:

$$\mathbf{u} = P_{C_\mathbf{q}} \mathbf{U}. \tag{2.54}$$

Replacing $P_{C_\mathbf{q}}$ by $\mathrm{Id} - P_{N_\mathbf{q}}$ leads to

$$\mathbf{u} + P_{N_\mathbf{q}} \mathbf{U} = \mathbf{U}.$$

Consequently, $t \mapsto \mathbf{q}(t)$ verifies

$$\dot{\mathbf{q}} + N_\mathbf{q} \ni \mathbf{U}(\mathbf{q}). \tag{2.55}$$

This formulation characterizes the trajectory $\mathbf{q}$ in the case in which one is interested in.

2.8.3 Theoretical Results

We present the theoretical results obtained from the above model here only briefly.

The monotone Case

We consider pedestrians moving straight through a narrow corridor. As a consequence,

$$Q_0 = \left\{ \mathbf{q} \in \mathbb{R}^N, \quad \mathbf{q}_{i+1} - \mathbf{q}_i \geq r_{i+1} + r_i \right\}.$$

Pedestrian's order is preserved because superposition is not allowed. Thus the ensemble of admitted distributions Q_0 is convex. We note

$$N_{\mathbf{q}} = \partial I_{Q_0}(\mathbf{q}), \tag{2.56}$$

where $\partial I_{Q_0}(\mathbf{q})$ denotes the subdifferential of Q_0. Therefor $\mathbf{q} \mapsto N_{\mathbf{q}}$ is maximal monotone [19]. Now one is able to apply the results of the theory for maximal monotone operators under the condition that $\mathbf{U}$ is Lipschitz-continuous, and one finally obtains the existence and uniqueness for the problem (2.55) with initial condition $\mathbf{q}(0) = \mathbf{q}_0 \in Q_0$.

Remark 2: *If one applies the results of the theory for maximal monotone operators, it is possible to show that in the above case a solution of* (2.55) *is also a solution of* (2.52)

If one regards a single person in a convex space, one obtains analogous results.

The general Case

We consider various persons moving through an arbitrary space. Q_0 is not convex any longer. One can prove that $\mathbf{q} \mapsto N_{\mathbf{q}}$ is not maximal monotone any longer, thus we can not apply the above procedure any more. $\mathbf{q}$ evolves arbitrarily in Q_0. Accordingly, we have to consider a sweeping process. Using the results of Moreau, one can prove that Q_0 is η-prox-ordered [19]. This means that there exists a real $\eta > 0$, and for all points $\tilde{\mathbf{q}}$ with distance $d < \eta$ in Q_0, the projection from $\tilde{\mathbf{q}}$ on Q_0 is well defined. With the results of Thibault and Edmond we finally obtain the following theorem (for details, see [19]):

Theorem 1: *Suppose* $\boldsymbol{q} \mapsto \boldsymbol{U}(\boldsymbol{q})$ *is Lipschitz-continuous. For all* $T > 0$, $\boldsymbol{q}_0 \in Q_0$, *there exists a unique solution* $\mathbf{q} \in W^{1,1}(0, T; Q_0)$ *of*

$$\begin{cases} \frac{d\mathbf{q}}{dt} + N_{\mathbf{q}} \ni \mathbf{U}(\mathbf{q}), \\ \mathbf{q}(0) = \mathbf{q}_0. \end{cases} \tag{2.57}$$

Remark 3: *The constant* η *depends in our case on the number of persons* N *and the radii of their discs.*

2.8.4 Numerical Method

Maury *et al.* propose following numerical procedure: Let $0 = t_0 < t_1 < ... < t_p = T$ be a uniform subdivision of the interval $[0, T]$ with $h = t_{n+1} - t_n$. $\mathbf{q}^n$ denotes the approximation of $\mathbf{q}(t_n)$, and $\mathbf{u}^n$ denotes the approximation of $\mathbf{u}(t_n)$. If $\mathbf{q}^n$ is known, one can compute $\mathbf{q}^{n+i}$ for $i > 0$ in using an explicit Euler method. It remains to determine the actual velocity $\mathbf{u}^n$ via the desired velocity $\mathbf{U}(\mathbf{q}^n)$. Still, the first one is the projection of the second one on the admitted velocities.

$$\begin{aligned} \text{Start}: \quad & \mathbf{q}^0 = \mathbf{q}_0 \\ \text{Iteration}: \quad & \mathbf{q}^n \quad \text{known} \\ & \mathbf{u}^n = P_{C_h(\mathbf{q}^n)}(\mathbf{U}(\mathbf{q}^n)) \\ & \text{with} \quad C_h(\mathbf{q}^n) = \left\{ \mathbf{v} \in \mathbb{R}^{2N}, \quad D_{ij}(\mathbf{q}^n) + h\mathbf{G}_{ij}(\mathbf{q}^n) \cdot \mathbf{v} \geq 0 \quad \forall i < j \right\} \\ & \mathbf{q}^{n+1} = \mathbf{q}^n + h\mathbf{u}^n \end{aligned}$$

One can show that this method works for the admitted distributions.

Proposition 3: *For all n and all $i \neq j$: $D_{ij}(\mathbf{q}^n) \geq 0$.*

Remark 4: *The actual velocity $\mathbf{u}^n$ is obtained as the orthogonal projection from $\mathbf{U}(\mathbf{q})$ on a closed convex set which contains 0. Thus the norms l^2 in $\mathbb{R}^{2N}$ satisfy $|\mathbf{u}^n| \leq |\mathbf{U}(\mathbf{q}^n)|$. It has to be mentioned that the maximum modulus principle does not hold any longer. Futhermore, a special numerical effect can occur: Some persons may move with a velocity that is larger than their desired velocity, even if the desired velocity is constant.*

2.8.5 Approximative Calculation of the effective Velocity

In this section, we specify the numerical method to calculate $\mathbf{u}^n$, according to [19]. To simplify the notations, we neglect the time-reference (the exponent n). The actual velocity $\mathbf{u}$ is the solution of a minimimazion problem under condition: $\min_{\mathbf{v}\in C_h(\mathbf{q})} |\mathbf{v} - \mathbf{U}(\mathbf{q})|^2$. The Lagrange function of this problem reads:

$$L(\mathbf{v}, \lambda) = \frac{1}{2} |\mathbf{v} - \mathbf{U}(\mathbf{q})|^2 - \sum_{1\leq i<j\leq N} \lambda_{ij}(D_{ij}(\mathbf{q}) + h\mathbf{G}_{ij}(\mathbf{q}) \cdot \mathbf{v}). \tag{2.58}$$

The existence of a critical point $(\mathbf{u}, \lambda)$ follows directly [19]. One obtains the relation:

$$\mathbf{u} = \mathbf{U}(\mathbf{q}) + h \sum_{1\leq i<j\leq N} \lambda_{ij}\mathbf{G}_{ij}(\mathbf{q}). \tag{2.59}$$

We define the linear maps:

$$\begin{array}{rccc} \Phi: & \mathbb{R}^{2N} & \to & \mathbb{R}^{\frac{N(N-1)}{2}} \\ & \mathbf{v} & \mapsto & -h(\mathbf{G}_{ij}(\mathbf{q}) \cdot \mathbf{v})_{i<j} \end{array} \tag{2.60}$$

$$\begin{array}{rccc} \Phi^*: & \mathbb{R}^{2N} & \to & \mathbb{R}^{2N} \\ & \lambda & \mapsto & -h\sum_{i<j} \lambda_{ij}\mathbf{G}_{ij}(\mathbf{q}). \end{array} \tag{2.61}$$

Now we can rewrite $C_h(\mathbf{q})$:

$$\begin{aligned} C_h(\mathbf{q}) &= \left\{ \mathbf{v} \in \mathbb{R}^{2N}, \quad \forall \lambda \in (\mathbb{R}^+)^{\frac{N(N-1)}{2}}, - \sum_{1\leq i<j\leq N} \lambda_{ij}(D_{ij}(\mathbf{q}) + h\mathbf{G}_{ij}(\mathbf{q}) \cdot \mathbf{v}) \leq 0 \right\} \\ &= \left\{ \mathbf{v} \in \mathbb{R}^{2N}, \quad \forall \lambda \in (\mathbb{R}^+)^{\frac{N(N-1)}{2}}, \quad \langle \lambda, \Phi(\mathbf{v}) - \mathbf{D}(\mathbf{q}) \rangle \leq 0 \right\} \end{aligned}$$

Maury *et al.* use the algorithm of Uzawa to determine $\mathbf{u}$:

$$\begin{aligned} \mu^0 &= 0 \\ \mathbf{v}^{k+1} &= \mathbf{U}(\mathbf{q}) - \Phi^*(\mu^{\mathbf{k}}) \\ \mu^{k+1} &= \Pi_+ \left(\mu^k + \rho \left[\Phi(\mathbf{v}^{k+1}) - \mathbf{D}(\mathbf{q}) \right] \right). \end{aligned} \tag{2.62}$$

Here, ρ is a constant, $\rho \geq 0$, and Π_+ is the orthogonal projection on $(\mathbb{R}^+)^{\frac{N(N-1)}{2}}$:

$$\mu \mapsto \Pi_+(\mu) = (\max(0, \mu_{ij}))_{i<j}. \tag{2.63}$$

This algorithm converges for $0 < \rho < \rho_{max} = 2/\left\|\Phi\right\|^2$ [19]. For the simulations, Maury *et al.* determined to hold on if the relative superposition is found below than a certain threshold.

Remark 5: *Although there always exists a Lagrange mulitiplier for this problem in finite dimension, uniqueness is not in general guaranteed. Accordingly the disposition of a sufficient large crowd of pedestrians is not unique. Besides, Φ^* is not in general injective. As a consequence, the set*

$$\Lambda = \left\{ \lambda \in (\mathbb{R}^+)^{\frac{N(N-1)}{N}}, \quad \mathbf{w} = \sum_{i<j} \lambda_{ij} \mathbf{G}_{ij}(\mathbf{q}) \right\}$$

is not in general a singleton. However, one can show that this set, which denotes the number of contacts between pedestrians, is limited.

Remark 6: *The number of contacts is clearly less than $\frac{N(N-1)}{2}$. In the case that all radii equal r, every disc has contact to six other disks. Thus the number of contacts is less than $3N$. As for the simulation, we consider constraints only for two nearby persons.*

2.8.6 Conclusions

This model is based on a completly different approach than the models above, namely on the Lagrange formalism. Maury *et al.* showed existence and uniqueness of a solution under reasonable assumptiones. Futhermore, they presented a numerical method. They simulated pedestrians leaving a train as well as pedestrians escaping from a room with two velocities. Running the simulations, they archieved good results in an equitable time.

2.9 Model based on Continuum Dynamics

We present a model for pedestrian flow that was literally used for traffic, according to [6]. Colombo *et al.* present a model for the flow of pedestrians which is able to describe typical features due to panic, in particular the possible overcompression in a crowd and the fall in the outflow through a door of a panicking crowd.

We start with the classical macroscopic Lighthill-Whitam and Richards model. The model reads

$$\partial_t \rho + \partial_x q(\rho) = 0. \tag{2.64}$$

Here, $\rho \in [0, R]$ denotes pedestrian's density. R denotes the maximal density. The flow function reads $\rho \mapsto q(\rho) = \rho v(\rho)$ with $v = v(\rho)$ being pedestrian's speed. The model is a consequence of only two assumptions:

- Conservation: the total number of pedestrians is constant,
- Speed law: v is a function of ρ.

A well known property of scalar conservation is the 'maximum principle':

If the initial distribution ρ_0 satisfies the bounds $\rho_0(x) \in [\rho_{min}, \rho_{max}]$ for all $x \in \mathbb{R}$, then the corresponding solution satisfies the same bounds for all times, i.e. $\rho(t,x) \in [\rho_{min}, \rho_{max}]$ for all $t \geq 0$ and $x \in \mathbb{R}$.

The maximum principle is a problem for the modelling of pedestrian flow because it prevents the increase of the initial maximal density. This is in contrast to the realistic description of panic, where a sort of 'overcompression' is found. The model we present in the following does not enjoy the maximum principle. The rise of panic depends essentially on the assumptions on the initial situation: the door needs to be 'small', the amount of people needs to be 'large' and the area covered by people is 'large' with respect to the distance of the people from the door.

Colombo *et al.* investigated only the 1D case, due to the mathematical theory used is based on non-clasical shocks, whose theory is essentially investigated in 1D only.

2.9.1 The Model

The model below is still based on conservation and speed law of the Lighthill-Whitam and Richards model. However, Colombo *et al.* modified speed law and the definition of a solution. They introduced a further characteristic density R^*, the maximal density in exceptional situations (panics). The speed law v is chosen so that the density flow diagram looks as in Figure 2.6.

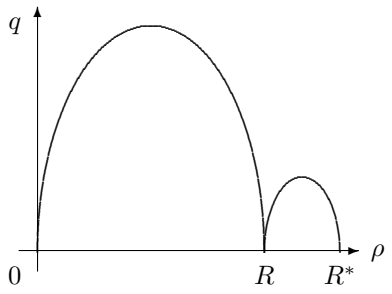

Figure 2.6: Possible flow function

Under normal circumstances, ρ varies in $[0, R]$. In panic situations, caused for instance by a sharp increase in the density, ρ enters the interval $[R, R^*]$. We introduce the following assumptions on the flow q [6]:

$q : [0, R^*] \mapsto [0, \infty]$ is smooth $\left(\in \mathbb{C}^0\left([0, R^*]\right) \cap \mathbb{C}^2\left([0, R^*] \setminus \{R\}\right)\right)$ and

- $q(\rho) = 0$ iff $\rho \in \{0, R, R^*\}$.
- q' is bounded on $[0, R^*]$. q' vanishes at a single point R_M in $]0, R[$. Similarly, q' vanishes at a single point R_M^* in $]R, R^*[$.
- q has at most one inflection point R_I in $]R_M, R[$ and at most another one, R_I^*, in $]R, R_M^*[$ and no other inflection points.

It is possible to consider the case in which q' is not defined at R. Therefore one has to assume that $q \in \mathbb{C}^2$. The case in which $q(R)$ is positive but very small can be recovered through a

merely technical extension. It is also possible to cover the case in which further inflection points exist. The boundedness of q' is required to ensure that information propagates with finite speed.

The mere introducion in the Lighthill-Whitam and Richards model of a fundamental diagram as in Figure 2.6 does not bypass the maximum principle. Hence Colombo *et al.* adopt non-classical solutions to scalar conservation laws. A solution to (2.64) can be constructed by means of solutions to Riemann problems. A Riemann problem is the following particular initial value problem:

$$\begin{cases} \partial_t \rho + \partial_x q(\rho) = 0 \\ \rho(0,x) = \begin{cases} \rho^l & \text{if } x < 0 \\ \rho^r & \text{if } x > 0. \end{cases} \end{cases} \tag{2.65}$$

By classical solutions to (2.65), we mean those defined in [18]. On the other hand, non-classical solutions satisfy (2.64) in its weak or integral form, but they may violate other usual admissibility conditions found in literature. A non-classical shock is a discontinuity that satisfies the Rankine-Hugoniot conditions, but not necessarily also Liu's entropy condition [18].

Colombo *et al.* proved the following results:

$q : [0, R^*] \mapsto [0, \infty[$ satisfies the above assumptions. The functions Φ and Ψ are defined in [6], as well as $\mathcal{C}$ and $\mathcal{N}$, subsets of the square $[0, R^*]^2$. Choose thresholds s and Δs such that

$$s \in]0, R_M[\text{ and } \Delta s \in]0, R - s[$$

Then there exists a unique Riemann solver $\mathcal{R} : [0, R^*]^2 \mapsto \mathbf{BV}(\mathbb{R})$ [6], satisfying

- If $\rho^l, \rho^r \in [0, R]$, then $\mathcal{R}(\rho^l, \rho^r)$ selects the classical solution unless

  $$\rho^l \geq s, \quad \rho^r > \Phi(\rho^l) \quad \text{and} \quad \rho^r - \rho^l > \Delta s.$$

  In this case, $\mathcal{R}(\rho^l, \rho^r)$ consists of a non-classical shock between ρ^l and $\Psi(\rho^l)$, followed by the classical solution of the Riemann problem with states $\Psi(\rho^l)$ and ρ^r.

- If $\rho^r < \rho^l$, then $\mathcal{R}(\rho^l, \rho^r)$ is the classical solution.

- If $\rho^l > R$ and $\rho^r > \rho^l$, then $\mathcal{R}(\rho^l, \rho^r)$ consists of a non-classical shock between ρ^l and a panic state followed by, possibly null, classical waves. More precisely,
  $\rho^r \in]R, \Psi(\rho^l)] : \mathcal{R}(\rho^l, \rho^r)$ consists of a non-classical shock between ρ^l and $\Psi(\rho^l)$, followed by classical waves;
  $\rho^r \in [\Psi(\rho^l), R^*[: \mathcal{R}(\rho^l, \rho^r)$ consists of a single shock.

Moreover,

- $\mathcal{R}$ is L^1_{loc}-continuous in $\mathcal{C}^\circ$, in $\mathcal{N}^\circ$ and also along the segment $\rho^l = \rho^r$ for $\rho^l \in]R, R^*]$.

- $\mathcal{R}$ is consistent in $\mathcal{C}^\circ$ and, separately, in $\mathcal{N}^\circ$.

The physical interpretation is as follows:

- Fix $\rho^l, \rho^r \in [0, R]$. If ρ^l is 'very low', i.e. below s, panic does not arise, independent from $\rho^r \in [0, R]$. If $\rho^r - \rho^l$ is 'very low', i.e. $\rho^r - \rho^l < \Delta s$, pedestrians are ready to stand the increase in the density without panicking. On the contrary, if pedestrian's density

is above the first threshold s and ρ^r is also 'high', then a 'sufficiently high'(above Δs) density increase causes panic, leading to the formation of a pedestrian jam, i.e. of an area where the density is greater than the usual maximum R. The higher ρ^l, the easier is the transition from ρ^l to a panic state.

- When pedestrians face a density lower than the one they are in, panic does not arise.

For more detail, we refer to [6].

2.9.2 Conclusions

Colombo *et al.* investigated pedestrian flow based on a traffic model. After having made some necessary assumptions, they could apply the model for cars to pedestrians. The model describes typical features due to panic. A disadvantage is that the model is bound in $\mathbf{BV}(\mathbb{R})$ and the lack of continuous dependence. As the model describes the one-dimensional case, it can be applied only if the evacuation route guides through a corridor, like the 1D social force model.

2.10 Model for Crowds

We present a model used for simulating large crowds with common goals, according to [15] and [27]. The model is a real time model based on continuum crowds. The problem which arises at simulating crowds of thousands of individuals at real time is the enormous computational effort. Therefore we do not consider an agent based model, but a continuum system. Motion is treated similarly to energy minimization. This formulation yields dynamic potential fields and velocity fields over the domain which guide all individual motion simultaneously. This approach unifies global path plannig and local collision avoidance into a single optimization framework.

It has to be noted that global path planning is often an unrealistic assumpion, due to limited vision and partial knowledge of the terrain. Global knowledge is only an approximation to more accurate long-term planning. The global planning assumption produces smoother and more realistic crowd motion than the assumption of strictly local knowledge. Furthermore we assume that smaller persons take their direction from taller ones, who have an overall view about the situation [15].

2.10.1 The Model

The model presented here is based on the fact that the total number of pedestrian is constant [15]. This approach is similar to the one introduced in Section 2.9. The latter was only investigated in the one dimensional case, here we consider the two dimensional case:

$$\frac{\partial \rho}{\partial t} + \frac{\partial}{\partial x}(\rho u) + \frac{\partial}{\partial y}(\rho v) = 0. \tag{2.66}$$

As before, ρ denotes pedestrian's density, u and v are the components of the velocity, x and y are the components of the location. Our next step is to formulate observations about crowd flow in precise hypotheses [27].

The essential assumption is that people have a destination or goal. Treuville *et al.* do not consider crowds which have no definable goal, such as people wandering through a mall. Goals can be specific (e.g. go to west side of town) or dynamic (e.g. explore unseen parts of the environment).

Hypothesis 1: Each person is trying to reach a geographic goal $G \subseteq \mathbb{R}^2$.

Pedestrians move at maximum speed possible given enviromental conditions, e.g. pedestrians going downhill increase their speed, walls are impassable, pedestrians cannot intersect.

Hypothesis 2: Pedestrians move at the maximum speed possible. This can be expressed as a maximum speed field f such that a person at location $\mathbf{x}$ moving in direction θ has velocity

$$\dot{\mathbf{x}} = f(\mathbf{x}, \theta)\mathbf{n}_\theta. \tag{2.67}$$

$\mathbf{n}_\theta = [\cos\theta, \sin\theta]^T$ denotes the unit vector pointing in direction θ.

Pedestrians have preferences for certain paths even without obstacles, e.g. they do not walk across the street until they reach a croswalk.

Hypothesis 3: There exists a discomfort field g. All things being equal, people would prefer to be at point $\mathbf{x}$ rather than $\mathbf{x}'$ if $g(\mathbf{x}') > g(\mathbf{x})$.

Whenever pedestrians choose paths, they choose the minimum distance path to their destination in general, but they also try to avoid congestion, time consuming situations and areas of high discomfort.

Hypothesis 4: Let Π be the set of all paths from $\mathbf{x}$ to some point in the goal. We assume the speed field f, discomfort g and goal G to be fixed. A person at location $\mathbf{x}$ will then pick the path $P^* \in \Pi$ minimizing

$$P^* = \min_{P\in\Pi} \underbrace{\alpha \int_P ds}_{\text{Path Length}} + \underbrace{\beta \int_P dt}_{\text{Time}} + \underbrace{\gamma \int_P g dt}_{\text{Discomfort}}. \tag{2.68}$$

Here, α, β and γ are weighted individually. ds means the integral is taken with respect to path length, dt means the integral is taken with respect to time. We use $ds = f dt$, f being the speed, and obtain

$$P^* = \min_{P\in\Pi} \alpha \int_P ds + \beta \int_P \frac{1}{f} ds + \gamma \int_p \frac{g}{f} ds. \tag{2.69}$$

We define the unit cost field

$$C = \frac{\alpha f + \beta + \gamma g}{f},$$

which leads to

$$P^* = \min_{P\in\Pi} \int_P C ds. \tag{2.70}$$

2.10.2 Optimal Path Computation

We suppose that the function $\phi : \mathbb{R}^2 \to \mathbb{R}$ is everywhere equal to the cost of the optimal path to the goal. Every person wants to minimize the cost of the path. The optimal strategy for this purpose is to move opposite the gradient of ϕ. This will decrease the cost most rapidly. The potential function ϕ is defined in the following way: in the goal we assume $\phi = 0$, everywhere else ϕ satisfies the eikonal equation

$$\|\nabla\phi(\mathbf{x})\| = C. \tag{2.71}$$

The unit cost C is evaluated in the direction of the gradient $\nabla\phi$. All optimal paths follow exactly the gradient of this function [27]. Every person moves in the direction opposite the gradient with velocity

$$\dot{\mathbf{x}} = -f(\mathbf{x}, \theta)\frac{\nabla\phi(\mathbf{x})}{\|\nabla\phi(\mathbf{x})\|}, \tag{2.72}$$

where $f(\mathbf{x}, \theta)$ is evaluated in the direction of motion.

Solving (2.71) is the slowest aspect of simulation. Hence we want to do it as few as possible. Therefore Treuville *et al.* devide the crowd whose motion is described into a set of groups. We assume that all pedestrians belonging to one group share an identical speed field, discomfort and goal. This is often the case in crowds when groups of pedestrians try to get to the same location at approximately the same speed. Thus we need to calculate the potential function of each group only once and we can derive optimal paths for all group members simultaneously. At each time step we construct a potential function ϕ for each group and then move the pedestrians in that group according to (2.72). We prefer to have as few groups as possible.

2.10.3 Speed

The speed field f measures the maximum permissible speed of motion for every point and every direction in the domain. Speed is a density-dependent variable. At low densities, speed is dominated by the terrain: Speed remains constant on flat surfaces but changes with the slope. At higher densities, speed becomes dominated by the movement of nearby pedestrians. This velocity dependent term is crucial for modeling 'lane formation', an phenomenon mentioned beforehand.

We begin with describing the crowd density field ρ, according to [27]. The individual density field for pedestrian i is denoted by ρ_i. This field should peak at location of person i and fall off radially. In a bounding disc of radius r this field should be above a threshold value $\bar{\rho}$, and below outside. The crowd density ρ is the sum of each individual density field

$$\rho = \sum_i \rho_i. \tag{2.73}$$

The average velocity field $\bar{\mathbf{v}}$ is computed as

$$\bar{\mathbf{v}} = \frac{\sum_i \rho_i \dot{\mathbf{x}}_i}{\rho}, \tag{2.74}$$

where $\dot{\mathbf{x}}_i$ denotes the velocity of the pedestrian i.

In areas of low densities ($\rho < \rho_{min}$ for some ρ_{min}) speed is equal to the topological speed f_T. We assume that the terrain is bounded between minimum and maximum slope s_{min} and s_{max}. The speed varies inversely with the slope:

$$f_T(\mathbf{x},\theta) = f_{max} + \left(\frac{\nabla h(\mathbf{x})\cdot\mathbf{n}_\theta - s_{min}}{s_{max}-s_{min}}\right)(f_{min}-f_{max}), \tag{2.75}$$

where $\nabla h(\mathbf{x})\cdot\mathbf{n}_\theta$ is the slope of the height field h in direction θ.

The flow speed $f_{\bar{\mathbf{v}}}$ in areas of high densities ($\rho \geq \rho_{max}$ for some ρ_{max}) is modelled according to

$$f_{\bar{\mathbf{v}}}(\mathbf{x},\theta) = \bar{\mathbf{v}}(\mathbf{x}+r\mathbf{n}_\theta)\cdot\mathbf{n}_\theta. \tag{2.76}$$

Flow speed is essentially the average velocity $\bar{\mathbf{v}}$ evaluated at a distance r from location $\mathbf{x}$. The offset has the effect that pedestrians evaluate the average velocity for the area into which they move in. Flow speed is non negative because pedestrians do not go backwards.

At medium densities ($\rho_{min} < \rho < \rho_{max}$) we linearily interpolate

$$f(\mathbf{x},\theta) = f_T(\mathbf{x},\theta) + \left(\frac{\rho(\mathbf{x}+r\mathbf{n}_\theta)-\rho_{min}}{\rho_{max}-\rho_{min}}\right)(f_{\bar{\mathbf{v}}}(\mathbf{x},\theta) - f_T(\mathbf{x},\theta)). \tag{2.77}$$

Density is evaluated at an offset for the same reason mentioned beforehand.

2.10.4 Minimum Distance Enforcement

The above model ensures in theory that two persons do not intersect. If they approach each other, they experience a so high density that their speed towards another will drop to zero. In practice however, this holds only to the resolution of the grid. Two pedestrians in the same cell may intersect. For this reason a pair-wise minimum distance between pedestrians in enforced. People are pushed apart so that a minimum distance holds [27].

2.10.5 Implementation

The simulation of the model can be carried out in real-time. For details for the implementation we refer to [27] and [32].

2.10.6 Conclusions

Treuille *et al.* presented a real time model for crowds of thousands of people. The model is based on continuum dynamics. Inspite of simplifying assumptions, it reproduces observed phenomena such as lane formation. The model could be further improved by taking into account two important aspects:

First of all *predictive discomfort*: Individuals already take into account moving obstacles, but not that the obstacles are moving. More intelligent pedestrians would take into account the expectd motion of the obstacles while computing their path.

Secondly, *expected periodic field changes*: pedestrians approaching a red traffic light experience a zero speed field. They would conclude that crossing is impossible and therefore pick another path. The expected speed should take into account the percentage of time of the taffic light beeing green. We note that this algorithm has been licensed for use in next generartion games. The model is attractive due to natural crowd behaviour, real time simulations, and integration of autonomous agents.

Chapter 3

1D Movement

In this chapter we focus on the 1D movement. We are interested in the relation between density and velocity for the single-file movement. We begin with an experimental setup investigated by Seyfried *et al.* and the results. The model used for this setup has been introduced in Sec.2.2. Afterwards we will make some extensions.

3.1 Experimental Setup

The experiental setup took place as follows: Test persons were walking through a corridor. The corridor was built up with chairs and ropes [25]. The width of the corridor in the measurement section was 0.8m. Passing was prevented and single-file movement was enforced. The corridor's shape was made up of two half-circles and two straight segments, which assured periodic boundary conditions. Furthermore it was broadened in the curve to reduce the effects of the curves in the measurement. The measured section was positioned in the center of the straight part of the corridor. The length of the measured section was 2m, the length of the whole corridor was 17.3m. The test persons were told not to overtake and not to hurry. This resulted in rather low free velocities. One is interested in different densities, therfore six cycles with N=1,15,20,25,30,34 test persons in the corridor were executed. For the cycle with N=1 every person passed alone through the corridor. For the other cycles the persons were distributed uniformly in the corridor. After the instruction get going, every person passed the corridor two or three times. At the end, the corridor was opened so that the persons could get out.

3.1.1 Measurement Setup

For every person i Seyfried *et al.* [25] collected the entrance time t_i^{in} (of the ear) in the measurement section and the exit time t_i^{out}. These two times allow calculation of individual velocities $v_i^{man} = l_m/(t_i^{out} - t_i^{in})$ and momentary number $n(t)$ of pedestrians at time t in the measured section. The definition of a momentary 'density' is problematic due to the small number of persons involved. $\tilde{\rho}^{man}(t) = n(t)/l_m$ jumps between discrete values. For a better definition, Seyfried *et al.* choose $\rho^{man}(t) = \sum_{i=1}^{N} \Theta_i(t)/l_m$, where $\Theta_i(t)$ denotes the 'fraction' with which person i is inside:

$$\Theta_i(t) = \begin{cases} \frac{t-t_i^{in}}{t_{i-1}^{in}-t_i^{in}} & : t \in \left[t_i^{in}, t_{i-1}^{in}\right] \\ 1 & : t \in \left[t_{i-1}^{in}, t_i^{out}\right] \\ \frac{t_{i-1}^{out}-t}{t_{i-1}^{out}-t_i^{out}} & : t \in \left[t_i^{out}, t_{i-1}^{out}\right] \\ 0 & : \text{otherwise.} \end{cases} \tag{3.1}$$

Crossing of an individual person with velocity v_i^{man} is regarded as a statistical event. This event is associated to the density ρ_i^{man}, mean value of density during the time slice $\left[t_i^{in}, t_i^{out}\right]$. For N=1, Seyfried *et al.* got a mean value of v_{free}^{man}=1.24m/s ($\pm$ 0.15m/s). The deviation of the literature value 1.34m/s according to Weidmann can be explained by the instruction to the test persons not to hurry.

3.1.2 Empirical Results

To compare the relation between velocity and density of the single-file movement (1D) with the movement in a plane (2D), one has to transform the line-density to an area-density [25]:

$$\rho_{1D\to 2D} = \rho_{1D}^2 + C(\rho). \tag{3.2}$$

The correction term $C(\rho)$ arises due to the fact that the ordering of pedestrians in two dimensions does not occur in a square lattice. Seyfried *et al.* propose $C(\rho)$=0.7m^{-2} [25]. Comparison of the relation of velocity and density for the single-file movement with movement in a plane shows surprising conformity. The qualitative agreement indicates that properties of two-dimensional movement, like internal friction and other lateral interferences, have no strong influence on the fundamental diagram, at least in the density domains considered [25].

There are a couple of 'microscopic' properties that determine the velocity-density relation: At intermediate densities and velocities, the distance to the person in front is related to step length and to safety margin. Step length and safety margin are connected with velocity. At high densities and small velocities, groups pass over into marching in step. Furthermore, utilization of the availabe space is optimized: Some pedestrians set their feet far right and left of the line of movement. This generates some overlap in the space occupied with the pedestrian in front. At intermediate densities and relatively high velocities, pedestrians concentrate on their movement. This leads to fast reactions on the movement of the pedestrian in front. At smaller velocities this concentration is reduced and leads to delayed reactions.

In the following we focus on the correlation of the distance between pedestrians and velocity. The distance to the person in front is the sum of step length and safety margin. This distance is the required length d of one person to move with velocity v. In a one-dimensional system the harmonic average of this quantity is the inverse of the density: $d = 1/\rho$. Hence we investigate the relation between required length and velocity via the velocity-density relation.

Seyfried *et al.* found out that the best fit to the data is given by the function d=0.36+1.06v [25]. Moreover, the walking velocity has a lower bound of $v \approx$0.5m/s. The linearity for the sum of step length and safety margin holds even and persists for velocities smaller than 0.5m/s. Possible explanations are the marching in steps and optimized utilization of the available space.

3.2 Results

We presented the model results in Sec.2.2.4. Seyfried *et al.* found out that b=0.56s resulted in good agreement with the empirical data. With b=1.06s they found a difference between the velocity-density relation predicted by the model and the empirical fundamental diagram. This means that a model which reproduces the right macroscopic dependency between density and velocity does not necessarily describe correctly the microscopic situation. Futhermore, space requirement of a person at average speed is much less than average space requirement. The explanation is that pedestrians adapt their speed not only to the person immediately in front, but to the situation further ahead. This behaviour gives a much smoother movement than the model predicts.

3.3 Investigations of the Model

If one applies the model of Seyfried *et al.* for hard bodies with remote action, one is confronted with several problems. The equations of motion read:

$$\frac{dr_i}{dt} = v_i \tag{3.3}$$

$$\frac{dv_i}{dt} = \begin{cases} \tilde{G}_i(t) & \text{, if } v_i(t) > 0 \\ \max(0, \tilde{G}_i(t)) & \text{, if } v_i(t) \leq 0, \end{cases} \tag{3.4}$$

with

$$\tilde{G}_i(t) = \frac{v_i^0 - v_i(t)}{\tau_i} - e_i \left(\frac{1}{r_{i+1}(t) - r_i(t) - d_i(t)} \right)^{g_i}. \tag{3.5}$$

Again, $d_i(t) = a_i + b_i v_i(t)$, e_i and g_i are constants.

The first problem of Seyfried's model arises from the fact that velocities of pedestrians may become negative if they approach an obstacle or another person. If the situation in front relaxes, pedestrians start moving forward again. This behaviour is not realistic because in real life situations pedestrians do stop if they have to, but almost never go backwards. In a two dimensional model negative velocities can be avoided, because pedestrians are able to walk around obstacles, which is not possible in the one dimensional case. Anyhow we are not allowed to restrict the right hand side of (3.3) to a certain intervall, because this would violate the Newton axioms.

The second problem is that the right handside of (3.4) is not Lipschitz-continuous. This is problematic because we want to show existence and uniqueness for local solutions of this model.

We tried to find an improved model. First of all we analyzed $\tilde{G}_i$. We propose for the new acceleration force:

$$G_i(t) = \begin{cases} \frac{v_i^0 - v_i(t)}{\tau_i} - \frac{e_i}{m_i} \left(\frac{h}{r_{i+1}(t) - r_i(t) - d_i(t)} \right)^{g_i} & \text{, } r_{i+1} - r_i - d_i > 0 \\ -\infty & \text{, else.} \end{cases}$$

The distinction of cases ensures the right handling in case that the denominator equals zero (the distance between two pedestrians is exactly the safty distance required). The constant h is measured in meter, this excludes problems for different values of g_i. Furthermore, the mass m_i makes sure that G_i models an acceleration (e_i is a force).

Our first approach for another model was introducing a new function which adjusts the acceleration:

$$\frac{dv_i}{dt} = G_i(t) \cdot H(v_i(t)). \tag{3.6}$$

The function $H(v_i(t))$ should be Lipschitz-continuous and satisfy

$$H(v_i) = \begin{cases} 0 & \text{, if } v_i \leq 0 \\ 1 & \text{, if } v_i > \epsilon, \end{cases} \tag{3.7}$$

ϵ being small with respect to v_i. However, this approach did not improve the situation very much, because we are still confrontated with the problem of negative velocities. Furthermore we assume that the function H should also be dependent of the acceleration G_i. Thus we propose

$$\frac{dv_i}{dt} = G_i(t) \cdot H(v_i(t), G_i(t)), \tag{3.8}$$

$$H(v_i(t), G_i(t)) = \begin{cases} 0 & \text{, if } \quad v_i(t) \leq 0 \quad \text{and} \quad G_i \leq 0 \\ 1 & \text{, if } \quad v_i(t) \geq \epsilon, \\ 1 & \text{, if } \quad G_i(t) \geq \delta \end{cases}$$

with $\epsilon > 0$ being small with respect to v_i and $\delta > 0$ being small with respect to G_i. The function H describes pedestrian's motion as follows: If the situation in front of a person would lead to a negative acceleration conntected with a negative velocity, the acceleration becomes zero (first case). If the velocity is larger than a certain value, the person is allowed to move on (second case). On the other hand, if the acceleration is larger than a threshold, the person is allowed to move on as well (third case). We interpolate for $0 \leq v_i(t) \leq \epsilon$ and $0 \leq G_i(t) \leq \delta$. $H(v_i(t), G_i(t))$ should be Lipschitz-continuous with respect to v_i and G_i.

This model is up to the function $H(v_i(t), G_i(t))$ and changes in G_i similar to Seyfried's model. The main difference is the interpolation, which has the following effect: We regard the case that the velocity is positive and close to zero (smaller than ϵ), and the acceleration is negative (in fact a deceleration). Then the interpolation leads to a decreased deceleration. We assume that this decreased deceleration leads to non-negative velocities at all the times.

We simulated the above model with the following function

$$H(v_i(t), G_i(t)) = \begin{cases} 0 & \text{, if } \quad v_i(t) \leq 0 \quad \text{and} \quad G_i \leq 0 \\ 1 & \text{, if } \quad G_i(t) \geq \delta \\ 1 & \text{, if } \quad v_i(t) \geq \epsilon \\ v_i/\epsilon & \text{, if } \quad 0 < v_i(t) < \epsilon \quad \text{and} \quad G_i < \frac{\delta}{\epsilon} v_i(t) \\ G_i/\delta & \text{, if } \quad 0 < G_i(t) < \delta \quad \text{and} \quad v_i(t) < \frac{\epsilon}{\delta} G_i(t). \end{cases} \tag{3.9}$$

We note that $H(v_i(t), G_i(t))$ described in (3.9) is Lipschitz-continuous with respect to v_i and G_i (almost everywhere differentiable, and the first-order derivations are bounded).

We found out in our simulations that pedestrians did not go backwards if the time steps were sufficiently small (Δt=0.01s). This is on the one hand due to the decreased deceleration in case that the velocities are small. On the other hand, deceleration before an obstacle is a complicated process: Pedestrians start deceleration sufficiently long before they approach an obstacle. The more a person decelerates, the less becomes the velocity and the required safety margin. The above mentioned properties lead to non negative velocities at all the times.

We want to present another, completely different, approach. We split the acceleration into the parts less and larger than zero. The equation of motion reads

$$\frac{dv_i}{dt} = \Theta(v_i^0 - v_i)G_i^+ + \Theta(v_i)G_i^- . \tag{3.10}$$

Θ denotes the Heaviside function

$$\Theta(x) = \begin{cases} 0 & , \text{if } x \leq 0 \\ 1 & , \text{if } x > 0. \end{cases}$$

G_i^+ and G_i^- describe positive and negative parts of G_i:

$$G_i^+ = \max\{G_i, 0\} \qquad G_i^- = \min\{G_i, 0\} .$$

If the actual velocity v_i is larger than or equal to the desired velocity v_i^0, the first term of (3.10) is zero, this means for the acceleration $\frac{dv_i}{dt} \leq 0$. On the other hand, if v_i is less than or equal to zero, the second term of (3.10) is zero, this means $\frac{dv_i}{dt} \geq 0$. In the third case, $0 < v_i < v_i^0$, both parts of (3.10) are taken into account. We neglected this model as we found out the model described in (3.8) worked well.

Our next step was to show that a solution for model (3.8) exists and that this solution is unique.

Lemma 1: *Let $r_{i+1}(0) - r_i(0) > d_i(0) \quad \forall i$. Then the ODE-System*

$$\begin{pmatrix} \dot{r_1} \\ \dot{v_1} \\ \dot{r_2} \\ \dot{v_2} \\ \vdots \\ \dot{r_N} \\ \dot{v_N} \end{pmatrix} = \begin{pmatrix} v_1 \\ G_1(t) \cdot H(v_1(t), G_1(t)) \\ v_2 \\ G_2(t) \cdot H(v_2(t), G_2(t)) \\ \vdots \\ v_N \\ G_N(t) \cdot H(v_N(t), G_N(t)) \end{pmatrix} \Leftrightarrow \dot{\mathbf{y}} = \mathbf{f}(t, \mathbf{y}) \tag{3.11}$$

has a local solution. The solution is unique.

Remark: *Lemma 1 applies in particular for uniformly distributed initial values*

$$r_i(0) = \frac{i-1}{N} \qquad v_i(0) = 0 \quad \forall i.$$

Proof: We use the theorem of Picard-Lindelöf (cf. Satz 60.2 in [13]). It is obvious that $\mathbf{f}(t, \mathbf{y})$ is continuous because $H(v_i(t), G_i(t))$ and $G_i(t)$ are continuous. We have to show that $\mathbf{f}(t, \mathbf{y})$ is Lipschitz-continuous. It is adequate to show that every component of $\mathbf{f}$ is differentiable with respect to y_i, $i = 1, ..., N$, almost everywhere.
For i odd: $f_i = v_i$:

$$\frac{\partial f_i}{\partial r_j} = 0 \quad j \neq i \qquad \frac{\partial f_i}{\partial r_i} = 0 \tag{3.12}$$

$$\frac{\partial f_i}{\partial v_j} = 0 \quad j \neq i \qquad \frac{\partial f_i}{\partial v_i} = 1. \tag{3.13}$$

For i even: $f_i = H(v_i, G_i) \cdot \left(\frac{v_i^0 - v_i}{\tau_i} - \frac{e_i}{m_i} \left(\frac{h}{r_{i+1} - r_i - d_i} \right)^{g_i} \right)$:

$$\frac{\partial f_i}{\partial r_j} = 0 \quad j \neq i \quad j \neq i+1$$
$$\frac{\partial f_i}{\partial r_{i+1}} = H(v_i, G_i) \cdot \left(\frac{e_i g_i}{m_i} \left(\frac{-h}{r_{i+1} - r_i - d_i} \right)^{g_{i-1}} \right)$$
$$\frac{\partial f_i}{\partial r_i} = H(v_i, G_i) \cdot \left(\frac{e_i g_i}{m_i} \left(\frac{h}{r_{i+1} - r_i - d_i} \right)^{g_{i-1}} \right)$$
$$\frac{\partial f_i}{\partial v_j} = 0 \quad i \neq j$$
$$\frac{\partial f_i}{\partial v_i} = \frac{\partial H(v_i, G_i)}{\partial v_i} - \frac{1}{\tau_i} H(v_i, G_i)$$

Due to $H(v_i, G_i)$ being Lipschitz-continuous, all these derivations are bounded. Hence we can apply the theorem of Picard-Lindelöf and obtain local existence of a unique solution. ■

3.4 Implementation

We tested the above model as follows: We simulated a corridor with periodic boundaries of length 17m and distributed the pedestrians uniformly about the available space. We chose values presented in Table 3.1 ($d_i = a_i + b_i v_i$). We found time steps $\Delta t = 0.01$s sufficient.

Parameter	**Mean**	**Standard Derivation**
v_i^0 [m/s]	1.24	0.15
τ_i [s]	0.61	0.01
e_i [N]	0.51	0.01
m_i [kg]	70	5
h [m]	1	0
a_i[m]	0.36	0.01
b_i [s]	0.56	0.01
g_i	2	0

Table 3.1: Values for 1D Model

The solver we selected for our ODE-system is based on an explicit Runge-Kutta (4,5) formula. It is a one step solver, this means that for computing $y(t_n)$ only the the solution at an immediately preceeding time point $y(t_{n-1})$ is needed.

On the one hand we were interested in density waves. Hence we divided the corridor in $\sqrt{N}$ partitions (N being the number of pedestrians) and run the simulation several times. We plotted the average number of pedestrians in each partition, thus we were able to see the density waves.

On the other hand we wanted to reproduce the velocity-density diagram. Therefore we run the simulation for each N again several times and calculated the average velocities for corresponding density ($\rho = N/17$m). We obtained the velocity-density relation shown in Figure 3.1. The experimental data are presented in Appendix A. We note that the velocity is high in case that the density is low. The velocity decreases with increasing density. The

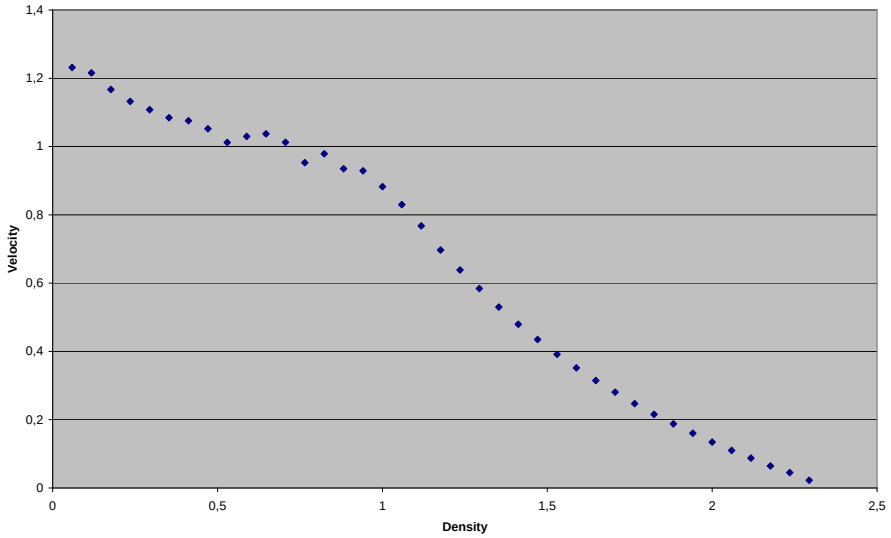

Figure 3.1: Velocity-Density Relation

high decay at densities of approximately 1/m arises due to the fact that the safety margin for velocities $v \approx 1.24$m/s is approximately 1m. At densities above 1/m pedestrians have to slow down considerably. The slight increase of velocities for densities below 1/m occures because we simulated Gaussian distributed velocities. Our results are consistent with the velocity-density diagrams found in literature (e.g. [25]).

3.5 Conclusions

In this section we presented Seyfried's experimental setup and results. We investigated his model and made some extensions. We found out that pedestrians did not go backwards in the extended model. We were able to prove existence and uniqueness for local solutions of the extended model.We showed how the density changes in time (density waves), and presented the velocity density diagram obtained from our implementation. Our results were in good agreement with the experimental data.

Chapter 4

Limiting Behaviour based on the BBGKY Approach

In this chapter we want to find an asymptotic continuum model when the number of pedestrians in the 1D model introduced above tends to infinity. Pedestrians correspond to particles. They interact via a force which is described by a potential. A lot work has been done for interacting particle systems (we refer to [26], [23], [5] and [20]). Diffenert forms of potentials for different scalings have been investigated (e.g. long- and short-ranged forces with weak respectively strong interactions). All approaches have in common that they investigate the case that each particle is influenced by every other particle, at least every particle within a certain radius [26], [20]. But our model approach is different: We consider the case that particle i is only influenced by particle $i+1$ in front. The potential is only dependent on the distance between particles $i+1$ and i, not on their positions.

The generalized equation of motion reads

$$\frac{dv_i}{dt} = \frac{v_i^0 - v_i}{\tau_i} + \frac{\alpha}{m} A'(\beta(x_{i+1} - x_i) - d_i), \tag{4.1}$$

where α and β specify the scaling of the potential. We assume all pedestrians to have equal masses. The safety distance d_i is assumed to be independent of the velocity. There are four cases that seem reasonable to be considered:

1. The case $\alpha = O(1)$ and $\beta = O(N)$
2. The case $\alpha = O(1)$ and $\beta = O(1)$
3. The cases $\alpha = O(1/N)$
4. The case $\alpha = O(N)$ and $\beta = O(N)$

The scaling with respect to the time is left open yet and will be performed in the next section.

4.1 Special Case: Deterministic Locations

We introduce an artificial variable s and start with the special case of deterministic distributed pedestrians in s. We introduce the continuous function:

$$u(s,t) = \Big\{ x_i(t) \quad s \in [\tfrac{i-1}{N}, \tfrac{i}{N}), \tag{4.2}$$

with $s \in [0,1]$. We proceed in the same way with v_i. Accordingly, we obtain for the acceleration

$$\frac{\partial v(s,t)}{\partial t} = \frac{dv_i(t)}{dt} = \frac{v_i^0 - v(s,t)}{\tau} - \frac{\alpha}{m} A'(\beta[u(s+\frac{1}{N},t) - u(s,t)] - d_i). \tag{4.3}$$

We introduce the distribution function for particles

$$F(x) = \frac{1}{N} \sum_{i=1}^{N} H(x - x_i),$$

where $H(x)$ denotes the Heaviside function. We identify u to be the inverse of the distribution function F, i.e.,

$$F(x) = u(x)^{-1}. \tag{4.4}$$

This means the following properties hold:

$$u\left(F(x,t),t\right) = x \tag{4.5}$$

and

$$F\left(u(s,t),t\right)) = s. \tag{4.6}$$

We set

$$V(x,t) = v(F(x,t),t). \tag{4.7}$$

Furthermore, the density is the derivative of the distribution function

$$\rho(x) = \frac{1}{N} \sum_{i=1}^{N} \delta(x - x_i) = \frac{\partial F(x)}{\partial x}. \tag{4.8}$$

Thus we obtain via the chain rule and $x = u(s,t)$

$$\rho(x,t) =: \rho(u(s,t)) = \frac{1}{\frac{\partial u(s,t)}{\partial s}}. \tag{4.9}$$

The derivative of (4.5) with respect to time yields

$$\frac{\partial u(s,t)}{\partial t} + \frac{\partial u(s,t)}{\partial s} \frac{\partial F(u(s,t),t)}{\partial t} = 0. \tag{4.10}$$

We obtain from (4.10) with all the above mentioned properties

$$V(x,t)\rho + \frac{\partial F(x,t)}{\partial t} = 0, \tag{4.11}$$

and after differentiation with respect to x we finally arrive at the continuity equation

$$\frac{\partial \rho(x,t)}{\partial t} + \frac{\partial}{\partial x}\left(V(x,t)\rho(x,t)\right) = 0. \tag{4.12}$$

Scaling with Respect to Time

We scaled the time t according to $t = \tilde{t}/\tau$. This ensures we regard a large time scale in the limit $\tau \to 0$. In the following we write t instead of $\tilde{t}$ again.

The derivation of (4.7) with respect to t taking into account $\frac{\partial u(s,t)}{\partial t} = V(x,t)$ yields (x is in the following a placeholder for $u(s,t)$)

$$\frac{\partial v(s,t)}{\partial t} = \frac{\partial V(x,t)}{\partial t} + \frac{\partial V(x,t)}{\partial x} V(x,t). \tag{4.13}$$

We inserted this into (4.3)

$$V(x,t) = v_i^0 - \tau \left(\frac{\partial V(x,t)}{\partial t} + \frac{\partial V(x,t)}{\partial x} V(x,t) + \frac{\alpha}{m} A' \left(\beta[u(s+\frac{1}{N},t) - u(s,t)] - d_i \right) \right)$$

Hence the potential A' is scaled according to $\frac{1}{\tau} A'$.

In the limit $\tau \to 0$ we obtain

$$V(u(s,t),t) = v_i^0 - \frac{\alpha}{m} A'(\beta[u(s+\frac{1}{N},t) - u(s,t)] - d_i).$$

4.1.1 Equation for V

The limiting equation for V is dependent on the scaling of A' with respect to the distance. We assume fluctuations in the individual values for pedestrians to be negligible

$$v_i^0 = v^0 + O(\frac{1}{N^\gamma}) \quad \text{and} \quad d_i = d + O(\frac{1}{N^\gamma}),$$

in particular

$$v_i^0 \overset{N\to\infty}{\longrightarrow} v^0 \quad \text{and} \quad d_i \overset{N\to\infty}{\longrightarrow} d \qquad \forall i.$$

We now further examine the different cases.

First Case ($\alpha = O(1)$, $\beta = O(N)$)

Without restriction of generality we choose α=1 and β=N

$$\beta[u(s+\frac{1}{N},t) - u(s,t)] = \frac{[u(s+\frac{1}{N},t) - u(s,t)]}{1/N} \overset{N\to\infty}{\longrightarrow} \frac{\partial u}{\partial s} = \frac{1}{\rho(u(s,t),t)} \tag{4.14}$$

We obtain in the limit $N \to \infty$

$$V(x,t) = v^0 - \frac{1}{m} A' \left(\frac{1}{\rho(x,t)} - d \right). \tag{4.15}$$

Second Case ($\alpha = O(1)$, $\beta = O(1)$) McKean-Vlasov Case

This case corresponds to the McKean-Vlasov case in literature (see [20]).

$$\beta[u(s+\frac{1}{N},t) - u(s,t)] = [u(s+\frac{1}{N},t) - u(s,t)] \overset{N\to\infty}{\longrightarrow} 0 \tag{4.16}$$

In this case we obtain in the limit $N \to \infty$

$$V(x,t) = v^0 - \frac{1}{m} A'(-d). \tag{4.17}$$

Third Case ($\alpha = O(1/N)$)

$$\begin{aligned} &\frac{\alpha}{m}A'(\beta[u(s+\frac{1}{N},t)-u(s,t)]-d(s)) = \\ &\frac{1}{Nm}A'(\beta[u(s+\frac{1}{N},t)-u(s,t)]-d(s)) \overset{N\to\infty}{\longrightarrow} 0 \end{aligned} \tag{4.18}$$

We obtain in the limit $N \to \infty$

$$V(x,t) = v^0. \tag{4.19}$$

Fourth Case ($\alpha = O(N)$, $\beta = O(N)$)

$$\beta[u(s+\frac{1}{N},t)-u(s,t)] = \frac{[u(s+\frac{1}{N},t)-u(s,t)]}{1/N} \overset{N\to\infty}{\longrightarrow} \frac{\partial u}{\partial s} = 1/\rho \tag{4.20}$$

We obtain in the limit $N \to \infty$

$$0 = \frac{1}{m}A'(1/\rho - d) \tag{4.21}$$

hence

$$V(x,t) = v^0. \tag{4.22}$$

This case is similar to the third case.

4.1.2 Conclusion

The formal asymptotics suggest that in the special case of deterministic locations all stochasic fluctuations disappear in the limit $N \to \infty$ and motion can be described by a deterministic equation, an analogon of the continuity equation

$$\frac{\partial \rho}{\partial t} + \frac{\partial}{\partial x}(V\rho) = 0. \tag{4.23}$$

The exact modes for V are given in (4.15), (4.17), and (4.19).

4.2 General Case

In this section we want to verify that the results received in the previous section hold indeed for all distributions. The equation of motion was

$$\frac{dv_i}{dt} = \frac{v_i^0 - v_i}{\tau} + \frac{\alpha}{\tau m}A'(\beta(x_{i+1}-x_i)-d_i). \tag{4.24}$$

The long-time limit $\tau \to 0$ leads to the first order ODE

$$\frac{dx_i}{dt} = v_i = v_i^0 - \frac{\alpha}{m}A'(\beta(x_{i+1}-x_i)-d_i). \tag{4.25}$$

We consider the particle distribution function $f^N = f^N(x_1, x_2, ..., x_N, t)$, which gives the probability density of finding at time t the first particle at x_1, the second particle at x_2, and so on. We know that the total number of pedestrians is constant, accordingly the one-dimensional transport equation holds (we use the notation ∂_x instead of $\frac{\partial}{\partial x}$)

$$\partial_t f^N + \sum_i \partial_{x_i} \left(\frac{dx_i}{dt} f^N \right) = 0, \tag{4.26}$$

in our case with (4.25)

$$\partial_t f^N + \sum_i \partial_{x_i} \left(\left[v_i^0 - \frac{\alpha}{m} A'(\beta(x_{i+1} - x_i) - d_i) \right] f^N \right) = 0. \tag{4.27}$$

We try to derive an analogon of what is called the BBGKY hiererchy in the classical kinetic theory (for reference, e.g. [2] and [3]). Therefore we define for $k = 1, ..., N$ the k-particle marginal

$$m_k^N(x_k, x_{k-1}, ..., x_1, t) = \int_{\mathbb{R}^{N-k}} f^N(x_1, x_2, ..., x_N, t) dx_{k+1} dx_{k+2} ... dx_N. \tag{4.28}$$

The k-particle marginal specifies the positions of the first k particles. To obtain an equation for the k-th particle marginal we integrate (4.27) with respect to $x_{k+1}, ...x_N$

$$\partial_t m_k^N + \sum_i \int_{\mathbb{R}^{N-k}} \partial_{x_i} \left(\left[v_i^0 - \frac{\alpha}{m} A'(\beta(x_{i+1} - x_i) - d_i) \right] f^N \right) dx_{k+1} dx_{k+2} ... dx_N = 0 \tag{4.29}$$

We split the sum in (4.29) into the parts with $i \leq k$ and $i > k$:

$$\begin{aligned} &\sum_{i \leq k} \int_{\mathbb{R}^{N-k}} \partial x_i \left(\left[v_i^0 - \frac{\alpha}{m} A'(\beta(x_{i+1} - x_i) - d_i) \right] f^N \right) dx_{k+1} dx_{k+2} ... dx_N = \\ &\sum_{i \leq k} \int_{\mathbb{R}} \partial x_i \left(\left[v_i^0 - \frac{\alpha}{m} A'(\beta(x_{i+1} - x_i) - d_i) \right] m_{k+1}^N \right) dx_{k+1} \end{aligned} \tag{4.30}$$

The second term is treated as:

$$\begin{aligned} &\sum_{i>k} \int_{\mathbb{R}^{N-k}} \partial x_i \left(\left[v_i^0 - \frac{\alpha}{m} A'(\beta(x_{i+1} - x_i) - d_i) \right] f^N \right) dx_{k+1} dx_{k+2} ... dx_N \overset{\text{Int. by parts}}{=} \\ &\sum_{i>k} \int_{\mathbb{R}^{N-k}} \partial x_i \left(\left[v_i^0 - \frac{\alpha}{m} A'(\beta(x_{i+1} - x_i) - d_i) \right] \right) f^N dx_{k+1} dx_{k+2} ... dx_N + \\ &\sum_{i>k} \int_{\mathbb{R}^{N-(k-1)}} \left(\left[v_i^0 - \frac{\alpha}{m} A'(\beta(x_{i+1} - x_i) - d_i) \right] \right) \overbrace{f^N|_{x_i=-\infty}^{x_i=\infty}}^{=0} dx_{k+1} dx_{k+2} ... dx_N - \\ &\sum_{i>k} \int_{\mathbb{R}^{N-k}} \partial x_i \left(\left[v_i^0 - \frac{\alpha}{m} A'(\beta(x_{i+1} - x_i) - d_i) \right] \right) f^N dx_{k+1} dx_{k+2} ... dx_N \\ &= 0. \end{aligned}$$

The equation for the k-particle marginal reads:

$$\partial_t m_k^N + \sum_{i \leq k} \int_{\mathbb{R}} \partial_{x_i} \left(\left[v_i^0 - \frac{\alpha}{m} A'(\beta(x_{i+1} - x_i) - d_i) \right] m_{k+1}^N \right) dx_{k+1} = 0. \tag{4.31}$$

We mention that m_{k+1}^N emerges in the equation for m_k^N. Hence we have to solve the equations for all m_k^N simultaneously. As usual we try to find a solution of simple form for $N \to \infty$.

4.2.1 Link between Special and General Approach

We want to derive the link between (4.31) and (x being the placeholder for $u(s,t)$ again)

$$\partial_t \rho(x,t) + \partial_x \left(\left[v^0 + O(\frac{1}{N^\gamma}) - \frac{\alpha}{m} A'(\beta[u(s+\frac{1}{N},t) - u(s,t)] - d + O(\frac{1}{N^\gamma})) \right] \rho(x,t) \right) = 0 \tag{4.32}$$

in the limit $N \to \infty$. We investigate the four cases mentioned above.

First Case ($\alpha = O(1), \beta = O(N)$)

We start with introducing

$$\delta^N(z) = N^{a+1} F(N^{a+1} z) \qquad a > 0.$$

$F(z)$ is a positive function with maximum at zero, furthermore decaying for $|z| \to \infty$. In the limit $N \to \infty$, δ^N converges to the Dirac-delta function.

We seek $m_k^N(x_k, ..., x_1, t)$ of the form

$$m_k^N(x_k, ..., x_1, t) = m_1^N(x_1, t) \prod_{i=1}^{k-1} \delta^N \left(N(x_{i+1} - x_i) - \frac{1}{m_1^N(x_i, t)} \right) + O(\frac{1}{N^\delta}).$$

We assume that the initial value for m_k^N at $t = 0$ depends only on m_1^N. The distances $x_{i+1} - x_i$ correspond to the distribution of x_{i+1} for $t = 0$. The assumption that the above form for δ^N holds implies that the variance is of higher order in $\frac{1}{N}$.

We assume φ_k to be a test function with compact support and $\varphi_k(x_k, ..., x_1, 0) = \varphi_k(x_k, ..., x_1, \infty) = 0$. To simplify the notations, we neglect the time dependence in the following. The weak formulation of (4.31) yields in the first case:

$$\int_{\mathbb{R}^k} \int_{\mathbb{R}^+} \partial_t \left[m_1^N(x_1) \prod_{i=1}^{k-1} \delta^N \left(N(x_{i+1} - x_i) - \frac{1}{m_1^N(x_i)} \right) \right] \varphi_k(x_k, ..., x_1, t) dx_1 ... dx_k dt +$$

$$\int_{\mathbb{R}^{k+1}} \int_{\mathbb{R}^+} \sum_{i \le k} \partial_{x_i} \left[\left(v_i^0 - \frac{1}{m} A'(N(x_{i+1} - x_i) - d_i) \right) m_1^N(x_1) \prod_{i=1}^{k} \delta^N \left(N(x_{i+1} - x_i) - \frac{1}{m_1^N(x_i)} \right) \right]$$

$$\times \varphi_k(x_k, ..., x_1, t) dx_1 ... dx_{k+1} dt = 0.$$

We obtain after integrating by parts

$$\int_{\mathbb{R}^k} \int_{\mathbb{R}^+} m_1^N(x_1) \prod_{i=1}^{k-1} \delta^N \left(N(x_{i+1} - x_i) - \frac{1}{m_1^N(x_i, t)} \right) \partial_t \varphi_k(x_k, ..., x_1) dx_1 ... dx_k dt +$$

$$\int_{\mathbb{R}^{k+1}} \int_{\mathbb{R}^+} \sum_{i \le k} \left(v_i^0 - \frac{1}{m} A'(N(x_{i+1} - x_i) - d_i) \right) \times$$

$$m_1^N(x_1) \prod_{i=1}^{k} \delta^N \left(N(x_{i+1} - x_i) - \frac{1}{m_1^N(x_i, t)} \right) \partial_{x_i} \varphi_k(x_k, ..., x_1) dx_1 ... dx_{k+1} dt = 0.$$

We substitute $z_j = N^a \left(N(x_j - x_{j-1}) - \frac{1}{m_1^N(x_{j-1})} \right)$, which is equivalent to

$$x_j = x_1 + \frac{1}{N^{a+1}} \sum_{i=2}^{j} z_i + \frac{1}{N} \sum_{i=1}^{j-1} \frac{1}{m_1^N(x_i)} = x_1 + \frac{1}{N} g_j(x_1, z_2, ..., z_j)$$

and obtain:

$$\begin{aligned}
&\int_{\mathbb{R}^k} \int_{\mathbb{R}^+} m_1^N(x_1) \prod_{i=1}^{k-1} \delta^N \left(\frac{z_{i+1}}{N^a} \right) \times \\
&\partial_t \varphi_k \left(x_1 + \frac{1}{N} g_k(x_1, z_2, ..., z_k), ..., x_1 + \frac{1}{N} g_1(x_1) \right) dx_1, dz_2 ... dz_k dt + \\
&\int_{\mathbb{R}^{k+1}} \int_{\mathbb{R}^+} \sum_{i \leq k} \left(v_i^0 - \frac{1}{m} A' \left(\frac{z_{i+1}}{N^a} + \frac{1}{m_1^N(x_1 + \frac{1}{N} g_i(x_1, z_2, ..., z_i))} - d_i \right) \right) \times \\
&m_1^N(x_1) \prod_{i=1}^{k} \delta^N \left(\frac{z_{i+1}}{N^a} \right) \times \\
&\partial_{x_i} \varphi_k \left(x_1 + \frac{1}{N} g_k(x_1, z_2, ..., z_k), ..., x_1 + \frac{1}{N} g_1(x_1) \right) dx_1, dz_2 ... dz_{k+1} dt = 0.
\end{aligned} \tag{4.33}$$

The Taylor expansion of φ_k up to first order is

$$\begin{aligned}
&\varphi_k \left(x_1 + \frac{1}{N} g_k(x_1, z_2, ..., z_k), ..., x_1 + \frac{1}{N} g_1(x_1) \right) = \\
&\varphi_k(x_1, ..., x_1) + \frac{1}{N} \nabla \varphi_k(x_1, ..., x_1)^T \mathbf{g}(x_1, z_2, ..., z_k) + O(1/N^2) \overset{N \to \infty}{\longrightarrow} \varphi_k(x_1, ..., x_1),
\end{aligned}$$

with

$$\mathbf{g} = \begin{pmatrix} g_1(x_1) \\ g_2(x_1, z_2) \\ \vdots \\ g_k(x_1, z_2, ..., z_k) \end{pmatrix}$$

We proceed in the same way with $m_1^N(x_1 + \frac{1}{N} g_i(x_1, z_2, ..., z_i))$. Furthermore we assume

$$m_1^N(x_1) \overset{N \to \infty}{\longrightarrow} \rho(x_1),$$

$\rho(x)$ being the density function. We also obtain

$$m_1^N \left(x_1 + \frac{1}{N} g_i(x_1, z_2, ..., z_i) \right) \overset{N \to \infty}{\longrightarrow} \rho(x_1).$$

With the above mentioned properties

$$v_i^0 = v^0 + O(\frac{1}{N^\gamma}) \quad \text{and} \quad d_i = d + O(\frac{1}{N^\gamma})$$

we obtain from (4.33) in the limit $N \to \infty$:

$$\int_{\mathbb{R}}\int_{\mathbb{R}^+} \rho(x_1)\partial_t\varphi_k(x_1,...,x_1)+$$
$$\sum_{i\leq k}\rho(x_1)\left[v^0-\frac{1}{m}A'\left(\frac{1}{\rho(x_1)}-d\right)\right]\partial_{x_i}\varphi_k(x_1,...,x_1)dtdx_1=0.$$

We rewrite this equation for test functions $\psi_k(x_1)=\varphi_k(x_1,...,x_1)$

$$\int_{\mathbb{R}}\int_{\mathbb{R}^+} \rho(x_1)\partial_t\psi_k(x_1)+$$
$$\sum_{i\leq k}\rho(x_1)\left[v^0-\frac{1}{m}A'\left(\frac{1}{\rho(x_1)}-d\right)\right]\partial_{x_i}\psi_k(x_1)dtdx_1=0.$$

The sum provides contribution only in case $x_i{=}x_1{:=}x$, this means we obtain after integrating by parts

$$\int_{\mathbb{R}}\int_{\mathbb{R}^+} \partial_t\rho(x,t)\psi_k(x,t)+$$
$$\partial_x\left(\rho(x,t)\left[v^0-\frac{1}{m}A'\left(\frac{1}{\rho(x,t)}-d\right)\right]\right)\psi_k(x,t)dtdx=0.$$

Because this equation holds for all x, t and test functions ψ_k with the above mentioned properties, we finally arrive at the deterministic equation

$$\partial_t\rho(x,t)+\partial_x\left(\left[v^0-\frac{1}{m}A'\left(\frac{1}{\rho(x,t)}-d\right)\right]\rho(x,t)\right)=0. \tag{4.34}$$

This result agrees with the special case (4.15) in Section 4.1. The continuum limit is hence a nonlinear conservation law for ρ. The limit of the marginals is given by $m_k=\rho(x_1)\prod_{i=1}^{k-1}\delta(x_{i+1}-x_i-\frac{1}{m_1(x_i)})$.

The other Cases

We proceed similarly in the second and third/fourth case. We can assume the marginals $m_k^N(x_k,...,x_1,t)$ to be slighly different, but also dependent on $m_1^N(x_1,t)$ and the distances $x_{i+1}-x_i$ for $i<k$. The limits coincide with (4.17) and (4.19), respectively.

4.2.2 Conclusions

We were able to prove that pedestrian's motion in the generalized 1D model in the limit $N\to\infty$, regarded on large time scales, can be described by a mean-field equation for the density ρ. This holds for different scalings for the potential A' and distances $x_{i+1}-x_i$. Motion can be described by an analogon of the continuity equation

$$\frac{\partial\rho}{\partial t}+\frac{\partial}{\partial x}(V\rho)=0 \tag{4.35}$$

with different choices for V in different scaling cases.

Chapter 5

Linear Stability

In this chapter we investigate the linear stability of several models. Linear stability is investigated around homogeneous flow. We want to know under which condition perturbations in homogeneous flow do not increase in time.

We start with the improved 1D social force model of Seyfried *et al.* for bodies with remote action. After that, we analyze Helbing's 2D social force model and the 2D NOMAD model. Finally we present the results of Nakayama *et al.* for the 2D optimal velocity model.

In this chapter, we write x_j instead of x_i, since we want to avoid confusion with the i denoting the imaginary part.

5.1 1D Social Force Model

We want to investigate linear stability for the 1D social force model. The equation of motion reads:

$$\frac{dv_j}{dt} = G_j(t) \cdot H(v_j(t), G_j(t)), \tag{5.1}$$

with

$$G_j(t) = \begin{cases} \frac{v_j^0 - v_j(t)}{\tau_j} - \frac{e_j}{m_j}\left(\frac{h}{r_{j+1}(t) - r_j(t) - d_j(t)}\right)^{g_j} & \text{, if} \quad r_{j+1}(t) - r_j(t) - d_j(t) > 0 \\ -\infty & \text{, else,} \end{cases} \tag{5.2}$$

and

$$H(v_j(t), G_j(t)) = \begin{cases} 0 & \text{, if} \quad v_j(t) \leq 0, \quad G_j \leq 0 \\ 1 & \text{, if} \quad G_j(t) \geq \delta \\ 1 & \text{, if} \quad v_j(t) \geq \epsilon \\ v_j/\epsilon & \text{, if} \quad 0 < v_j(t) < \epsilon, \quad G_j < \frac{\delta}{\epsilon} v_j(t) \\ G_j/\delta & \text{, if} \quad 0 < G_j(t) < \delta, \quad v_j(t) < \frac{\epsilon}{\delta} G_j(t), \end{cases} \tag{5.3}$$

as above.

We want to analyze the model around homogeneous flow, i.e. constant velocities, zero acceleration and uniform distances. Homogeneous flow is realized in situations where $H(v_j, G_j)$ equals one, this means the pedestrians are able to walk and accelerate freely. Otherwise homogeneous flow is not possible.

The homogeneous flow solution is given by $\tilde{x}_j(t) = \tilde{h}j + \tilde{v}t + \text{const}$. All pedestrians walk with the same velocity $\tilde{v}$ and have the same headway $\tilde{h}$. One obtains $\tilde{v} = \frac{d\tilde{x}}{dt}$ by solving the equation

$$0 = \frac{v^0 - \frac{d\tilde{x}}{dt}}{\tau} - \frac{e}{m}\left(\frac{h}{\tilde{h} - a - b\frac{d\tilde{x}}{dt}}\right)^g =: f(\frac{d\tilde{x}}{dt}). \tag{5.4}$$

Again, e, a, b and g are constants, defined in Section 2.2.2.

We obtain an explicit equation for $\tilde{v}$ for small relaxation time. We insert the linear approximation

$$\tilde{v} = v^0 + \tau\tilde{w} + O(\tau^2) \tag{5.5}$$

into (5.4) and the equation for the velocity in case $g > 1$ reads:

$$\tilde{v} = v^0 - \tau\frac{e}{m}\left(\frac{h}{\tilde{h} - a - bv^0}\right)^g + O(\tau^2). \tag{5.6}$$

We consider a perturbation

$$x_j(t) = \tilde{x}_j(t) + y_j(t). \tag{5.7}$$

We obtain via the Taylor-expansion up to first order and because of $f(\tilde{v}) = 0$:

$$\begin{aligned}\frac{d^2y_j(t)}{dt^2} &= f\left(\frac{dx_j(t)}{dt}\right) = f\left(\tilde{v} + \frac{dy_j(t)}{dt}\right)\\ &= f(\tilde{v}) + f'(\tilde{v})\frac{dy_j}{dt} = f'(\tilde{v})\frac{dy_j}{dt}.\end{aligned} \tag{5.8}$$

$y_j(t)$ can be expanded into Fourier modes, $y_j(t) = \exp[ikj + i\omega t]$, with $\omega = \omega_1 + i\omega_2$. Stability means that perturbations do not increase in time. We rewrite

$$y_j(t) = \exp[ikj + i\omega t] = \exp[ikj + i(\omega_1 + i\omega_2)t] = \exp[ikj + i\omega_1 t - \omega_2 t].$$

Thus we find the condition for stability $\omega_2 \geq 0$, or ω does not have negative imaginary part.

Inserting the exponential form into (5.8), we obtain

$$-\omega^2 = f'(\tilde{v})i\omega, \tag{5.9}$$

and in case $\omega \neq 0$ (otherwise the model is always stable)

$$\omega = -f'(\tilde{v})i \quad \Rightarrow \quad w_2 = -f'(\tilde{v}) \geq 0 \tag{5.10}$$

This finally leads to the stability condition $f'(\tilde{v}) \leq 0$, which is in fact a condition for the relaxation time τ:

$$\tau \geq -\frac{m}{ebg}\left(\frac{\tilde{h} - a - b\tilde{v}}{h}\right)^{g+1}. \tag{5.11}$$

Here, the constants m, e, b, g, and $\tilde{h} - a - b\tilde{v}$ are larger than zero as a matter of fact, this means we obtain the sufficient condition

$$\tau \geq 0. \tag{5.12}$$

This condition holds automatically, thus homogeneous flow is always stable in the 1D model.

5.2 2D Social Force Model of Helbing

Helbing's 2D social force model reads:

$$\frac{d\mathbf{v}_j}{dt} = \frac{v_j^0 \mathbf{e}_j^0 - \mathbf{v}_j}{\tau_j} + \frac{1}{m_j} \sum_{k(\neq j)} \mathbf{f}_{jk} + \frac{1}{m_j} \sum_W \mathbf{f}_{jW}. \tag{5.13}$$

f_{jk} are the repulsive interaction forces

$$\begin{aligned} \mathbf{f}_{jk} = {} & A_j \exp\left[\left(R_{jk} - d_{jk}\right)/B_j\right] \cdot \mathbf{n}_{jk} + kg\left(R_{jk} - d_{jk}\right)\mathbf{n}_{jk} \\ & + \kappa g\left(R_{jk} - d_{jk}\right)\Delta v_{jk}^t \mathbf{t}_{jk}, \end{aligned} \tag{5.14}$$

defined in Section 2.1.2. f_{jW} are the forces of the walls, also defined in Section 2.1.2. d_{jk} and $\mathbf{n}_{jk}$ were defined as:

$$d_{jk} = \left\|\mathbf{r}_j - \mathbf{r}_k\right\|, \qquad \mathbf{n}_{jk} = \frac{\mathbf{r}_j - \mathbf{r}_k}{d_{jk}}.$$

We are interested in the homogeneous flow solution (see Figure 5.1), thus we do not have to consider the forces of the walls. Futhermore we assume that pedestrians do not touch each other, accordingly $g(x) = 0$.

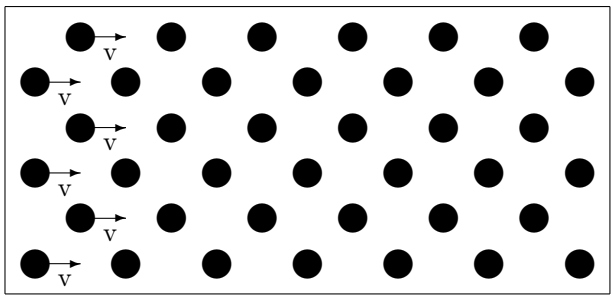

Figure 5.1: Homogeneous Flow

Homogeneous flow is expressed by the solution

$$\mathbf{r}_j = \mathbf{X}_j + \mathbf{v}t = (r_{jx}, r_{jy}). \tag{5.15}$$

Here, $\mathbf{X}_j = (X_j, Y_j)$ is a constant vector which represents a site on a regular lattice. $\mathbf{v}$ is a constant velocity with which all pedestrians move. We assume equal sizes, masses and interaction constants: $R_{jk} = 2R$, $m_j = m$ and $A_j = A$. For convenience, we set $\mathbf{e}_j^0 = (1, 0) \quad \forall j$. This means all pedestrians are supposed to move in the positive direction of the x-axis. Futhermore, all pedestrians have the same distance to each other, $d_{jk} = d$.

We are now able to compute $\mathbf{v}$ and introduce $\mathbf{f}$:

$$\begin{aligned} \mathbf{f} = (f_x, f_y) &= A \cdot \exp[(2R - d)/B] \frac{\mathbf{r}_k - \mathbf{r}_j}{d} \\ \mathbf{v}_x &= v^0 - \frac{\tau}{m} \sum_k A \cdot \exp[(2R - d)/B] \frac{r_{kx} - r_{jx}}{d} \\ &=: v^0 - \frac{\tau}{m} \sum_k f_x(\mathbf{r}_k - \mathbf{r}_j), \end{aligned} \tag{5.16}$$

$$\begin{aligned}\mathbf{v}_y &= -\frac{\tau}{m}\sum_k A\cdot\exp[(2R-d)/B]\frac{r_{ky}-r_{jy}}{d}\\ &=: -\frac{\tau}{m}\sum_k f_y(\mathbf{r}_k-\mathbf{r}_j).\end{aligned} \tag{5.17}$$

We add a perturbation $\mathbf{x}_j(t)=(x_j(t),y_j(t))$, i.e.

$$r_{jx}\to X_j+v_xt+x_j(t)\quad r_{jy}\to Y_j+v_yt+y_j(t). \tag{5.18}$$

After inserting this into our model, we obtain via Taylor-expansion up to first order linearized equations

$$\frac{d^2}{dt^2}x_j=-\frac{1}{m}\sum_k\left[A_{kj}(x_k-x_j)+B_{kj}(y_k-y_j)\right]-\frac{1}{\tau}\frac{d}{dt}x_j, \tag{5.19}$$

$$\frac{d^2}{dt^2}y_j=-\frac{1}{m}\sum_k\left[C_{kj}(x_k-x_j)+D_{kj}(y_k-y_j)\right]-\frac{1}{\tau}\frac{d}{dt}y_j. \tag{5.20}$$

The parameters A_{kj}, B_{kj}, C_{kj} and D_{kj} are defined by

$$A_{kj}=\partial_x f_x(x,y)|_{x=X_k-X_j,y=Y_k-Y_j}, \tag{5.21}$$

$$B_{kj}=\partial_y f_x(x,y)|_{x=X_k-X_j,y=Y_k-Y_j}, \tag{5.22}$$

$$C_{kj}=\partial_x f_y(x,y)|_{x=X_k-X_j,y=Y_k-Y_j}, \tag{5.23}$$

$$D_{kj}=\partial_y f_y(x,y)|_{x=X_k-X_j,y=Y_k-Y_j}. \tag{5.24}$$

We consider the case that the perturbation propagates at the angle φ with the x-axis. Then the wave vector is $\mathbf{k}=(k_x,k_y)=(k_x,pk_x)$, with $p=\tan\varphi$. Two-dimensional waves are classified into two types of modes: longitudinal modes and transverse modes. Londitudinal modes in the φ direction are written by [21]

$$x_j=\exp[i\omega t+i\mathbf{k}\cdot\mathbf{x}]=\exp[i\omega t+i\theta(X_j+pY_j)],\qquad y_j=px_j. \tag{5.25}$$

Here, $\theta=k_x$. We can rewrite the linearized equations (5.19) and (5.20) as

$$\frac{d^2}{dt^2}x_j=-\frac{1}{m}\sum_k\left(A_{kj}+pB_{kj}\right)(x_k-x_j)-\frac{1}{\tau}\frac{d}{dt}x_j \tag{5.26}$$

$$0=-\frac{1}{m}\sum_k\left(A_{kj}+pB_{kj}-\frac{1}{p}C_{kj}-D_{kj}\right)(x_k-x_j). \tag{5.27}$$

The second equation is obtained by subtracting (5.20) from (5.19).

For the transverse modes we have [21]

$$x_j=\exp[i\omega t+i\mathbf{k}\cdot\mathbf{x}]=\exp[i\omega t+i\theta(X_j+pY_j)],\qquad y_j=-\frac{1}{p}x_j. \tag{5.28}$$

In this case we note $\theta=k_y$. The linearized equations are

$$\frac{d^2}{dt^2}x_j=-\frac{1}{m}\sum_k\left(A_{kj}-\frac{1}{p}B_{kj}\right)(x_k-x_j)-\frac{1}{\tau}\frac{d}{dt}x_j \tag{5.29}$$

$$0=-\frac{1}{m}\sum_k\left(A_{kj}-\frac{1}{p}B_{kj}+pC_{kj}-D_{kj}\right)(x_k-x_j). \tag{5.30}$$

In homogeneous flow, the interaction with the nearest neighbour is dominant and we neglect the interaction with further particles, which is justified for fast decay of the interaction potential compared to next-nearest neighbour distances. We take the summation over k for six particles around the jth one. We assign the indices shown in Figure 5.2.

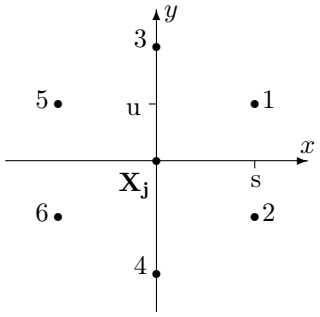

Figure 5.2: Indices of the Particles

For example, the position of particle 1 is $(s,u) = \left(\sqrt{3}\frac{d}{2}, \frac{d}{2}\right)$. Here, d denotes the distance between two nearest-neighbour particles. The exact forms of the parameters defined in (5.21) - (5.24) are shown in Appendix B.

We investigate the cases φ=0 (p=0, modes along the x-axis), φ=$\pi/2$ (p=∞, modes along the y-axis) and the general case ($0 < \varphi < \pi/2$) seperatly. Thus we carry out the analysis in three cases of direction (i) x-axis, (ii) y-axis and (iii) other directions for each two polarizations (a) longitudinal modes and (b) transverse modes. We investigated the stability in the six cases mentioned above. A necessary condition for stability is that ω does not have negative imaginary part (Section 5.1). The results are shown in the following. The details are explained in Appendix B.

We note that A and B, the interaction constants, are positive. The condition for the longitudinal mode along the x-axis is

$$d \geq \frac{B}{3}.$$

The condition for the transverse mode along the x-axis reads

$$d \geq 3B.$$

We now consider the case of $\varphi = \pi/2$ (y-axis). In the longitudinal case, we obtain

$$d \geq \frac{3B}{5 + 4\cos\theta u}.$$

The condition for the transverse mode is

$$d \geq \frac{B\,(5 + 4\cos\theta u)}{3}.$$

We investigated the general case ($0 < \varphi < \pi/2$) and found solutions only in two cases: For $\varphi = \pi/3$ and $\varphi = \pi/6$.

The condition for the longitudinal mode for $\varphi = \pi/3$ reads

$$d \geq \frac{B}{3},$$

and the condition for the transverse mode reads

$$d \geq 3B.$$

For $\varphi = \pi/6$, we obtain in the longitudinal mode

$$d \geq 3B$$

and in the transverse mode

$$d \geq \frac{B}{3}.$$

5.2.1 Conclusions

We investigated the linear stability of Helbing's 2D social force model and obtained six stability conditions for three directions and two polarizations. The conditions depend only on the distance d, the interaction distance B, and the wave vector $\mathbf{k}$. If d is sufficiently large (depending on B, sometimes on $\mathbf{k}$), this means the density is low, homogeneous flow in Helbing's social force model is stable.

5.3 NOMAD Model

We investigate the stability of the basic NOMAD model, introduced in Section 2.3.1. The model reads

$$\frac{d\mathbf{v}_j}{dt} = \frac{\mathbf{v}_j^0 - \mathbf{v}_j}{\tau_j} - A_j \sum_{j \in Q_i} \mathbf{u}_{jk} e^{-\frac{d_{jk}}{B_j}}, \tag{5.31}$$

with

$$d_{jk} = \|\mathbf{r}_k - \mathbf{r}_j\|, \quad \mathbf{u}_{jk} = [\mathbf{r}_k - \mathbf{r}_j] / d_{jk}. \tag{5.32}$$

We consider the homogeneous flow solution

$$\mathbf{r}_j = \mathbf{X}_j + \mathbf{v}t \tag{5.33}$$

introduced above. For convenience, we set $\mathbf{v}_j^0 = (v^0, 0) \quad \forall j$. All pedestrians have the same distance $d_{jk} = d$ to each other and the same interaction constant A.

We compute $\mathbf{v}$ and introduce $\mathbf{f}(\mathbf{r}_k - \mathbf{r}_j) = (f_x, f_y) = A\exp\left(\frac{-d}{B}\right)\frac{\mathbf{r}_k - \mathbf{r}_j}{d}$:

$$v_x = v^0 - \tau A \sum_{k \in Q_j} \frac{r_{kx} - r_{jx}}{d} \exp\left(\frac{-d}{B}\right) = v^0 - \tau \sum_{k \in Q_j} f_x(\mathbf{r}_k - \mathbf{r}_j), \tag{5.34}$$

$$v_y = -\tau A \sum_{k \in Q_j} \frac{r_{kx} - r_{jx}}{d} \exp\left(\frac{-d}{B}\right) = -\tau \sum_{k \in Q_j} f_y(\mathbf{r}_k - \mathbf{r}_j). \tag{5.35}$$

We add a perturbation in the same way as in the previous section and obtain via Taylor-expansion the linearized equations

$$\frac{d^2}{dt^2}x_j = -\sum_{k\in Q_j}\left[A_{kj}(x_k - x_j) + B_{kj}(y_k - y_j)\right] - \frac{1}{\tau}\frac{d}{dt}x_j, \tag{5.36}$$

$$\frac{d^2}{dt^2}y_j = -\sum_{k\in Q_j}\left[C_{kj}(x_k - x_j) + D_{kj}(y_k - y_j)\right] - \frac{1}{\tau}\frac{d}{dt}y_j. \tag{5.37}$$

The parameters A_{kj}, B_{kj}, C_{kj} and D_{kj} are defined the same way as in Section 5.2.

We obtain for the longitudinal modes

$$\frac{d^2}{dt^2}x_j = -\sum_{k\in Q_j}\left(A_{kj} + pB_{kj}\right)(x_k - x_j) - \frac{1}{\tau}\frac{d}{dt}x_j, \tag{5.38}$$

$$0 = -\sum_{k\in Q_j}\left(A_{kj} + pB_{kj} - \frac{1}{p}C_{kj} - D_{kj}\right)(x_k - x_j), \tag{5.39}$$

and for the transverse modes

$$\frac{d^2}{dt^2}x_j = -\sum_{k\in Q_j}\left(A_{kj} - \frac{1}{p}B_{kj}\right)(x_k - x_j) - \frac{1}{\tau}\frac{d}{dt}x_j, \tag{5.40}$$

$$0 = -\sum_{k\in Q_j}\left(A_{kj} - \frac{1}{p}B_{kj} + pC_{kj} - D_{kj}\right)(x_k - x_j). \tag{5.41}$$

We again regard the set of pedestrians that influence person j, $k \in Q_j$, as the six pedestrians next to person j.

Once again, we have the necessary condition that ω does not have negative imaginary part. We have to investigate the same six cases as in Section 5.2. The results are shown in the following, the exact forms of the parameters A_{kj}, B_{kj}, C_{kj}, D_{kj} and the details are explained in Appendix C. We note that A and B, the interaction constants, are positive.

The condition for the longitudinal mode along the x-axis is $d \geq B/3$, and for the transverse mode $d \geq 3B$.

For modes along the y-axis, we obtain in the longitudinal case $d \geq \frac{3B}{(5+4\cos\theta u)}$. In the transverse case we get $d \geq B(5 + 4\cos\theta u)/3$.

We found soultions in the general case only for $\varphi = \pi/3$ and $\varphi = \pi/6$. In the longitudinal case for $\varphi = \pi/3$, the solution reads $d \geq B/3$, and in the transverse case $d \geq 3B$.

For $\varphi = \pi/6$ we obtain in the longitudinal case $d \geq 3B$, and in the transverse case $d \geq B/3$.

5.3.1 Conclusions

The NOMAD model is similar to Helbing's model. Differences are the number of pedestrians who influence person i, forces of walls and forces that arise in case of physical interaction which are not included in the NOMAD model. Furthermore the interaction term is different. In the NOMAD model the interaction term is independent of pedetrian's radii. In the investigation of the model forces of walls and of physical interactions are neglected. For convenience we regarded only nearest neighbours. Accordingly, as only difference remained the depencence of the radii in the interaction term. We found out that this dependence has no effect on the conditions for linear stability, this means we obtained the same conditions for Helbing's model and the NOMAD model.

5.4 Optimal Velocity Model

In this section we present the results of Nakayama *et al.* for investigation of linear stability of the optimal velocity model. The details are explained in [21]. The model reads

$$\frac{d}{dt}\mathbf{v}_j(t) = a\left(\mathbf{v}^0 + \sum_k \mathbf{f}(\mathbf{r}_k(t) - \mathbf{r}_j(t)) - \mathbf{v}_j(t)\right). \tag{5.42}$$

5.4.1 Linear Analysis

Nakayama *et al.* started with some simplifications: They set $\mathbf{v}^0 = (v^0, 0)$ and $c = -1$. Thus $g < 0$, this means the interaction is repulsive. α was set to $1/4$. Furthermore, they rescaled $t \to t/a$, $v^0 \to av^0$ and $\mathbf{f} \to a\mathbf{f}$. After this, (5.42) reads

$$\frac{d}{dt}\mathbf{v}_j(t) = \mathbf{v}^0 + \sum_k \mathbf{f}(\mathbf{r}_k(t) - \mathbf{r}_j(t)) - \mathbf{v}_j(t). \tag{5.43}$$

The homogeneous flow solution reads

$$\mathbf{r}_j = \mathbf{X}_j + \mathbf{v}t, \tag{5.44}$$

with constant velocity

$$\mathbf{v} = (v_x, v_y) = \mathbf{v}^0 + \sum_k \mathbf{f}(\mathbf{X}_k - \mathbf{X}_j). \tag{5.45}$$

Distances between any nearest-neighbour pairs are the same, d. Distance is used as a parameter instead of density. After considering a perturbation one obtains linearized equations

$$\frac{d^2}{dt^2}x_j = \sum_k \left[A_{kj}(x_k - x_j) + B_{kj}(y_k - y_j)\right] - \frac{d}{dt}x_j, \tag{5.46}$$

$$\frac{d^2}{dt^2}y_j = \sum_k \left[C_{kj}(x_k - x_j) + D_{kj}(y_k - y_j)\right] - \frac{d}{dt}y_j, \tag{5.47}$$

with parameters A_{kj}, B_{kj}, C_{kj} and D_{kj} defined as above. The exact forms are given in [21].

Nakayama *et al.* obtaineded for longitudinal modes

$$\frac{d^2}{dt^2}x_j = \sum_k (A_{kj} + pB_{kj})(x_k - x_j) - \frac{d}{dt}x_j, \tag{5.48}$$

$$0 = \sum_k \left(A_{kj} + pB_{kj} - \frac{1}{p}C_{kj} - D_{kj}\right)(x_k - x_j), \tag{5.49}$$

and for transverse modes

$$\frac{d^2}{dt^2}x_j = \sum_k \left(A_{kj} - \frac{1}{p}B_{kj}\right)(x_k - x_j) - \frac{d}{dt}x_j, \tag{5.50}$$

$$0 = \sum_k \left(A_{kj} - \frac{1}{p}B_{kj} + pC_{kj} - D_{kj}\right)(x_k - x_j). \tag{5.51}$$

The interaction with nearest neighbours is dominant, so interaction with further particles is neglected. Solving the linearized equations, one again finds that ω does not have negative imaginary part [21]. For modes along the x-axis, the condition for the longitudinal mode is

$$a > \frac{3[3g' + 2(g/d)]^2}{2[3g' + (g/d)]}, \tag{5.52}$$

d being the distance between two nearest-neighbor particles, g the function from (2.30), and g' its derivative. The stability condition for the transverse mode reads

$$a > \frac{3[g' + 2(g/d)]^2}{2[g' + 3(g/d)]}. \tag{5.53}$$

The instability arises first from the longest wavelength mode for both cases.

For off-x-axis modes, there exist three remarkable points: First of all, mode solutions only exist in the directions $\varphi = n\pi/6$ ($n = 1, 2, 3, 4, 5, 7, 8, 9, 10, 11$). Secondly, only the shortest wavelength mode is allowed in each direction and for each polarization. Thirdly, the stability condition is decided only by the distance d and independent of the sensitivity a [21].

φ	longitudinal mode	transverse mode
0	(5.52)	(5.53)
$\pi/6$	d>1.05	d>0.59
$\pi/3$	d>0.59	d>1.05
$\pi/2$	d>1.05	d>0.94

Table 5.1: Stability conditions for all modes

In Table 5.1, stability conditions are shown for α=1/4, β=2.5, b=1.9 and c=-1.0. Two critical values, $d = 0.59$ and $d = 1.05$, are common for various modes. These values also appear as the singularity of stability condition for the modes alongthe x-axis: (5.52) is singular at $d = 0.59$ and (5.53) is singular at $d = 1.05$. It is left to future research why these values turn up in both modes.

For the phase diagram it has to be noticed that there are four different phases: Homogeneous flow is stable in phase A. In phase B, only the transverse modes along the x-axis are unstable. In phase C, only longitudinal modes along the x-axis are unstable. Several modes become unstable simultaneously in phase D. Here it is unpredictable how the flow breaks.

Nakayama *et al.* suggest a mechanism for blocking phenomena observed in counter flow based on their analysis. For sufficiently large distance d and sensitivity a, clear lanes are formed where particles are moving in opposite directions. Each lane can be considered as unidirectional flow. The stability condition is roughly the same as that obtained for unidirectional flow. When the distance among particles is little smaller than the critical value obtained by the analysis for unidirectional flow, temporal lane formation is observed, but these lanes are unstable. The final states in such cases are blocking states. At shorter distances ($d < 1$), no temporal lane formation is observed and blocking states emerge immediately. The conclusions from numerical simulations are that lane formation occurs in region A where the homogeneous flow is stable, and the blocking occurs in regions where homogeneous flow is unstable. We mention for the phase diagram that there are two phases: In one phase lane formation occurs, in the other phase blocking occurs. The boundary between the above phases exists near the boundary between regions A and B (C).

5.4.2 Conclusions

Nakayama *et al.* investigated the linear stability of the homogeneous flow solution in the two-dimensional OV model. They pointed out the stability conditions and drew the phase diagram from the result. They also performed numerical simulations of counterflow. The results can be understood as follows: Whenever lanes are formed, each can be considered as unidirectional flow and is stable at densities where homogeneous flow is stable (low densities). If the density is a little higher, lanes are formed temporally. Each lane can not be maintained due to unstable modes and the blocking phenomena occur finally. At much higher densities, several modes in the off-x-direction are unstable simultaneously, and blocking states emerge immediately. As a conclusion, the two-dimensional OV model can present a unified understanding of these phenomena in pedestrian flow.

Chapter 6

Numerical Results for a 2D Social Force Model

In this chapter we implemented Helbing's social force model. The simulations were calculated with Matlab. The calculation time was approximately 2 minutes. We implemented the following scenario. We considered a quadradic room of size 15m. The room has two exits of size 2m. The doors are located in the middle of left and right wall. We assume a circular shaped column of size 0.5m positioned asymetrically in front of the right door. 20 persons want to leave the room. Their initial distribution was choosen randomly. They are not in the state of panic. Pedestrians chose the nearest exit without taking density into account. Each exit is used by ten pedestrians.

The equation of motion reads [11]:

$$\begin{aligned} m_i \frac{d\mathbf{v}_i(t)}{dt} &= m_i \frac{v_i^0 \mathbf{e}_i^0(t) - \mathbf{v}_i(t)}{\tau_i} \\ &+ \sum_{j(\neq i)} \left\{ A_i \cdot \exp[(R_{ij} - d_{ij})/B_i] + kg(R_{ij} - d_{ij}) \right\} \mathbf{n}_{ij} + \kappa g(R_{ij} - d_{ij}) \Delta v_{ji}^t \mathbf{t}_{ij} \\ &+ \sum_{W} \left\{ A_i \cdot \exp[(R_i - d_{iW})/B_i] + kg(R_i - d_{iW}) \right\} \mathbf{n}_{iW} - \kappa g(R_i - d_{iW})(\mathbf{v}_i \cdot \mathbf{t}_{iW}) \mathbf{t}_{iW} \end{aligned} \tag{6.1}$$

with values presented in Table 6.1. We found out that time steps Δt=0.01s were sufficient.

We can see in Figures 6.5 - 6.8 that the column in front of the exit ensures smoother flow. Pedestrians do not interfere with other pedestrians and are able to leave the room faster. The column may obstruct a small number of pedestrians. The effect of the column gets even more important in case of panic: the cloumn avoids building up of dangerous pressures. This case was not the focus of this simulation.

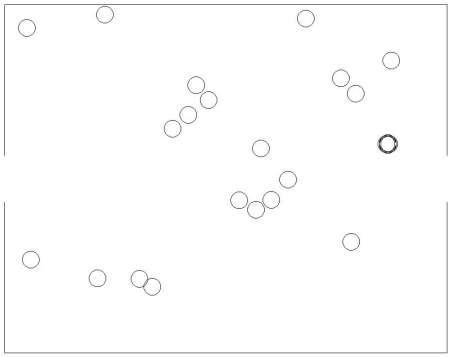

Figure 6.1: t=0s

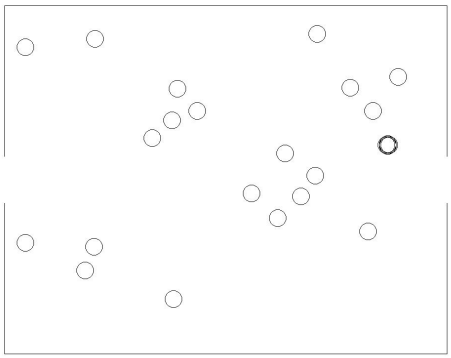

Figure 6.2: t=1s

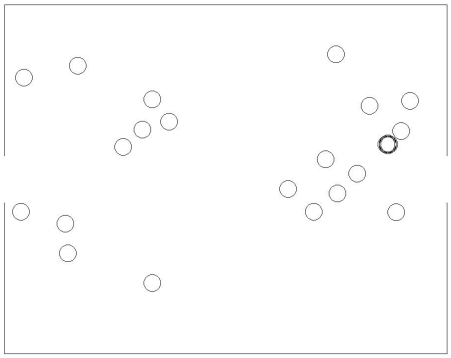

Figure 6.3: t=2s

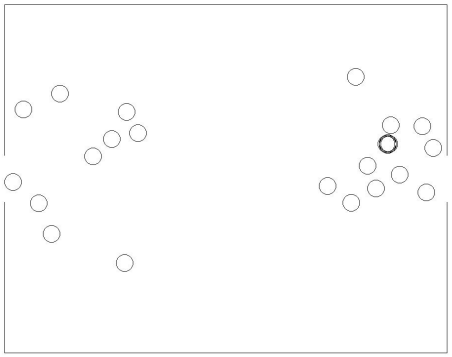

Figure 6.4: t=3s

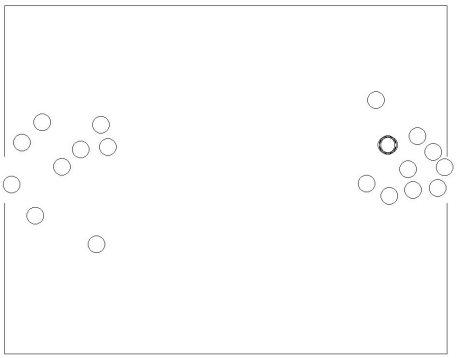

Figure 6.5: t=4s

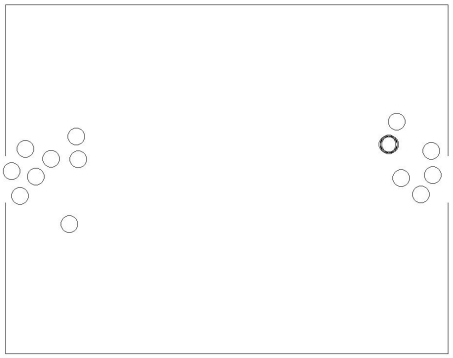

Figure 6.6: t=5s

Figure 6.7: t=6s

Figure 6.8: t=7s

Figure 6.9: t=8s

Parameter	**Mean**	**Standard Derivation**
m_i [kg]	70	5
v_i^0 [m/s]	1.24	0.15
τ_i [s]	0.5	0.01
r_i [m]	0.3	0.05
A_i [N]	$2{\cdot}10^3$	0
B_i [m]	0.08	0
k [kg/s^2]	$1.2{\cdot}10^5$	0
κ [kg/ms)	$2.4{\cdot}10^5$	0

Table 6.1: Values for 2D Model

Chapter 7

Outlook

In the last recent years a lot of work has been done in modelling for pedestrian motion, but there is still a lot to do.

Helbing pointed out that an obstacle in front of a door leads to smoother flow. We simulated his model with a circular shaped column as an obstacle. We found out that his ideas are correct. This leads to the question how the optimal shape for an obstacle would be and where the optimal place is. The effect of complex shaped obstacles could be investigated by means of the work of R. Tsai, especially with the sweeping method [4], [28], [29].

Furthermore, derivation of two dimensional continuum models is still an open problem. We leave this interesting problem to future research.

Pedestrian's behaviour in the state of panic is not fully understand by now. There are different approaches: On the one hand, data from various evacuation scenarios, e.g. plane evacuation, airport evacuation and hotel evacuation are still evaluated and survivors interviewed. One tries to understand how people really behave in case of smoke, etc. On the other hand, experimental setups are performed. Experiments do not reflect pedestrian's behaviour in case of real panic, but in adjusting special situations one gains an insight into standardized behaviour: For train evacuation modelling, e.g., it is essential to understand how pedestrians leave a train without a platform.

Results from investigations for pedestrian's motion have many applications in different socio-economic or biological systems, in which individuals compete for limited resources. Jamming and herding behaviour can be found in various systems, from markets and economics to animal colonies. Investigating pedestrian's motion may help to understand more complex human behaviour in the future.

Appendix A

Experimental Data

Tab.A.1 presents the corresponding experimental data for Figure 3.1, derived from the extended 1D model:

$$\frac{dv_i}{dt} = G_i(t) \cdot H(v_i(t), G_i(t)),$$

with

$$G_i(t) = \begin{cases} \frac{v_i^0 - v_i(t)}{\tau_i} - \frac{e_i}{m_i} \left(\frac{h}{r_{i+1}(t) - r_i(t) - d_i(t)} \right)^{g_i} & , r_{i+1} - r_i - d_i > 0 \\ -\infty & , \text{else} \end{cases}$$

and

$$H(v_i(t), G_i(t)) = \begin{cases} 0 & , \text{if} \quad v_i(t) \leq 0, \quad G_i \leq 0 \\ 1 & , \text{if} \quad G_i(t) \geq \delta \\ 1 & , \text{if} \quad v_i(t) \geq \epsilon \\ v_i/\epsilon & , \text{if} \quad 0 < v_i(t) < \epsilon, \quad G_i < \frac{\delta}{\epsilon} v_i(t) \\ G_i/\delta & , \text{if} \quad 0 < G_i(t) < \delta, \quad v_i(t) < \frac{\epsilon}{\delta} G_i(t). \end{cases}$$

We run the simulation 25 times. The desired velocities v_i^0 were Gaussian distributed. Values for τ_i, e_i, m_i a_i, b_i, h_i and g_i are given in Section 3.4. The length of the corridor was 17m, thus the density equals N/17m. We calculated the average velocity from all pedestrians. The results are shown in Table A.1.

Number of Pedestrians	**Density**	**Average Velocity**
1	0.06	1.23
2	0.12	1.22
3	0.18	1.17
4	0.24	1.13
5	0.29	1.11
6	0.35	1.08
7	0.41	1.08
8	0.47	1.05
9	0.53	1.01
10	0.59	1.03
11	0.65	1.04
12	0.71	1.01
13	0.76	0.95
14	0.82	0.98
15	0.88	0.94
16	0.94	0.93
17	1	0.88
18	1.06	0.83
19	1.12	0.77
20	1.18	0.7
21	1.24	0.64
22	1.29	0.58
23	1.35	0.53
24	1.41	0.48
25	1.47	0.43
26	1.53	0.39
27	1.59	0.35
28	1.65	0.31
29	1.71	0.28
30	1.76	0.25
31	1.82	0.22
32	1.88	0.19
33	1.94	0.16
34	2	0.13
35	2.06	0.11
36	2.12	0.08
37	2.18	0.06
38	2.24	0.05
39	2.29	0.02

Table A.1: Experimental Data for 1D Model

Appendix B

Details for Linear Stability of Helbings Model

B.1 Exact Forms of A, B, C and D

The parameters defined by (5.21) - (5.24) are expressed as $A_1, A_2, \ldots, A_6, B_1, \ldots, D_6$. For example, $A_1 = \partial_x f_x(x,y)|_{x=s,y=u}$, with $\mathbf{f} = A \cdot \exp[(2R-d)/B]\frac{\mathbf{r}_k - \mathbf{r}_j}{d}$ and $(s,u) = \left(\sqrt{3}\frac{d}{2}, \frac{d}{2}\right)$. The exact forms are as follows:

$$\begin{aligned}
A_1 = A_2 = A_5 = A_6 &= \partial_x f_x(x,y)|_{x=\pm s, y=\pm u} \\
&= A \cdot \exp\left[(2R-d)/B\right]\left(\frac{1}{4d} - \frac{3}{4B}\right), \qquad \text{(B.1)} \\
A_3 = A_4 &= \partial_x f_x(x,y)|_{x=0, y=\pm 2u} \\
&= A \cdot \exp\left[(2R-d)/B\right]\left(\frac{1}{d}\right), \qquad \text{(B.2)} \\
B_1 = -B_2 = -B_5 = B_6 &= \partial_y f_x(x,y)|_{x=\pm s, y=\pm u} \\
&= A \cdot \exp\left[(2R-d)/B\right]\left(\frac{-\sqrt{3}}{4B} - \frac{\sqrt{3}}{4d}\right), \qquad \text{(B.3)} \\
B_3 = B_4 &= \partial_y f_x(x,y)|_{x=0, y=\pm 2u} \\
&= 0, \qquad \text{(B.4)} \\
C_1 = -C_2 = -C_5 = C_6 &= \partial_x f_y(x,y)|_{x=\pm s, y=\pm u} \\
&= A \cdot \exp\left[(2R-d)/B\right]\left(\frac{-\sqrt{3}}{4B} - \frac{\sqrt{3}}{4d}\right), \qquad \text{(B.5)} \\
C_3 = C_4 &= \partial_x f_y(x,y)|_{x=0, y=\pm 2u} \\
&= 0, \qquad \text{(B.6)}
\end{aligned}$$

$$D_1 = D_2 = D_5 = D_6 = \partial_y f_y(x,y)|_{x=\pm s, y=\pm u}$$
$$= A \cdot \exp\left[(2R-d)/B\right]\left(\frac{3}{4d} - \frac{1}{4B}\right), \tag{B.7}$$
$$D_3 = D_4 = \partial_y f_y(x,y)|_{x=0, y=\pm 2u}$$
$$= A \cdot \exp\left[(2R-d)/B\right]\left(\frac{-1}{B}\right). \tag{B.8}$$

B.2 Modes along the x-axis

B.2.1 Longitudinal Modes

In this case, $p = 0$, the equations corresponding to (5.25) - (5.27) are

$$x_j = \exp[i\omega t + i\mathbf{k}\cdot\mathbf{x}] = \exp[i\omega t + i\theta X_j], \qquad y_j = 0 \tag{B.9}$$

and

$$\frac{d^2}{dt^2}x_j = -\frac{1}{m}\sum_k A_{kj}(x_k - x_j) - \frac{1}{\tau}\frac{d}{dt}x_j, \tag{B.10}$$
$$0 = \frac{1}{m}C_{kj}(x_k - x_j) \tag{B.11}$$

We can easily find that (B.11) is automatically satisfied:

$$\begin{aligned}\sum_k C_{kj}(x_k - x_j) &= \sum_k C_{kj}\left[e^{i\theta X_k} - e^{i\theta X_j}\right]e^{i\omega t} \\ &= \left[(C_1 - C_1)\left(e^{i\theta s} - 1\right) + ((-C_1) + C1)\left(e^{-i\theta s} - 1\right)\right]e^{i\omega t} \\ &= 0.\end{aligned} \tag{B.12}$$

From (B.10) we obtain

$$-\omega^2 = -A_1\frac{4}{m}(\cos\theta s - 1) - \frac{1}{\tau}i\omega. \tag{B.13}$$

We examine the real part of this equation in case $\omega_2 = 0$ (stability) and find the stability condition

$$3d \geq B.$$

B.2.2 Transverse Modes

Transverse modes along the x-axis are expressed as

$$x_j = 0, \qquad y_j = \exp[i\omega t + i\mathbf{k}\cdot\mathbf{x}] = \exp[i\omega t + i\theta X_j]. \tag{B.14}$$

We obtain from (5.19) and (5.20)

$$0 = -\frac{1}{m}B_{kj}(y_k - y_j) \tag{B.15}$$
$$\frac{d^2}{dt^2}y_j = -\frac{1}{m}\sum_k D_{kj}(y_k - y_j) - \frac{1}{\tau}\frac{d}{dt}y_j. \tag{B.16}$$

It is easy to verify that (B.15) is satisfied in the same way as (B.11). Futhermore, (B.16) yields a similar equation to (B.10). Therefore the stability condition for this mode is

$$d \geq 3B.$$

B.3 Modes along the y-axis

B.3.1 Longitudinal Modes

In case $p = \infty$, the equations corresponding to (5.19) and (5.20) are

$$x_j = 0, \qquad y_j = \exp[i\omega t + i\mathbf{k}\cdot\mathbf{x}] = \exp[i\omega t + i\theta Y_j] \tag{B.17}$$

and

$$0 = -\frac{1}{m}B_{kj}(y_k - y_j), \tag{B.18}$$

$$\frac{d^2}{dt^2}y_j = -\frac{1}{m}\sum_k D_{kj}(y_k - y_j) - \frac{1}{\tau}\frac{d}{dt}y_j, \tag{B.19}$$

(B.18) is satisfied in the same way as (B.11). From (B.19) we obtain

$$-\omega^2 = -D_1\frac{4}{m}(\cos\theta u - 1) - D_3\frac{2}{m}(\cos 2\theta u - 1) - \frac{1}{\tau}i\omega \tag{B.20}$$

Hence we have to solve

$$D_1\frac{4}{m}(\cos\theta u - 1) + D_3\frac{2}{m}(\cos 2\theta u - 1) \geq 0. \tag{B.21}$$

Taking into account $\cos 2\theta u = \cos^2\theta u - \sin^2\theta u$ and $\frac{-\sin^2\theta u}{\cos\theta u - 1} = 1 + \cos\theta u$, we obtain

$$d(5 + 4\cos\theta u) \geq 3B.$$

B.3.2 Transverse Modes

Transverse modes along the y-axis are expressed as

$$x_j = \exp[i\omega t + i\mathbf{k}\cdot\mathbf{x}] = \exp[i\omega t + i\theta Y_j], \qquad y_j = 0. \tag{B.22}$$

We obtain from (5.19) and (5.20)

$$\frac{d^2}{dt^2}x_j = -\frac{1}{m}\sum_k A_{kj}(x_k - x_j) - \frac{1}{\tau}\frac{d}{dt}x_j, \tag{B.23}$$

$$0 = -\frac{1}{m}C_{kj}(x_k - x_j). \tag{B.24}$$

(B.24) is satisfied in the same way as (B.11). (B.23) leads to

$$-\omega^2 = -A_1\frac{4}{m}(\cos\theta u - 1) - A_3\frac{2}{m}(cos 2\theta u - 1) - \frac{1}{\tau}i\omega, \tag{B.25}$$

hence we have to solve

$$2A_1(\cos\theta u - 1) - A_3(\cos 2\theta u - 1) \geq 0, \tag{B.26}$$

which leads to the condition

$$3d \geq B(5 + 4\cos\theta u)$$

B.4 Modes in General Direction

B.4.1 Longitudinal Modes

For stability of longitudinal modes in direction $(0 < \varphi < \pi/2, 0 < p < \infty)$, we simplify (5.27). We use (5.25) and obtain

$$\begin{aligned}
0 = &\left(e^{i\theta(s+pu)} - 1\right)\left(A_1 + pB_1 - \frac{1}{p}C_1 - D_1\right) \\
&+ \left(e^{i\theta(s-pu)} - 1\right)\left(A_1 - pB_1 + \frac{1}{p}C_1 - D_1\right) \\
&+ \left(e^{2i\theta pu} - 1\right)(A_3 - D_3) + \left(e^{-2i\theta pu} - 1\right)(A_3 - D_3) \\
&+ \left(e^{-i\theta(s-pu)} - 1\right)\left(A_1 - pB_1 + \frac{1}{p}C_1 - D_1\right) \\
&+ \left(e^{-i\theta(s+pu)} - 1\right)\left(A_1 + pB_1 - \frac{1}{p}C_1 - D_1\right).
\end{aligned} \tag{B.27}$$

We simplify by the replacement $p = \sqrt{3}/q$, q being a real number. The exact meaning of this parametrization is shown in [21]. The arguments of the exponential functions in (B.27) become

$$2\theta pu = \frac{\sqrt{3}}{q} r\theta \equiv 2\Phi, \qquad \theta(s \pm pu) = (q \pm 1)\Phi. \tag{B.28}$$

We rewrite (B.27) as

$$\begin{aligned}
0 = &e^{i(q+1)\Phi}\left(A_1 + pB_1 - \frac{1}{p}C_1 - D_1\right) \\
&+ e^{i(q-1)\Phi}\left(A_1 - pB_1 + \frac{1}{p}C_1 - D_1\right) \\
&+ e^{2i\Phi}(A_3 - D_3) + e^{-2i\Phi}(A_3 - D_3) \\
&+ e^{-i(q-1)\Phi}\left(A_1 - pB_1 + \frac{1}{p}C_1 - D_1\right) \\
&+ e^{-i(q+1)\Phi}\left(A_1 + pB_1 - \frac{1}{p}C_1 - D_1\right)
\end{aligned} \tag{B.29}$$

and obtain

$$\begin{aligned}
0 = &-\left(\frac{1}{d} + \frac{1}{B}\right)(\cos(q+1)\Phi + \cos(q-1)\Phi) + 2\left(\frac{1}{d} + \frac{1}{B}\right)\cos 2\Phi \\
&+ \frac{\sqrt{3}}{2}\left(\frac{1}{p} - p\right)\left(\frac{1}{d} + \frac{1}{B}\right)(\cos(q+1)\Phi - \cos(q-1)\Phi).
\end{aligned} \tag{B.30}$$

We found solutions only two cases: First of all, $2\Phi = \pi$ and $q = 1 (p = \sqrt{3})$, this equals $\varphi = \frac{\pi}{3}$. Moreover in case $2\Phi = \pi$ and $q = 3 (p = 1/\sqrt{3})$, this equals $\varphi = \frac{\pi}{6}$.

We start with the case $2\Phi = \pi$ and $q = 1$. Inserting this into (5.26), we find

$$-\omega^2 = \frac{4}{m}(A_1 + \sqrt{3}B_1 + A_3) - \frac{1}{\tau}i\omega \tag{B.31}$$

and obtain the stability condition

$$3d \geq B.$$

For $2\Phi = \pi$ and $q = 3$, we obtain

$$-\omega^2 = \frac{4}{m}(A_1 + \frac{1}{\sqrt{3}}B_1 + A_3) - \frac{1}{\tau}i\omega, \tag{B.32}$$

hence

$$d \geq 3B.$$

B.4.2 Transverse Modes

In this case, condition (5.30) is the same as condition (5.27), because of $B_{kj} = C_{kj}$. Accordingly we have solutions only in the two cases mentioned above. For the first case, (5.29) becomes

$$-\omega^2 = \frac{4}{m}\left(A_1 - \frac{1}{\sqrt{3}}B_1 + A_3\right) - \frac{1}{\tau}i\omega, \tag{B.33}$$

and the stability condition reads

$$d \geq 3B.$$

For the second case, (5.29) becomes

$$-\omega^2 = \frac{4}{m}\left(A_1 + \sqrt{3}B_1 + A_3\right) - \frac{1}{\tau}i\omega, \tag{B.34}$$

and the stability condition reads

$$3d \geq B.$$

Appendix C

Details for Linear Stability of the NOMAD Model

C.1 Exact Forms of A, B, C and D

The exact forms of the parameters A_{kj}, B_{kj}, C_{kj} and D_{kj} for the NOMAD model are as follows (with $\mathbf{f} = \exp\left(\frac{-d}{B}\right)\frac{\mathbf{r}_k - \mathbf{r}_j}{d}$):

$$\begin{aligned}
A_1 = A_2 = A_5 = A_6 &= \partial_x f_x(x,y)|_{x=\pm s, y=\pm u} \\
&= A \cdot \exp\left[-d/B\right]\left(\frac{1}{4d} - \frac{3}{4B}\right), && \text{(C.1)} \\
A_3 = A_4 &= \partial_x f_x(x,y)|_{x=0, y=\pm 2u} \\
&= A \cdot \exp\left[-d/B\right]\left(\frac{1}{d}\right), && \text{(C.2)} \\
B_1 = -B_2 = -B_5 = B_6 &= \partial_y f_x(x,y)|_{x=\pm s, y=\pm u} \\
&= A \cdot \exp\left[-d/B\right]\left(\frac{-\sqrt{3}}{4d} - \frac{\sqrt{3}}{4B}\right), && \text{(C.3)} \\
B_3 = B_4 &= \partial_y f_x(x,y)|_{x=0, y=\pm 2u} \\
&= 0, && \text{(C.4)} \\
C_1 = -C_2 = -C_5 = C_6 &= \partial_x f_y(x,y)|_{x=\pm s, y=\pm u} \\
&= A \cdot \exp\left[-d/B\right]\left(\frac{-\sqrt{3}}{4d} - \frac{\sqrt{3}}{4B}\right), && \text{(C.5)} \\
C_3 = C_4 &= \partial_x f_y(x,y)|_{x=0, y=\pm 2u} \\
&= 0, && \text{(C.6)}
\end{aligned}$$

$$D_1 = D_2 = D_5 = D_6 = \partial_y f_y(x,y)|_{x=\pm s, y=\pm u}$$
$$= A \cdot \exp\left[-d/B\right]\left(\frac{3}{4d} - \frac{1}{4B}\right), \tag{C.7}$$
$$D_3 = D_4 = \partial_y f_y(x,y)|_{x=0, y=\pm 2u}$$
$$= A \cdot \exp\left[-d/B\right]\left(\frac{-1}{B}\right). \tag{C.8}$$

C.2 Modes along the x-axis

C.2.1 Longitudinal Modes

The corresponding equations to (5.38) and (5.39) are

$$\frac{d^2}{dt^2}x_j = -\sum_k A_{kj}(x_k - x_j) - \frac{1}{\tau}\frac{d}{dt}x_j, \tag{C.9}$$
$$0 = -\sum_k C_{kj}(x_k - x_j). \tag{C.10}$$

It is easy to see that (C.10) is in the same way satified as (B.11). From (C.9) we obtain

$$-\omega^2 = -4A_1(\cos\theta s - 1) - \frac{1}{\tau}i\omega \tag{C.11}$$

and find the stability condition

$$3d \geq B.$$

C.2.2 Transverse Modes

We have

$$0 = -\sum_k B_{kj}(y_k - y_j), \tag{C.12}$$
$$\frac{d^2}{dt^2}y_j = -\sum_k D_{kj}(y_k - y_j) - \frac{1}{\tau}\frac{d}{dt}y_j. \tag{C.13}$$

(C.12) is automatically satisfied and (C.13) is similar to (C.11), therefore we obtain the condition

$$d \geq 3B.$$

C.3 Modes along the y-axis

C.3.1 Longitudinal Modes

The constraint

$$0 = -\sum_k B_{kj}(y_k - y_j) \tag{C.14}$$

is automatically satisfied and from

$$\frac{d^2}{dt^2}y_j = -\sum_k D_{kj}(y_k - y_j) - \frac{1}{\tau}\frac{d}{dt}y_j \tag{C.15}$$

we obtain

$$-\omega^2 = -2\left[2D_1(\cos\theta u - 1) - D_3(\cos 2\theta u - 1)\right] - \frac{1}{\tau}i\omega. \tag{C.16}$$

Therefore we have to solve

$$2D_1(\cos\theta u - 1) + D_3(\cos 2\theta u - 1) \geq 0, \tag{C.17}$$

which leads to

$$d(5 + 4\cos\theta u) \geq 3B.$$

C.3.2 Transverse Modes

We obtain similar equations to (C.14) and (C.15), which finally leads to

$$3d \geq B(5 + 4\cos\theta u).$$

C.4 Modes in General Directon

C.4.1 Longitudinal Modes

We have

$$\begin{aligned}
0 = &\left(e^{i\theta(s+pu)} - 1\right)\left(A_1 + pB_1 - \frac{1}{p}C_1 - D_1\right) \\
&+ \left(e^{i\theta(s-pu)} - 1\right)\left(A_1 - pB_1 + \frac{1}{p}C_1 - D_1\right) \\
&+ \left(e^{2i\theta pu} - 1\right)(A_3 - D_3) + \left(e^{-2i\theta pu} - 1\right)(A_3 - D_3) \\
&+ \left(e^{-i\theta(s-pu)} - 1\right)\left(A_1 - pB_1 + \frac{1}{p}C_1 - D_1\right) \\
&+ \left(e^{-i\theta(s+pu)} - 1\right)\left(A_1 + pB_1 - \frac{1}{p}C_1 - D_1\right),
\end{aligned} \tag{C.18}$$

and after the same replacement as in B.4.1 we have to solve

$$\begin{aligned}
0 = &-\left(\frac{1}{d} + \frac{1}{B}\right)(\cos(q+1)\Phi + \cos(q-1)\Phi) + 2\left(\frac{1}{d} - \frac{1}{B}\right)\cos 2\Phi \\
&+ \frac{\sqrt{3}}{2}\left(\frac{1}{p} - p\right)\left(\frac{1}{d} + \frac{1}{B}\right)(\cos(q+1)\Phi - \cos(q-1)\Phi).
\end{aligned} \tag{C.19}$$

Again, we found solutions only in the cases $2\Phi = \pi$, $q = 1 (p = \sqrt{3})$ and $2\Phi = \pi$, $q = 3 (p = \frac{1}{\sqrt{3}})$. We obtain in the first case

$$-\omega^2 = 4(A_1 + \sqrt{3}B_1 + A_3) - \frac{1}{\tau}i\omega, \tag{C.20}$$

which leads to the condition

$$3d \geq B.$$

In the second case we obtain

$$-\omega^2 = 4(A_1 - \frac{1}{\sqrt{3}}B_1 + A_3) - \frac{1}{\tau}i\omega, \tag{C.21}$$

which leads to

$$d \geq 3B.$$

C.4.2 Transverse Modes

The transverse modes lead to the same equation as in C.4.1, due to $B_{kj} = C_{kj}$. Hence we have in the case $2\Phi = \pi$, $q = 1$ the equation

$$-\omega^2 = 4(A_1 - \frac{1}{\sqrt{3}}B_1 + A_3) - \frac{1}{\tau}i\omega \tag{C.22}$$

and the stability condition

$$d \geq 3B.$$

In case $2\Phi = \pi$, $q = 3$ we have

$$-\omega^2 = 4A(A_1 + \sqrt{3}B_1 + A_3) - \frac{1}{\tau}i\omega \tag{C.23}$$

and find the stability condition

$$3d \geq B.$$

Bibliography

[1] C. Burstedde. *Simulation von Fußgängerverhalten mittels zweidimensionaler zellulärer Automaten*,
Diploma Thesis, Institute for Theoretical Physics, University of Cologne (2001)

[2] C. Cercignani, D. Sattinger. *Scaling limits and models in physical processes*,
Birkheuser (1998), **6-35**

[3] C. Cercignani, R. Illner, M. Pulvirenti. *The Mathematical Theory of Dilute Gases*,
Applied Mathematical Sciences 106, Springer (1994)

[4] L. Chen, R. Tsai. *Redistancing by flow of time dependent eikonal equation*,
Journal of Computational Physics 227(8) (2008), **4002-4017**

[5] F. Golse. *The meann-field limit for dynamics of large particle systems*,
Journées équations aux dérivées partielles 9 (2003)

[6] R. Colombo, M. Rosini. *Pedestrian flows and non-classical shocks*,
in *Mathematical Methods in the Applied Sciences* (2005), **1553-1567**

[7] D. Helbing. *Sicherheit in Fußgängermengen bei Massenveranstaltungen*,
in W. Freyer, S. Groß (eds) *Sicherheit in Tourismus und Verkehr* (2004), **253-288**
Preprint: http://www.age-info.de/PDF/SicherheitHelbing.pdf

[8] D. Helbing. *Traffic and related self-driven many particle systems*,
Reviews of Modern Physics 73 (2001), **1067-1141**

[9] D. Helbing, I. Farkas, P. Molnár, T. Vicsek. *Simulation von Fußgängermengen in normalen Situationen und im Evakuierungsfall*,
Vortrag bei der AGE Zentralveranstaltung 2002 in Essen
Preprint: http://www.age-info.de/PDF/essen-helbing.pdf

[10] D. Helbing, I. Farkas, T. Vicsek. *Freezing by heating in a driven mesoscopic system*,
Physical Review Leters 84 (2000), **1240-1243**

[11] D. Helbing, I. Farkas, T. Vicsek. *Simulating dynamical features of escape panic*,
Letters to Nature 407 (2000), **487-490**

[12] D. Helbing, P. Molnar. *Social force model for pedestrian Dynamics*,
Physical Rewiew Letters E51 (1995), **4282-4286**

[13] H. Heuser. *Gewöhnliche Differentialgleichungen*,
Teubner, Stuttgart (1995)

[14] S. Hoogendorn, W. Daamen, R. Landman. *Microscopic calibration and validation of pedestrian models - Cross-comparison of models using experimental data*,
in N. Waldau, P. Gattermann, H. Knoflacher, M. Schreckenberg (eds) *Pedestrian and Evacuation Dynamics 2005* (2007), **253-265**

[15] R. Hughes. *A continuum theory for the flow of pedestrians*,
Transportation Research Part B36 (2002), **507-535**

[16] H. Klüpfel. *A cellular automaton model for crowd movement and egress simulation*,
PhD Thesis, Faculty 4 - Natural Science, University Duisburg-Essen (2003)

[17] T. Kretz, M. Schreckenberg. *Moore and more and symmetry*,
in N. Waldau, P. Gattermann, H. Knoflacher, M. Schreckenberg (eds) *Pedestrian and Evacuation Dynamics 2005* (2007), **297-308**

[18] T. Liu. *The Riemann problem for general systems of conservation laws*,
Journal of Differential Equations (1975), **218-234**

[19] B. Maury, J. Venel. *Un modèle de mouvements de foule*,
Esaim: Proceedings 18 (2007), **143-152**

[20] D. Morale, V. Capasso, K. Oelschläger. *An interacting particle system modelling aggregation behavior: from individuals to populations*,
Journal of Mathematical Biology 50 (2005) **49-66**

[21] A. Nakayama, K. Hasebe, Y. Sugiyama. *Instability of pedestrian flow and phase structure in two-dimensional optimal velocity model*,
Physical Review Letters E71 (2007), 036121

[22] A. Nakayama, Y. Sugiyama, K. Hasebe. *Instability of pedestrian flow in two-dimensional optimal velocity model*,
in N. Waldau, P. Gattermann, H. Knoflacher, M. Schreckenberg (eds) *Pedestrian and Evacuation Dynamics 2005* (2007), **321-331**

[23] S. Ollo, S.R.S. Varadhan. *Scaling limit for interacting Ornstein-Uhlenbeck Processes*,
Communications in Mathematical Physics 135 (1991), **355-378**

[24] M. Schultz, S. Lehmann, H. Fricke. *A discrete microscopic model for pedestrian dynamics to manage emergency situations in airport terminals*,
in N. Waldau, P. Gattermann, H. Knoflacher, M. Schreckenberg (eds) *Pedestrian and Evacuation Dynamics 2005* (2007), **367-375**

[25] A. Seyfried, B. Steffen, W. Klingsch, T. Lippert, M. Boltes. *Steps toward the fundamental diagram - empirical results and modelling*,
in N. Waldau, P. Gattermann, H. Knoflacher, M. Schreckenberg (eds) *Pedestrian and Evacuation Dynamics 2005* (2007), **377-390**

[26] H. Spohn. *Kinetic equations from Hamilton dynamics: Markovian limits*,
Reviews of Modern Physics 53 (1980), **569-616**

[27] A. Treuille, S. Cooper, Z. Popovic. *Continuum crowds*,
ACM Transactions on Graphics 25(3) (2006) **1160-1168**
Preprint: http://grail.cs.washington.edu/projects/crowd-flows/78-treuille.pdf

[28] R. Tsai. *Rapid and accurate computation od the distance function using grids*, Journal of Computational Physics 178 (2002) **175-195**

[29] R. Tsai, L. Cheng, S. Osher, H. Zhao. *Fast sweeping algorithms for a class of Hamilton-Jacobi equations*, SIAM Journal of Numerical Analysis 41(2) (2003) **673-694**

[30] U. Weidmann. *Transporttechnik der Fußgänger*, Schriftenreihe des IVT 90, Zurich, (1992)

[31] M. Wölki, A. Schadschneider, M. Schreckenberg. *Fundamental diagram of a one-dimensional cellular automaton model for pedestrian flow - the ASEP with shuffled update*, in N. Waldau, P. Gattermann, H. Knoflacher, M. Schreckenberg (eds) *Pedestrian and Evacuation Dynamics 2005* (2007), **423-428**

[32] Y. Xia, S.C. Wong, M. Zhang, C.-W- Shu, W.H.K. Lam. *An efficient discontinuous Galerkin method on triangular meshes for a pedestrian flow model*, International Journal for Numerical Methods in Engineering, to appear Preprint: http://www.dam.brown.edu/scicomp/scg-media/report_files/BrownSC-2007-18.pdf

List of Figures

2.1 Lane Formation 7
2.2 'Freezing by heating' 8
2.3 Archlike Blockings at the Exit 9
2.4 Speed neighborhoods 20
2.5 Cell Neighborhood and Preference Matrix 22
2.6 Possible flow function 32

3.1 Velocity-Density Relation 45

5.1 Homogeneous Flow 57
5.2 Indices of the Particles 59

6.1 t=0s 66
6.2 t=1s 66
6.3 t=2s 66
6.4 t=3s 67
6.5 t=4s 67
6.6 t=5s 67
6.7 t=6s 68
6.8 t=7s 68
6.9 t=8s 68

List of Tables

2.1 Overview of estimation results 16
2.2 Speed and related neighbourhoods 20
2.3 Average walking times 21

3.1 Values for 1D Model 44

5.1 Stability conditions for all modes 63

6.1 Values for 2D Model 69

A.1 Experimental Data for 1D Model 74

Eidesstattliche Erklärung

Hiermit versichere ich, dass ich die vorliegende Arbeit selbstständig verfasst habe und neben den Programmen MATLAB und EXEL keine weiteren als die im Literaturverzeichnis angegebenen Hilfsmittel verwendet habe. Alle auf der CD beigefügten Programme sind von mir selbst erstellt worden.

Münster, 21.04.2008 _____

Unterschrift